INSIGHTS ON PUFA-CONTAINING LIPID MEMBRANES PROBED BY MD SIMULATIONS

by

Xiaoling Leng

A Dissertation

Submitted to the Faculty of Purdue University

In Partial Fulfillment of the Requirements for the degree of

Doctor of Philosophy

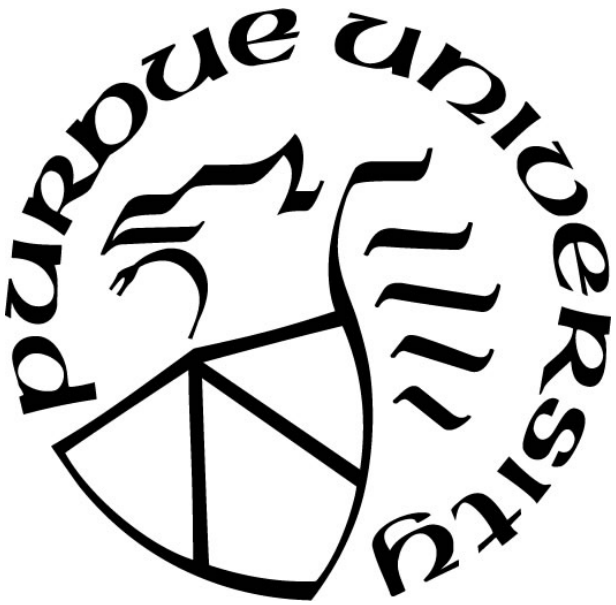

Department of Physics

West Lafayettee, Indiana

May 2017

THE PURDUE UNIVERSITY GRADUATE SCHOOL
STATEMENT OF DISSERTATION APPROVAL

Dr. Stephen R. Wassall , Chair
Department of Physics
Dr. Horia I. Petrache
Department of Physics
Dr. Fangqiang Zhu
Department of Physics
Dr. Le Luo
Department of Physics
Dr. Jorge H. Rodríguez
Department of Physics

Approved by:
Dr. Ricardo S. Decca
Head of the Departmental Graduate Program

For my wife Yuanyuan Zhou and daughterXiaoqing Leng

ACKNOWLEDGMENTS

I would like to thank my advisor for his guidance and encouragement through the research and writing process. I am grateful to all my committee members for the time and energy they have put into helping me complete my research.

My family, especially my wife, supported me during this long process. It means a lot to me. Thank you.

TABLE OF CONTENTS

LIST OF TABLES

LIST OF FIGURES

Appendix Figures

ABSTRACT

Author: Leng, Xiaoling . Ph.D.
Institution: Purdue University
Degree Received: May 2017
Title: Insights On PUFA-Containing Lipid Membranes Probed By MD Simulations
Major Professor: Stephen Wassall

The cell membrane serves as a barrier between the interior and exterior of a living cell. Its main structural component is the lipid bilayer, which is composed of various kinds of lipids that segregate into domains. These lipid domains, distinguished in composition and physical properties from the bulk lipids that surround them, are believed to modulate the function of resident proteins by providing an appropriate lipid environment. Polyunsaturated fatty acids (PUFA) are a type of fatty acid that contain multiple C=C double bonds. They have a lot of health benefits, which may originate in part due to their incorporation into lipids in the plasma membrane. Hypotheses that PUFA-containing lipids laterally separate into domains and/or modulate the structure of existing domains have been raised to explain the fundamental role played by PUFA. In our research, we use molecular dynamics (MD) simulations to simulate model membranes composed of PUFA-containing phospholipids and to investigate their interaction with cholesterol and vitamin E that are influential membrane constituents.

The presumptive function for vitamin E in membranes is to protect PUFA against oxidation. Although the chemistry of the process is well established, the role played by the molecular structure that we address with atomistic molecular dynamics (MD) simulations remains controversial. We compared the behavior of vitamin E in lipid bilayers composed of 1-stearoyl-2-docosahexaenoylphosphatidylcholine (SDPC, 18:0-22-6PC) and 1-stearoyl-2-oleoylphosphatidylcholine (SOPC, 18:0-18:1PC) via all-atom MD simulations at 37° C. SDPC represents a PUFA-containing lipid, and SOPC serves as monounsaturated control. From the calculation of van der Waals energy of interaction between vitamin E and fatty acid (FA) chains, we found higher probability that the PUFA chains surround the chromanol head group on vitamin E. This is further demonstrated by probability density maps of acyl chains around vitamin E molecules. Also, an ability to more easily penetrate

deep into the PUFA containing bilayer of vitamin E is detected by faster flip-flop rate of vitamin E observed in the SDPC bilayers. These results showed that the high disorder of polyunsaturated docosahexaenoic acid (DHA) chains allows vitamin E to easily tunnel down into the bilayer and often brings the PUFA chains up to the surface of the bilayer, improving the likelihood that the reactive (hydroxyl) group on vitamin E would encounter a lipid peroxyl radical and terminate the oxidation process. Thus, the simulations indicate that the molecular structure of vitamin E supports its role as an antioxidant in a PUFA-containing membrane.

A subsequent study on the partitioning of vitamin E into PUFA-containing lipids was done by analyzing the binding energy of vitamin E in the corresponding lipid bilayer. The binding energy is obtained from the potential of mean force (PMF) profile of vitamin E alone the membrane normal direction (z), which is calculated from umbrella sampling MD simulations. We found the binding in SDPC is smaller in SOPC, indicating that vitamin E does not prefer PUFA-containing phospholipids. The flip-flop rate was also estimated from the PMF profile, confirming that vitamin E flip-flops across the SDPC bilayer more easily than the SOPC bilayer. From the simulations it was noted that the membrane deforms as vitamin E is pulled out, which suggests interactions between the phospholipids contribute to the binding energy of the vitamin E.

In a final study, a comparison was made between the effect on membrane organization of the three types of long chain omega-3 (n-3) PUFA found in fish oils: eicosapentaenoic acid (EPA, 20:5), DHA (22:6) and docosapentaenoic acid (DPA, 22:5). MD simulations were run on lipid bilayers composed of 1-stearoyl-2-eicosapentaenoylphosphatidylcholine (EPA-PC, 18:0-20:5PC), 1-stearoyl-2-docosapentaenoylphosphatidylcholine (DPA-PC, 18:0-22:5PC), SDPC (DHA-PC, 18:0-22:6PC) and, as a monounsaturated control, SOPC (OA-PC, 18:0-18:1PC) in the absence and presence of cholesterol. By analyzing the physical properties such as membrane order and thickness, we found all three n-3 PUFAs disorder the membrane. The disordering is greatest with EPA and least with DPA. Unique among the n-3 PUFA-containing membranes, there is region of high order in the upper portion of the DPA chain. The PUFA-containing lipids were found to less favorably interact with cholesterol compared to the

OA-containing lipid, which is caused by their disorder. We speculate that differences between DPA, DHA and EPA might potentially modulate their effect on lipid domain formation.

CHAPTER 1. CELL MEMBRANES AND POLYUNSATURATED FATTY ACIDS

The cell membrane, also called plasma membrane, serves as a barrier between the interior and exterior of a living cell and cellar organelles in eukaryotes [1]. Its main structural component is a bilayer of lipid molecules about 5 nm in thickness. Membrane proteins, carbohydrates and other biological molecules are also embedded or inserted in this lipid bilayer. The real plasma membrane then is associated with a lot of biological functions, such as cell signaling [2], endocytosis [3], ion transportation [4], and so on.

There is a great complexity in cell membranes. Many types of lipids and membrane proteins exist, and the corresponding number of types of lipid-lipid, lipid-protein and protein-protein interactions are diverse. The cell membrane itself is also a very dynamic system, which is a key for the role it plays in cellar processes [5]. All these facts make it a challenging task to understand the structure and dynamics of cell membrane accurately.

One way to study the fundamental properties of cell membrane is to investigate on a simpler lipid-only bilayer system which is called a model membrane. Model membranes are protein-free with a controlled lipid content [6]. In this thesis we focus on the influence of polyunsaturated fatty acid (PUFA) incorporated into lipids in model membranes. The PUFAs are a type of fatty acids that contain multiple C=C double bonds. They have a lot of health benefits, which may originate from their physical properties [7]. In our research, we use molecular dynamics (MD) simulations to simulate model membranes composed of PUFA-containing phospholipids. Especially we investigated their interaction with cholesterol and vitamin E that are influential membrane constituents.

1.1 Cell membranes

The existence of cell membranes became accepted in the early 20 th century [8]. In 1925, the basic structure of cell membranes was revealed by Gorter and Grendel with a famous experiment [9]. They compared the surface area of the plasma membrane measured microscopically from mammalian erythrocytes with the area measured by spreading it out

as a lipid monolayer at an air/saline interface. The ratio between these two areas is approximately 1:2, so that the hypothesis of the bilayer structure of plasma membrane was established. Based on the lipid bilayer model, the fluid mosaic model was subsequently proposed [10] to further explain the organization and structure of plasma membranes in the 1960-1970s. In this model, the lipid molecules tend to form bilayer structure in water solution driven by their amphiphilic properties. By this we mean their hydrophobic tails are embedded in the center of the bilayer avoiding contact with water and their hydrophilic head groups are exposed at the aqueous interface interacting with water. Membrane proteins are bound to the bilayer. The proteins, lipid molecules and a small amount of carbohydrates together form a two dimensional fluid matrix that comprises the plasma membrane. The fluidity of the membrane is provided by the lipid molecules. Membrane proteins diffuse laterally within the bilayer (Fig. 1.1a).

More recently, the fluid mosaic model has been revised. Different types of lipids in the plasma membrane are no longer thought to be homogenously distributed. Patches of lipids called lipid domains are formed in the membrane that are different from the "average" lipids in composition and physical properties. Lipid domains were first identified in model membranes by Jain and White in 1977 [11], and then further confirmed by Karnovsky in 1982 [12]. Now, the concept of inhomogeneous distribution of lipids in the plasma membrane is well accepted. Some membrane proteins have their conformation sensitive to the lipid local environment, so that the specific local environment provided by the lipid domains is essential for resident proteins to perform their functions [13] (Fig. 1.1b).

1.2 Lipids

Lipids constitute the fundamental structural component of plasma membrane. The major types of lipid molecule in animal plasma membrane are the phospholipids, sphingolipids and cholesterol.

1.2.1 Phospholipids

The chemical structure of 1-stearoyl-2-oleoyl phosphatidylcholine (18:0-18:1 PC), a typical phospholipid, is shown in Fig. 1.2a. It is composed of a hydrophilic head group and

two hydrophobic fatty acyl (FA) chains, all attached to a glycerol backbone. With different combinations of various head groups and FA chains, there are many kinds of phospholipid. The head group is attached at the sn-3 position of the glycerol back bone. The most common type of phospholipid found in animal plasma membranes is phosphatidylcholine (PC) with a phosphorylcholine head group. Phosphatidylethanolamine (PE) with a phosphorylethanolamine head group, and phosphatidylserine (PS) with a phosphorylserine head group are other examples [14].

The hydrocarbon FA chains have an even number of carbons and are ester-linked at the sn-1 and sn-2 positions of the glycerol back bone. The length of FA chains typically varies from 14 to 22 carbons, and the number of C=C bonds varies from 1 to 6. In the plasma membrane, the sn-1 chain is usually saturated (no double bonds) while the sn-2 chain is unsaturated (Fig. 1.2a). Less common PUFA are also typically incorporated at the sn-2 position (Fig. 1.2b), although in some extreme cases they are found at both positions [15]. Stearic acid (SA 18:0) with 18 carbons is one of the most common saturated long FA attached at sn-1 position of phospholipids. Oleic acid (OA 18:1) with 18 carbons and 1 double bond is the most common unsaturated FA chain attached at the sn-2 position.

Both the types of head groups and FA chains determine the behavior/dynamic properties of a phospholipid in the membrane, which affect the physical property of the corresponding membrane lipid environment. In our studies we mostly focused on how FA chains affect the physical properties of model membranes.

1.2.2 Sphingolipids

Sphingomyelin (SM) is the main type of sphingolipid in plasma membranes. Its chemical structure contains three parts: a sphingosine backbone, a FA chain and a phosphocholine head group (Fig. 1.2c). The sphingosine backbone has a “sn-1 like” saturated chain with a trans C=C bond near the top, and is esterified to a phosphocholine group and amide-linked to a “sn-2 like” FA chain. The “sn-2 like” FA chain is usually saturated, which is different from the common phospholipids. SM has greater affinity to cholesterol compared to bulk lipids. The planar structure of cholesterol (will be discussed later) results in strong van der Waals interaction with the long linear saturated FA chains on SM, and there is hydrogen bonding between the hydroxyl group on the sterol and the amide group on the sphingosine

backbone [16]. This association between SM and cholesterol is responsible for the formation of lipid raft domains that are enriched with SM and cholesterol. Raft domains have different physical properties from the bulk lipids region, serving as the platform for signaling proteins [17].

1.2.3 Cholesterol

Cholesterol is the major type of sterol lipid in animal plasma membranes. It can make up as much as 50 mol% of total lipid in some cases [18]. The chemical structure of cholesterol molecule is shown in Fig 1.3a. The main structural component is a rigid tetracyclic moiety with a short branched chain at one end. A hydroxyl group at the other end of the sterol ring provides the amphiphilic feature for the molecule. Inside a membrane the hydroxyl group is usually located near the aqueous interface, while the long molecular axis of the molecule lies almost parallel to the membrane normal and extends towards the middle of the membrane. The planar structure of the sterol ring is asymmetric due to the two methyl substituents at the C10 and C13 position that stick out on one side. In this case we call the smooth side the α face, and the other (bumpy) side is called the β face. Cholesterol plays an important role in modulating membrane physical properties and lipid domain formation [19, 20]. By restricting the motion of neighboring FA chains, cholesterol increases membrane order and so stiffens the membrane. It is considered to be essential for function [21].

1.3 Model membranes

1.3.1 Single component model membrane

Model membranes are lipid bilayers prepared with controlled lipid content [6]. Their study can help elucidate the structure and organization of regions lipid bilayer that exist in certain region of real plasma membranes. The bilayers are hydrated, so that the lipid polar head groups are confined at the aqueous interface and the FA chains comprise the hydrophobic interior. Model membranes composed of a single phospholipid have different phases at different temperatures [22]. Under physiological temperature, a liquid-crystalline phase in which the FA chains are melted and undergo a lot of motion is usually adopted. The

dynamic properties of the FA chains are responsible for a range of physical features of phospholipid membranes, such as mechanical properties [23], phase behaviors [24, 25] and lipid domain formation. These features work collectively to influence the biological function of the plasma membrane.

There are many experimental methods used to explore the dynamic properties of FA chains in model membranes. NMR spectroscopies, in particular, have been successfully applied. They are non-destructive, and directly measure the dynamic properties of the associated atoms/molecule moieties on different time scales. Among them, solid state ^{2}H NMR is frequently used to investigate the molecular organization of the FA chains in hydrated model membrane samples [26]. This method measures the degree of anisotropy, quantified in terms of an order parameter (S_{CD}), of the motion of lipid chain segments in which hydrogen is replaced by deuterium. The profile of S_{CD} along a lipid chain is an important indicator of lipid structural and dynamical characteristics, and is correlated with other properties like hydrocarbon thickness, membrane rigidity and area expansion modulus, elastic properties (compressibility) and phase transition properties [27]. The definition of S_{CD} is

$$S_{CD} = \frac{1}{2}\langle 3cos^2\beta - 1\rangle \qquad (1.1)$$

where β is the angle between the carbon-deuterium bond and membrane normal, and the angular bracket refers to a time average. It is a function of carbon position along a FA chain, usually falling between 0-0.5 in magnitude since in most cases $\beta = 90^\circ$ is the most probable orientation. The lower value is associated with greater isotropic motion (most disorder), while the upper value is associated with a lipid chain undergoing axial rotation in all-trans conformation (most order). However, there exist some situations, such as the carbon position on the cis double bond in in an oleic acid (18:1) chain where $\beta = 90^\circ$ is not most probable, in which case S_{CD} is also involves a geometrical factor.

The profile of S_{CD} along the perdeuterated sn-1 chain in [$^2H_{35}$] stearoyl-2-oleoyl phosphatidylcholine (SOPC-d_{35}) is shown in Figure 1.3a. Its shape is typical of membranes in the liquid crystalline state. The S_{CD} values were calculated from the quadrupole splitting of peaks assigned to deuterium atoms. The profile starts with a plateau region of slowly decreasing order parameters in the upper portion of the chain (C2-C9), and then order

decreases progressively move quickly in the lower portion (C10-C18). It reflected that the motion of the top part of the chain is restricted, mainly staying parallel to the membrane normal while undergoing fast axial rotation. In the bottom half of the chain towards the center of bilayer, the motion becomes less restricted and there is an increase in the probability of gauche segments. Ultimately, the methyl group at the end of the chain moves almost isotropically and has a very low S_{CD}.

Order parameter profiles derived from MD simulation reproduce the experimental data. The profile shown for SOPC (Figure 1.4b) follows the same trend as the one from NMR (Figure 1.3a) except at the top region (C2-C9). This is because the S_{CD} values from the MD simulations are calculated explicitly from each carbon position, so the profile contains detail missed in the smoothed profile from NMR that assumes order varies monotonically with position. In practice, ^{2}H NMR S_{CD} profiles are often used to validate MD simulations.

1.3.2 Cholesterol's effect on model membrane

Cholesterol restricts the reorientation of phospholipid chains in liquid-crystalline phase. The profile obtained in MD simulations of S_{CD} along the sn-1 chain in SOPC in the presence of 20 mol% cholesterol is an example of this ordering effect (Figure 1.4b). There is an increase of 40% in the average order. The increase in S_{CD} is greater in the upper portion of the chain, which reflects the constraints imposed by the rigid steroid moiety that sits approximately parallel to the bilayer normal with its hydroxyl group near the aqueous interface. A higher cholesterol content (> 30 mol%), a liquid ordered phase (lo) is formed in which the chains are largely extended in all–trans conformation and undergo fast axial rotation.

1.3.3 Mixtures of lipids – lipid domains

Mixtures of saturated phospholipid, unsaturated phospholipid and cholesterol crudely mimic the lipid composition of biological membranes. They trend to separate into domains that are enriched in saturated phospholipid but depleted in cholesterol. These domains are believed to form in real membranes and provide the environment to support the function of resident proteins.

The lipid raft is the lipid domain that has been most studied [28]. It is a liquid ordered (lo) region ranging from 10-200 nm in size, that is enriched in cholesterol and saturated sphingomyelin. The rigid steroid moiety on the cholesterol stiffens the long saturated chains on sphingomyelin, causing the raft to be more ordered, thicker and less fluid compared with the surrounding bulk lipid region that is more unsaturated. Signaling proteins that are anchored in lipid rafts are purported to become functional when lipid rafts cluster together [29]. Thus the dynamics, size and stabilization of lipid rafts is a topic that receives a lot of attention.

1.4 PUFA

1.4.1 Molecular structure

PUFA contain multiple (≥3) double bonds in a repeating =C-C-C= unit (Fig. 1.3c). They cannot be synthesized in mammals, but are required to maintain health. Designated according to the position of the final double bond relative to the terminal methyl, there are 2 categories: omega-3 and omega-6. The former means the last double bond is at the 3rd carbon from the omega terminal methyl end of the chain, while omega-6 means that the last double bond is at the 6th carbon from the end. Numerous health benefits are associated with dietary consumption of n-3 PUFA found in fish oils [30]. The mechanism remains unclear and is the subject of ongoing investigation. Incorporation of n-3 PUFA into membrane phospholipids, which then modulate molecular organization and, as a result, protein activity is one possibility [31].

1.4.2 Membrane properties

Unlike saturated FA, PUFA are highly disordered. There is a shallow energy barrier for the dihedral rotation of C-C bonds next to the C=C bond, which produces a chain that is highly flexible. It can explore its whole conformational space within 50 ns by rapid isomerization [32]. Compared to more common saturated and mono-unsaturated chains, PUFA chains are able to adopt bent conformations that even have their lower portion moving up close to the aqueous interface [33, 34]. When incorporated into phospholipid, usually at the sn-2 position, they alternate some basic physical properties of the bilayer. Compared to less

unsaturated FA-containing phospholipid bilayers, PUFA containing phospholipid bilayers have low lipid order, larger area per lipid, thinner membrane thickness, greater water permeability, and more fluidity.

PUFA chains have poor affinity for cholesterol. Their rapid changes in conformation are unfavorable for close contact with the rigid steroid moiety of cholesterol. NMR and X-ray studies show a lower solubility for cholesterol in polyunsaturated phospholipid membrane, and binding coefficients measured for cholesterol are reduced in polyunsaturated bilayers [35]. MD simulations indicate cholesterol prefers the saturated (stearoyl, 18:0) sn-1 chain over the polyunsaturated (docosahexaenoyl, 22:6) sn-2 chain in a mixed chain PC [36].

The high disorder of PUFA and their aversion for cholesterol have given rise to the hypothesis that modulation of the architecture of the plasma membrane may, in part, explain the biological function of PUFA. One model has domains forming that are enriched in PUFA-containing phospholipids but depleted in the sterol [37]. A cartoon illustrating this model is shown in Figure 1.4. It is based upon the results of a series of experiments on docosahexaenoic acid (DHA, 22:6)-containing PE [38-40]. The basic idea is that the PUFA enriched domain provide a platform for suitable proteins that require a disordered environment to function [37]. However, other models that suggest PUFA target lipid rafts – modifying their molecular architecture - have also been proposed. The matter, thus, is still under debate.

1.4.3 Vitamin E

Alpha tocopherol (αtoc) is the biologically active form of vitamin E that is retained in the human body. It is the major lipid soluble, chain-breaking anti-oxidant that protects polyunsaturated phospholipids from oxidation by terminating a chemical chain reaction by which oxidation propagates [41, 42]. The chemical structure of αtoc is shown in Fig. 1.3b. Similar to cholesterol, αtoc's major structural components are a rigid head group with a polar hydroxyl group at one end and a hydrophobic chain at the other end. The difference is that the chromanol head group on αtoc is smaller than the steroid moiety on cholesterol, and the phytyl side (16 carbons) chain on αtoc is longer than the branched chain (5 carbons) on the sterol. The hydroxyl on the chromanol group is responsible for αtoc's anti-oxidant

function. It needs to come into close contact with a lipid peroxyl radical to scavenge it before it attacks another lipid.

1.5 Aims of research

1.5.1 Interaction of α-tocopherol with a polyunsaturated phospholipid

In conventional all-atom MD simulations and umbrella sampling MD simulations, we investigated the molecular organization and binding of αtoc in model membranes composed of a PUFA-containing lipid. We compared the interaction of αtoc with 1-steroyl-2-docosahexaenoyl phosphatidylcholine (SDPC) and 1-stearoly-2-oleoyl phosphatidylcholine (SOPC). SDPC is polyunsaturated while SOPC is a monounsaturated control.

While the chemistry of how αtoc works as an antioxidant has been extensively studied [43], the role its molecular structure plays is unclear. Whether it preferentially interacts with PUFA-containing phospholipids that are most susceptible to oxidation remains unanswered. This question is addressed in Chapter 3 and 4. Chapter 3 presents the results from all-atom MD simulations of the molecular organization of αtoc in an SDPC bilayer. In Chapter 4 the binding of αtoc to SDPC is measured by umbrella sampling MD simulations.

1.5.2 EPA vs DHA vs DPA

DHA has most often been studied as representative of n-3 PUFAs. In fact, EPA (20:5) and DPA (22:5) are also long-chain n-3 PUFAs found in fish oils that appear in the diet and are taken up into membrane phospholipids [44]. These three n-3 PUFAs have similar chemical structures with slightly varying unsaturation and chain length (Fig. 1.3c). It is not clear if they differ in their effects [44, 45]. In Chapter 5 all-atom MD simulations of membranes comparing these three PUFAs and their interaction with cholesterol are reported.

1.6 References

[1] B. Alberts, A. Johnson, J. Lewis, M. Raff, K. Roberts and P. Walter, Molecular Biology of the Cell, New York: Garland Science, 2002.

[2] W. Cho and R. V. Stahelin, "Membrane-protein interactions in cell signaling and membrane trafficking," *Annu. Rev. Biophys. Biomol. Struct.,* vol. 34, pp. 119-151, 2005.

[3] B. Alberts, A. Johnson, J. Lewis, M. Raff, K. Roberts and P. Walter, Transport into the cell from the plasma membrane: endocytosis., 2002.

[4] H. Lodish, B. A., S. L. Zipursky and e. al., Molecular Cell Biology. 4th edition, New York: W. H. Freeman, 2000.

[5] G. Lenaz, "Lipid fluidity and membrane protein dynamics," *Bioscience reports,* vol. 7, no. 11, pp. 823-837, 1987.

[6] Y. H. M. Chan and S. G. Boxer, "Model membrane systems and their applications," *Current opinion in chemical biology,* vol. 11, no. 6, pp. 581-587, 2007.

[7] S. R. Shaikh, J. J. Kinnun, X. Leng, J. A. Williams and S. R. Wassall, "How polyunsaturated fatty acids modify molecular organization in membranes: insight from NMR studies of model systems," *Biochimica et Biophysica Acta (BBA)-Biomembranes,* vol. 1848, no. 1, pp. 211-219, 2015.

[8] J. Lombard, " Once upon a time the cell membranes: 175 years of cell boundary research," *Biology direct,* vol. 9, p. 1, 2014.

[9] G. E and G. F., "On bimolecular layers of lipoids on the chromocytes of the blood," *The Journal of experimental medicine,* vol. 41, no. 4, pp. 439-443, 1925.

[10] S. S. J and N. G. L, "The fluid mosaic model of the structure of cell membranes," *Membranes and Viruses in Immunopathology; Day, SB, Good, RA, Eds,* pp. 7-47, 1972.

[11] M. K. Jain and H. 3. White, "Long-range order in biomembranes," *Adv. Lipid Res,* vol. 15, no. 1, 1977.

[12] M. J. Karnovsky, A. M. Kleinfeld, R. L. Hoover and R. D. Klausner, "The concept of lipid domains in membranes," *The Journal of cell biology,* vol. 94, no. 1, pp. 1-6, 1982.

[13] K. Simons and D. Toomre, "Lipid rafts and signal transduction," *Nature reviews Molecular cell biology,* vol. 1, no. 1, pp. 31-39, 2000.

[14] G. van Meer, D. R. Voelker and G. W. Feigenson, "Membrane lipids: where they are and how they behave," *Nature reviews Molecular cell biology,* vol. 9, pp. 112-124, 2008.

[15] M. I. Aveldano, "Dipolyunsaturated species of retina phospholipids and," *Biomembranes and Nutrition,* vol. 195, pp. 87-96, 1989.

[16] R. E. Brown, "Sphingolipid organization in biomembranes: what physical studies of model membranes reveal," *Journal of cell science,* vol. 111, no. 1, pp. 1-9, 1998.

[17] P. C. Calder and P. Yaqoob, "Lipid rafts—composition, characterization, and controversies," *The Journal of nutrition,* vol. 137, no. 3, pp. 545-547, 2007.

[18] T. Róg, M. Pasenkiewicz-Gierula, I. Vattulainen and M. Karttunen, "Ordering effects of cholesterol and its analogues," *Biochimica et Biophysica Acta (BBA)-Biomembranes,* vol. 1788, no. 1, pp. 97-121, 2009.

[19] K. Simons and R. Ehehalt, "Cholesterol, lipid rafts, and disease," *The Journal of clinical investigation,* vol. 110, no. 5, pp. 597-603, 2002.

[20] J. R. Silvius, "Role of cholesterol in lipid raft formation: lessons from lipid model systems," *Biochimica et Biophysica Acta (BBA)-Biomembranes,* vol. 1610, no. 2, pp. 174-183, 2003.

[21] H. Martinez-Seara, T. Róg, M. Karttunen, I. Vattulainen and R. Reigada, "Cholesterol induces specific spatial and orientational order in cholesterol/phospholipid membranes," *PloS one,* vol. 5, no. 6, p. e11162, 2010.

[22] G. Cevc, "How membrane chain-melting phase-transition temperature is affected by the lipid chain asymmetry and degree of unsaturation: an effective chain-length model," *Biochemistry,* vol. 30, no. 29, pp. 7186-7193, 1991.

[23] S. Ollila, M. T. Hyvönen and I. Vattulainen, "Polyunsaturation in lipid membranes: dynamic properties and lateral pressure profiles," *The Journal of Physical Chemistry B,* vol. 111, no. 12, pp. 3139-3150, 2007.

[24] M. R. Morrow, J. P. Whitehead and D. Lu, "Chain-length dependence of lipid bilayer properties near the liquid crystal to gel phase transition," *Biophysical journal,* vol. 63, no. 1, pp. 18-27, 1992.

[25] L. L. Holte, S. A. Peter, T. M. Sinnwell and K. Gawrisch, "2H nuclear magnetic resonance order parameter profiles suggest a change of molecular shape for phosphatidylcholines containing a polyunsaturated acyl chain," *Biophysical journal,* vol. 68, no. 6, pp. 2396-2403, 1995.

[26] A. Seelig and J. Seelig, "Dynamic structure of fatty acyl chains in a phospholipid bilayer measured by deuterium magnetic resonance," *Biochemistry,* vol. 13, no. 23, pp. 4839-4845, 1974.

[27] L. S. Vermeer, B. L. De Groot, V. Réat, A. Milon and J. Czaplicki, "Acyl chain order parameter profiles in phospholipid bilayers: computation from molecular dynamics simulations and comparison with 2H NMR experiments," *European Biophysics Journal,* vol. 36, no. 8, pp. 919-931, 2007.

[28] D. Lingwood and K. Simons, "Lipid rafts as a membrane-organizing principle," *Science,* vol. 327, no. 5961, pp. 46-50, 2010.

[29] J. Fantini, N. Garmy, R. Mahfoud and N. Yahi, " Lipid rafts: structure, function and role in HIV, Alzheimers and prion diseases," *Expert reviews in molecular medicine,* vol. 2, no. 1, pp. 1-22, 2002.

[30] W. Stillwell, "Docosahexaenoic acid: a most unusual fatty acid," *Chem. Phys. Lipids,* vol. 153, pp. 1-2.

[31] S. R. Wassal and W. Stillwell, "Polyunsaturated fatty acid–cholesterol interactions: Domain formation in membranes," *Biochimica et Biophysica Acta,* vol. 1788, pp. 24-32, 2008.

[32] O. Soubias and K. Gawrisch, "Docosahexaenoyl chains isomerize on the sub-nanosecond time scale," *Journal of the American Chemical Society,* vol. 129, no. 21, pp. 6678-6679, 2007.

[33] L. Saiz and M. L. Klein, "Structural properties of a highly polyunsaturated lipid bilayer from molecular dynamics simulations," *Biophysical journal,* vol. 81, no. 1, pp. 204-216, 2001.

[34] S. E. Feller, K. Gawrisch and A. D. MacKerell, "Polyunsaturated Fatty Acids in Lipid Bilayers: Intrinsic and Environmental Contributions to Their Unique Physical Properties," *Journal of the American Chemical Society,* vol. 124, no. 2, pp. 318-326, 2002.

[35] S. R. Shaikh, V. Cherezov, M. Caffrey, S. P. Soni, D. LoCascio, W. Stillwell and S. R. Wassall, "Molecular organization of cholesterol in unsaturated phosphatidylethanolamines: X-ray diffraction and solid state 2H NMR reveal differences with phosphatidyl- cholines," *Journal of the American Chemical Society,* vol. 128, no. 16, pp. 5375-5383, 2006.

[36] M. C. Pitman, F. Suits, A. D. MacKerell and S. E. Feller, "Molecular-level organization of saturated and polyunsaturated fatty acids in a phosphatidylcholine bilayer containing cholesterol," *Biochemistry,* vol. 43, no. 49, pp. 15318-15328, 2004.

[37] S. R. Wassall and W. Stillwell, "Polyunsaturated fatty acid–cholesterol interactions: domain formation in membranes," *Biochimica et Biophysica Acta (BBA)-Biomembranes,* vol. 1788, no. 1, pp. 24-32, 2009.

[38] A. Polozova and B. J. Litman, "Cholesterol dependent recruitment of di22: 6-PC by a G protein-coupled receptor into lateral domains," *Biophysical journal,* vol. 79, no. 5, pp. 2632-2643, 2000.

[39] S. R. Shaikh, A. C. Dumaual, A. Castillo, D. LoCascio, R. A. Siddiqui, W. Stillwell and S. R. & Wassall, "Oleic and docosahexaenoic acid differentially phase separate from lipid raft molecules: a comparative NMR, DSC, AFM, and detergent extraction study," *Biophysical journal,* vol. 87, no. 3, pp. 1752-1766, 2004.

[40] S. P. Soni, D. S. LoCascio, Y. Liu, J. A. Williams, R. Bittman, W. Stillwell and S. R. Wassall, "Docosahexaenoic acid enhances segregation of lipids between raft and non-raft domains: 2H NMR study," *Biophysical journal,* vol. 95, no. 1, pp. 203-214, 2008.

[41] G. W. Burton and K. U. Ingold, "Vitamin E: application of the principles of physical organic chemistry to the exploration of its structure and function," *Accounts of chemical research,* vol. 19, no. 7, pp. 194-201, 1986.

[42] M. Alessi, T. Paul, J. Scaiano and K. Ingold., "The contrasting kinetics of peroxidation of vitamin E-containing phospholipid unilamellar vesicles and human low-density lipoprotein," *Journal of the American Chemical Society,* vol. 124, no. 24, pp. 6957-6965, 2002.

[43] G. W. Burton and K. U. Ingold, "Vitamin E as an in Vitro and in Vivo Antioxidanta," *Annals of the New York Academy of Sciences,* vol. 570, no. 1, pp. 7-22, 1989.

[44] D. Mozaffarian and J. H. Wu, "(n-3) fatty acids and cardiovascular health: are effects of EPA and DHA shared or complementary?," *The Journal of nutrition,* vol. 142, no. 3, pp. 614S-625S, 2012.

[45] S. C. Dyall, "Long-chain omega-3 fatty acids and the brain: a review of the independent and shared effects of EPA, DPA and DHA," *Frontiers in aging neuroscience,* vol. 7, no. 52, 2015.

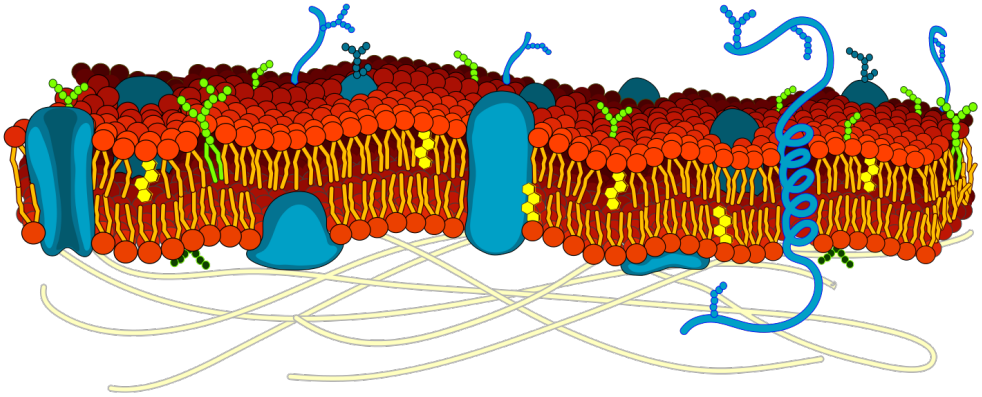

a)

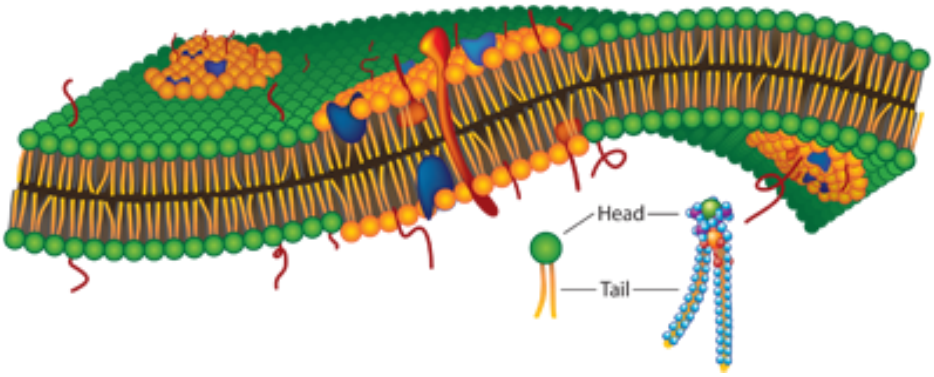

b)

Figure 1.1

a) The fluid mosaic model of plasma membrane. Phospholipids (red head group and yellow chains), carbohydrate (green) and cholesterol (yellow rigid sterol) form the bilayer. Proteins (blue) inserted or embedded in the fluid bilayer. (https://upload.wikimedia.org/wikipedia/commons/d/da/Cell_membrane_detailed_diagram_en.svg)

b) Lipid raft hypothesis. Raft domain (orange head group) associated with raft proteins are floating in a sea of bulk lipids (green head group). (http://molmod.ugent.be/subject/modeling-oxygen-diffusion-through-biological-lipid-membranes-using-inverse-monte-carlo)

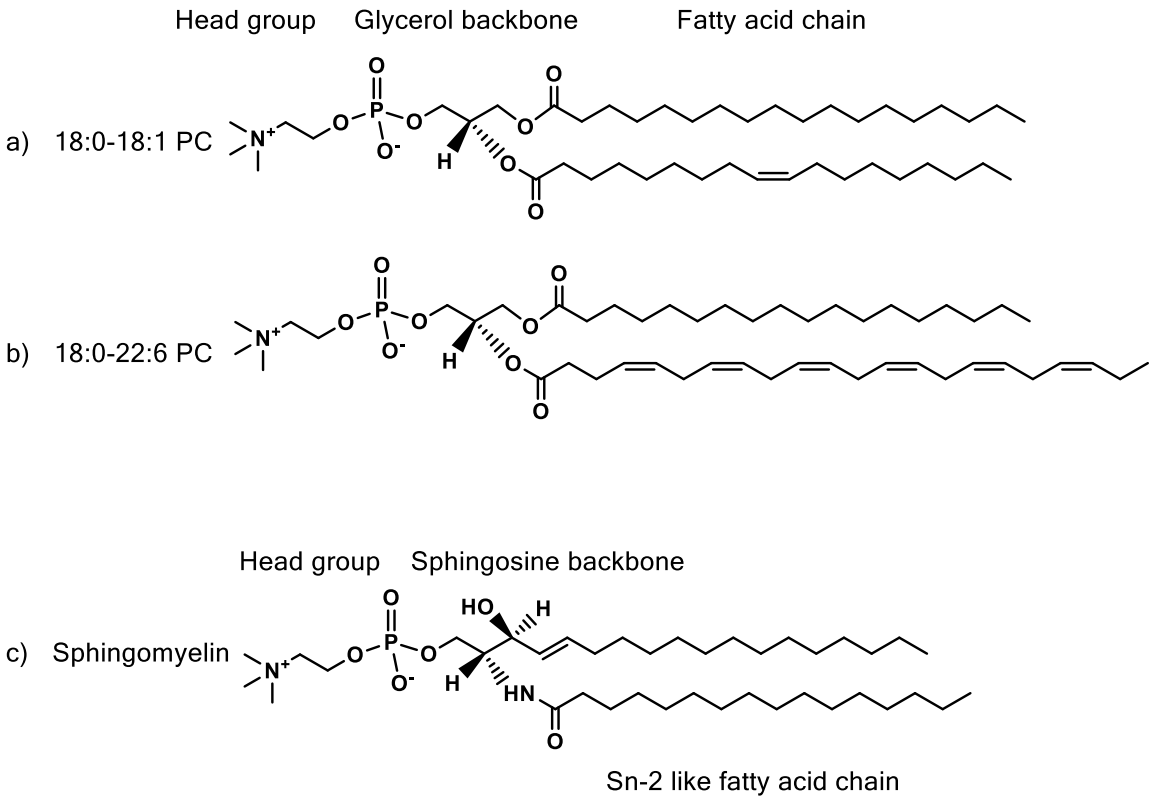

Figure 1.2

Chemical structures of different lipids

a) Phosphatidylcholine with 1- stearic (18:0 saturated) 2-oleic (18:1 unsaturated) chain.

b) Phosphatidylcholine with 1- stearic (18:0 saturated) 2-docosahexanoic (22:6 polyunsaturated) chain.

c) Sphingosylphosphorylcholine with N-palmitoyl (16:0) D-erythro (18:1 trans unsatruated) chain.

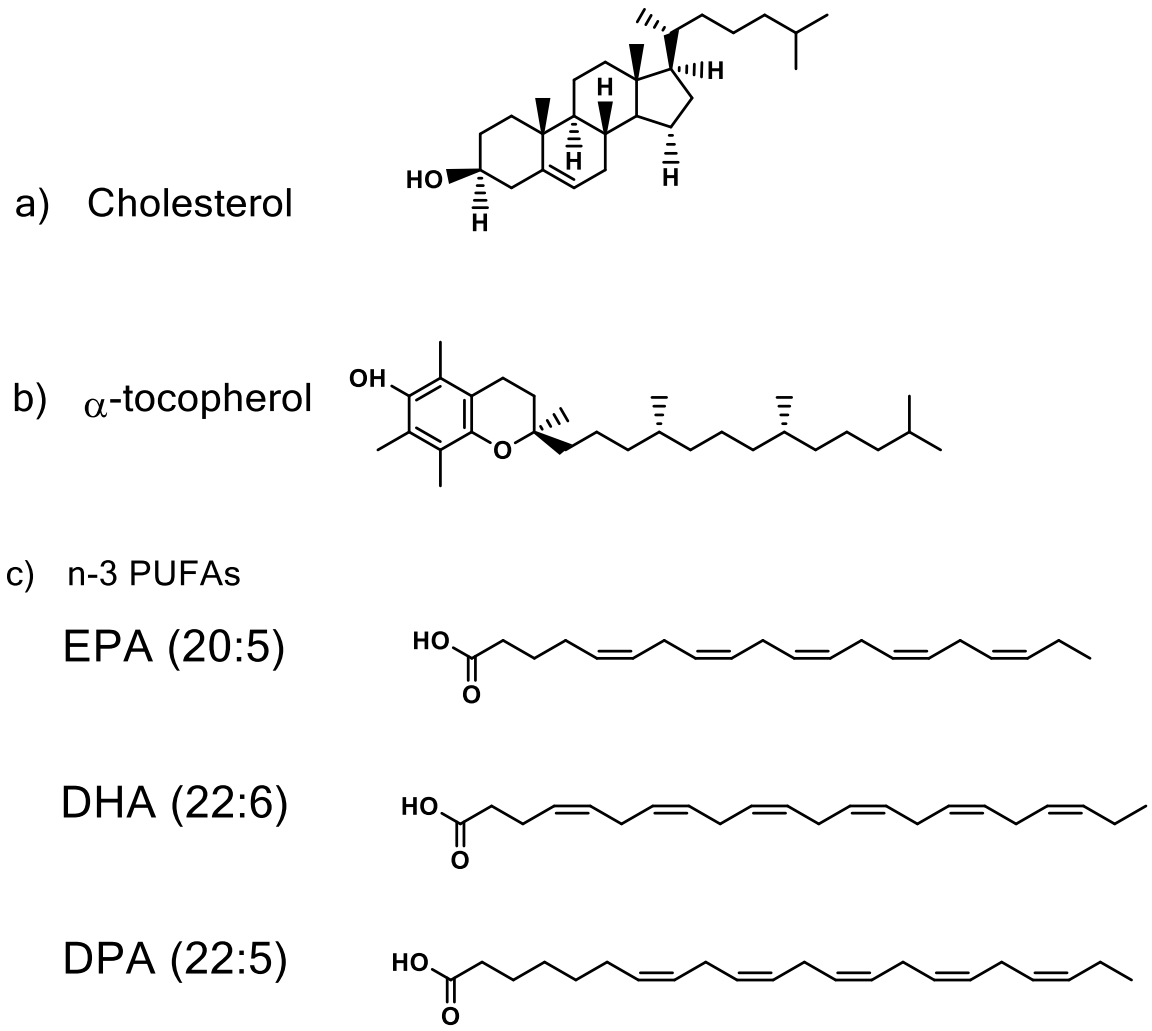

Figure 1.3

Chemical structures of a) Cholesterol. b) α-tochopherol (Vitamin E). c) Three types of n-3 Polyunsaturated fatty acids (PUFAs).

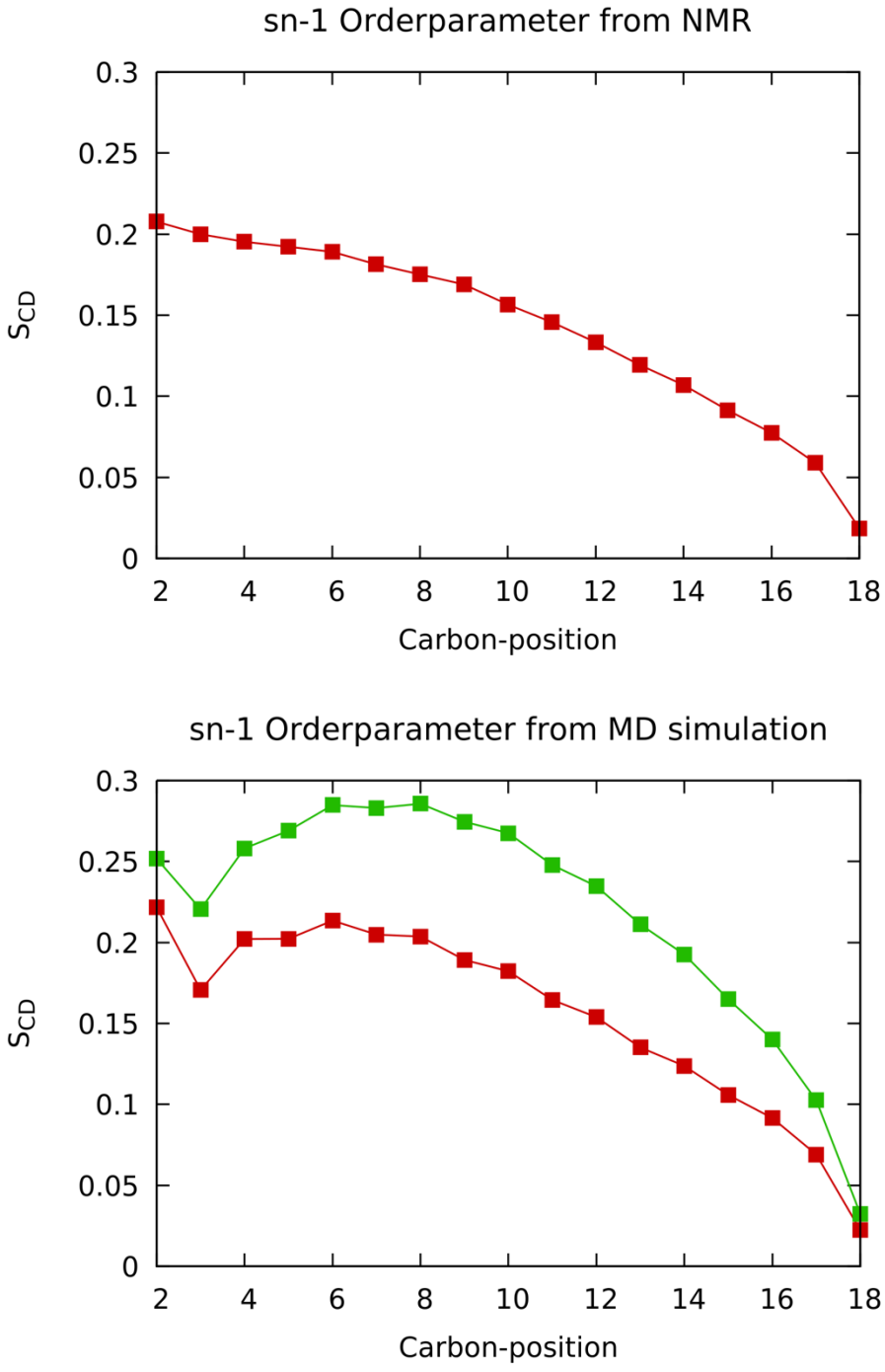

Figure 1.4

Sn-1 chain Order parameter (S_{CD}) profile of SOPC. a) S_{CD} of d-35 SOPC sample at 37°C from ^{2}H NMR experiment. b) S_{CD} of SOPC from NPT MD simulation at 37°C, 1 atm. red: Pure SOPC bilayer sample. Green: 80 mol% SOPC + 20 mol% cholesterol.

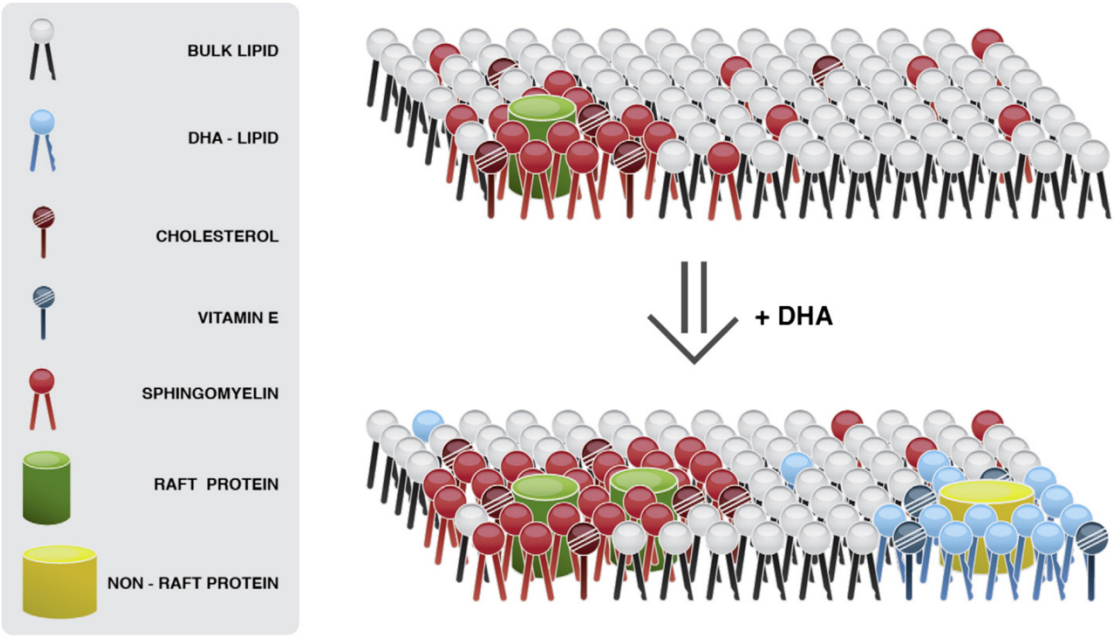

Figure 1.5

A cartoon illustration of the model of domain formation enhanced by the depletion of cholesterol from PUFA containing lipids. On the upper panel is the raft protein siting in a lipid raft domain enriched with cholesterol and sphingomyelin. With the addition of PUFA (DHA) incorporated lipid, the cholesterols are further excluded from these PUFA lipids which co-localized into the "non-raft" domain. Thus the size and stability of lipid raft is enhanced. At the meantime, non-raft protein are also sitting in the PUFA enriched non-raft domain.

Acknowledgement

Figure1.5 is reprinted from Biochimica et Biophysica Acta (BBA)-Biomembranes, 1788(1), Wassall, S. R., & Stillwell, W., Polyunsaturated fatty acid–cholesterol interactions: domain formation in membranes, 24-32, copyright (2008), with permission from Elsevier.

CHAPTER 2. MD SIMULATION

Molecular dynamics (MD) simulation is a powerful tool to study biological systems on the molecular level. It was first introduced in protein folding research [1]. Then as computing power grew exponentially over the past few decades, MD simulations have been applied widely to a lot of molecular biological systems, including model membranes [2]. There are several types of MD simulations suitable for biological system on different scales of size and time, such as all-atom MD and coarse-grained MD. In our research on model membranes we chose to use all-atom MD simulations with explicit solution. They are able to give us a detailed description of how changes in the structure of phospholipid molecules affect molecular organization in a bilayer, although are limited on the scale of the simulation size and time.

2.1 Standard atomistic simulation

The starting point for simulations is to build the lipid bilayer at the atomic level. CHARMM GUI was used [3]. The initial structures for each lipid molecule are randomly selected from a corresponding lipid structural library [4], and the lateral location of each lipid molecule is randomized in the leaflet. Water molecules are also explicitly modeled (Figure 2.1). Then a summation (integral) of all the pairwise interactions for each atom in the system is performed to calculate the force acting on it. The interactions are calculated from a set of potential functions ("force field") that we will discuss later. Once the force and acceleration for each atom at each time step can be calculated, Newton's second law can be applied to generate the motion of atoms and to obtain their trajectories.

In practice, the velocity Verlet integration method [5] is applied. This method works as follows. Suppose that at time frame n, the position of an atom is $\overrightarrow{r_n}$. The acceleration $\overrightarrow{a_n}$ is

$$\vec{a}_n = \frac{\Delta^2 \vec{r}_n}{\Delta t^2} = \frac{\frac{\overrightarrow{r_{n+1}} - \vec{r}_n}{\Delta t} - \frac{\vec{r}_n - \overrightarrow{r_{n-1}}}{\Delta t}}{\Delta t} = \frac{\overrightarrow{r_{n+1}} - 2\vec{r}_n + \overrightarrow{r_{n-1}}}{\Delta t^2} \tag{2.1}$$

so that the position of the atom for next step is

$$\overrightarrow{r_{n+1}} = 2\vec{r_n} - \overrightarrow{r_{n-1}} + \vec{a_n}\Delta t^2 \tag{2.2}$$

and the acceleration of that atom is given by the force acting on it through Newton's second law

$$\vec{a_n} = -\vec{\nabla} U_{total} \tag{2.3}$$

The U_{total} for an atom at frame n is a summation of the pairwise interaction potential energies accounting for the atoms in the rest of the system. The interaction potential energy function is the "force field" that we mentioned earlier. In all our simulations, we have used the standard CHARMM C36 force [6] and its C36p modification for polyunsaturated fatty acids [7].

The potential energy function of the force field is generally considered in 2 parts:

$$U_{total} = U_{bond} + U_{non-bond} \tag{2.4}$$

where U_{bond} stands for the bonded interaction energy, and $U_{non-bond}$ for non-bonded interaction. In the CHARMM force field, U_{bond} takes the following form [8]

$$U_{bond} = \sum_{bonds} K_b(b - b_0)^2 + \sum_{angles} K_\theta(\theta - \theta_0)^2 + \sum_{dihedrals} K_\gamma[1 + \cos(n\gamma - \delta)] + \sum_{impropers} K_\varphi(\varphi - \varphi_0)^2 + \sum_{Urey-Bradly} K_{UB}(r_{1,3} - r_{1,3_0})^2 \tag{2.5}$$

Figure 2.2 illustrates each term. The 1st term describes the bond stretching energy. It is approximated by a harmonic potential energy function with a force constant K_b, where b is the bond length and b_0 is the equilibrium value. The 2nd term describes the contribution to the energy from the angle between adjacent bonds. It is also approximated by a harmonic potential energy function with a force constant K_θ, in this case, where θ is the angle between 2 adjacent bonds and θ_0 is the equilibrium value. The 3rd term, in which γ is the dihedral angle between the planes of atoms ABC and BCD, describes the constraint on rotation around bond BC. Because the rotation of a covalent bond usually has more than one equilibrium conformation, the dihedral potential energy is approximated by a cosine function. The number of minima in this energy function is represented by n and δ defines the location of the minima, while K_r is the force constant. The 4th term, which is called the improper dihedral angle potential, is applied to maintain the correct geometry of atoms. It is approximated by a harmonic potential function with a force constant K_φ, where angle φ

is defined as the improper angle between the planes of atoms ABC and BCD while φ_0 is the equilibrium value. The 5th term comprises an additional angular term that is called the Urey-Bradley potential. It is represented by a harmonic potential function in which K_{UB} is the force constant, and $r_{1,3}$ is the distance between atoms 1 and 3 on atom 2 in a triple of atoms and $r_{1,3o}$ is the equilibrium distance. The parameters in all of these energy functions were determined from empirical techniques and quantum mechanics calculation [6-8]. For MD simulations of lipid bilayers, the first three terms are the most important, while the last two terms are minor.

The non-bonded interactions are basically divided into 2 parts. The first term describes the electrostatic interaction energy and the second term represents the van der Waals interaction (vdW) energy:

$$U_{non-bond} = \sum_{ij} \frac{q_i q_j}{\varepsilon r_{ij}} + \sum_{ik} \varepsilon_{ij} \left[\left(\frac{R_{\min i,j}}{r_{ij}} \right)^{12} - 2 \left(\frac{R_{\min i,j}}{r_{ij}} \right)^{6} \right] \quad (2.6)$$

Here r_{ij} is the distance between the ith and jth atoms, and q_i and q_j are the respective charges on the ith and jth atoms. For atoms that are attached on covalent bonds, q_i and q_j are the partial charges that are assigned to them due to the separation of the positive and negative charge distribution on the covalent bond (Figure 2.3a). The dielectric constant ε is 1 in explicit solvent simulation. The vdW energy is approximated by the standard Lennard-Jones 6-12 potential, where the term ε_{ij} refers to the vdW energy at its minimum and $R_{\min i,j}$ is the equilibrium distance (where vdW energy is minimum) (Figure 2.3b). Only atom pairs with atoms that are separated by more than 3 covalent bones are included in calculating non-bonded interactions. To avoid the high computational cost associated with long-range non-bonded interaction, the vdW interaction and the short range electrostatic interactions are truncated by switching functions at a certain distance (10 Å). The long-range contribution to the electrostatic interactions was calculated using the particle-mesh Ewald method [9].

The size of our simulation cell is limited to a patch of membrane containing about 100 lipid molecules. In order to deal with the atoms and molecules that are near the edge of the cell, a periodic boundary condition was applied. The idea is to duplicate the system along each axis in all directions, so that the simulation system is surrounded by its images (Figure 2.4).

Whenever a molecule moves out of the boundary of the simulation box, the image of the molecule appears and moves in from the opposite side of the boundary. Also these images still contribute to the non-bounded interactions of the atoms in the original cell.

To make our simulation better represent the real situation, we chose to use the constant number of particles, constant pressure and constant temperature (NPT) type of simulation. The pressure and temperature were kept at 1 atm. and 310 K, respectively, to correspond with the physiological conditions. The extended system algorithm with Nose-Hoover thermostat and Langevin piston was applied for temperature and pressure control. With this method, the system is coupled with an external pressure piston and heat reservoir. Additional degrees of freedom representing the pressure piston and heat reservoir were added to the Hamiltonian. The volume of the system and velocity of the atoms are scaled to maintain the pressure and temperature. While the volume is changing, the x-y directions of the simulation cell change together while the z direction changes independently [10-13].

2.2 MD simulation on lipid membrane

All-atom MD simulation has been successfully applied in the study of model membranes over the past few decades. In that time, the simulations have progressed dramatically in size, duration and sophistication. The major force fields parameterized for lipid simulation are GROMOS and CHARMM. The GROMOS force field is used in the GROMACS simulation software. It applies united atom models that represent the non-polar parts (CH, CH_2 and CH_3) to reach a greater efficiency. The CHARMM force field is used in CHARMM and NAMD simulation software. It applies explicit all-atom model for the lipid molecules, and has a more detailed description on the inter and intra molecular interactions [14]. We chose to use the CHARMM force field in our work.

The original CHARMM lipid force field C22 was released in the early 1990's [15]. It successfully reproduced experimental data in constant particle number, normal pressure and temperature (NPAT) ensemble simulations. In a series of simulations done on a 1,2-dipalmitoyl-sn-glycero-3-phosphocholine (DPPC) bilayer, the simulated S_{CD} profile showed good agreement with experimental data from ^2H NMR at an area per lipid (62.9 $Å^2$) measured by X-ray scattering (Figure 2.5) [16]. Another simulation on 1,2-dioleoyl-

sn-phosphatidylcholine (DOPC) with 59.3 $Å^2$ for the area per lipid reproduced neutron and X-ray scattering density profiles [17]. Subsequent refinements of the force field (as C27 [18] and then C36 [19]) have improved the quality of simulations. Now good agreement with experiment is achieved in simulations run in NPT ensemble on patches of bilayer containing 100 or more lipid molecules for 200 ns or longer (Fig. 2.6). The C36 force field, for example, yields accurate head group areas for different types of lipid in NPT ensemble [19]. Simulations published for lipid-cholesterol systems are also able to reproduce experimental results [20, 21], as are the few reports of vitamin E in bilayers [22, 23] that qualitative agreed with experiments.

MD simulations can provide a detailed visualization of molecular ongoing action in a membrane that is unattainable in experiment. Their purpose is no namely to replicate experiment. They played a crucial role in the development of understanding polyunsaturated phospholipids. Quantum mechanical calculations performed on vinyl-methylene bonds revealed a low energy barrier for torsion [24]. The simulations then run on SDPC showed, as seen in experiment, low order parameters ($S_{CD} < 0.05$) throughout most of the DHA chain at the sn-2 position (Fig. 2.6). They established that high disorder, and not a geometry that produces a low order parameter, was responsible.

2.3 Umbrella sampling

Whether α-tocopherol (α-toc) preferentially interacts with PUFA-containing lipids is one of the topics that our research intends to test. Details of the motivation will be described later. Here we introduce the technique that was used to calculate the binding energy of α-toc to lipid bilayers using the potential of mean force (PMF). The PMF describes the free energy change of a system along a reaction coordinate. It can basically be expressed as a function of a reaction coordinate, which in the case of our system is chosen to be the distance z between the center of mass of the chromanol group in an α-toc molecule and the center of the membrane along the membrane normal direction [25]

$$G(z) = k_B T \ln P(z) \tag{2.7}$$

G(z) is the system free energy, or potential of mean force (PMF) along z, zeroed at arbitrary location. $P(z)$ is the probability density of the system as a function of its coordinate z with

all possible conformations. k_B is the Boltzmann constant and T is the temperature of the system. A schematic illustration of *G(z)* is shown as figure 2.6. The change in free energy (ΔG) of the system from $z = z_{eq}$ (where the chromanol group of α-toc is at the equilibrium depth) to z greater than the sum of mono-layer thickness plus the length of α-toc molecule (where the entire α-toc molecule is totally in water) should represent the free energy change in pulling the α-toc out from the lipid bilayer.

It is usually impossible to get the fully sampled $P(z)$ of a system in ordinary MD simulation because its time scale is too short. A poor sampling would especially happen when a free energy barrier exists along the z coordinate, which would mean the system takes a very long time to evolve across the barrier only by the thermal energy. A solution to the problem is to apply a series of constraints on the system along z to push the system through the energy barrier. This approach is called umbrella sampling [26]. In practice, the simulation is copied to multiple windows, and in each window there is a harmonic constraint on z centered at different z values. The constraint $W_i(z)$ in window i is called the bias potential

$$W_i(z) = K(z - z_i)^2 \tag{2.8}$$

where z_i is the position of the center of the constraining potential in the i-th window. In our case, the distance between successive z_i is 1 Å, and there are 45 windows as z_i changes from 0 Å to 44 Å. The initial structures of the windows are prepared by a pulling simulation that uses an artificial force to pull α-toc from the center of bilayer to the water. When we get the trajectory from the pulling simulation, a snapshot of a conformation with its reaction coordinate z close to z_i is then selected to represent the initial conformation of each window. By dividing z into bins, we can obtain the probability distribution p_{il} of bin l in window i, under the bias potential W_i.

To calculate the unbiased probability distribution p_l, the Weighted Histogram Analysis Method (WHAM) is then applied as follows [27]. Suppose p_l is given, then the expected biased probability p_{il} in window i and bin l can be written as

$$p_{il} = f_i c_{il} p_l \tag{2.9}$$

where c_{il} is a bias factor that is determined by the bias potential in window i

$$c_{il} = \exp\ \frac{W_i(z_l)}{k_B T} \tag{2.10}$$

and f_i is used to keep the $\{p_{il}\}$ in window i summed up to 1.

$$f_i = \frac{1}{\sum_l c_{il} p_l} \tag{2.11}$$

According to the maximum likelihood theorem [27], we can minimize the quantity A

$$A = \left(-\sum_i^S N_i \ln f_i - \sum_l^M M_l \ln p_l\right) \tag{2.12}$$

to derive another equation for p_l

$$p_l = \frac{M_l}{\sum_i N_i f_i c_{il}} \tag{2.13}$$

Here S is the total number of windows, M is the total number of bins, N_i is the total number of counts in window i, and M_l is the total number of counts in bin l from all the windows. Equations (2.11) and (2.13) together form the traditional WHAM equations. Starting with an arbitrary set of $\{p_l\}$ and $\{f_i\}$, and iteratively substituting them into these equations, we can finally get a set of $\{p_l\}$ and $\{f_i\}$ that satisfy both equations so that the WHAM equations are solved. However, the above method can be slow in reaching convergence. In order to optimize calculating p_l, we use a variable substitution for f_i

$$g_i = \ln f_i$$

$$\Delta g_i = g_{i+1} - g_i$$

$$f_i = \exp\left(\sum_{j=1}^{i-1} \Delta g_i\right) \tag{2.14}$$

Substituting equation (2.14) into (2.12), we can get the $\hat{A}$ as a function of Δg_i

$$\hat{A}(\Delta g_1, \Delta g_2, \ldots \Delta g_{s-1}) = -\sum_{i=2}^{S} N_i \sum_{j=1}^{i-1} \Delta g_i - \sum_l M_l \ln\left(\frac{M_l}{\sum_i N_i c_{il} \exp\left(\sum_{j=1}^{i-1} \Delta g_i\right)}\right) \tag{2.15}$$

In practice, the $\hat{A}$ is minimized by the Broyden–Fletcher–Goldfarb–Shanno (BFGS) method. After that, the unbiased probability $\{p_l\}$ can be determined, and thus the potential of mean force at each bin l along z can be calculated from equation (2.7).

2.4 Applications of USMD simulation to lipid bilayers

Profiles of PMF with respect to depth within a membrane have been reported for a range of membrane constituents on the basis of USMD simulations [28]. Cholesterol is a

membrane constituent, somewhat similar in structure to αtoc that is a focus in this thesis, for which PMF profiles have been published. Illustrative examples of estimates of binding energy that were obtained are presented in Table 2.1. As seen in experiments, they show cholesterol has greater affinity for more ordered, saturated lipids such as raft-forming SM than more disordered, unsaturated phospholipids.

Just one PMF profile for vitamin E has been reported so far from USMD simulation [29]. The binding energy in 1,2-dipalmitoylphosphatidycholine (DPPC) that we estimate (by eyeball) from that PMF is approximately 18 kcal/mol.

2.5 References

[1] J. McCammon, B. Gelin and M. Karplus, "Dynamics of folded proteins," *Nature,* vol. 267, pp. 585-590, 1977.

[2] S. E. Feller, "Molecular dynamics simulations of lipid bilayers," *Current opinion in colloid & interface science,* vol. 5, no. 3, pp. 217-223, 2000.

[3] S. Jo, T. Kim, V. Iyer and W. Im, "CHARMM-GUI: A Web-based Graphical User Interface for CHARMM," *J. Comput. Chem,* vol. 29, pp. 1859-1865, 2008.

[4] S. Jo, J. Lim, J. Klauda and W. Im, "CHARMM-GUI Membrane Builder for Mixed Bilayers and Its Application to Yeast Membranes," *Biophys J.,* vol. 97, pp. 50-58, 2009.

[5] M. P. Allen and . J. Tildesley, Computer Simulation of Liquids, Oxford University Press, 1989.

[6] J. B. Klauda, R. M. Venable, J. A. Freites, J. W. O'Connor, D. J. Tobias, C. Mondragon-Ramirez, I. Vorobyov, A. D. M. Jr. and R. W. Pastor, "Update of the CHARMM All-Atom Additive Force Field for Lipids: Validation on Six Lipid Types," *J Phys Chem B,* vol. 114, pp. 7830-7843, 2010.

[7] J. B. Klauda, V. Monje, T. Kim and W. Im, "Improving the CHARMM force field for polyunsaturated fatty acid chains," *The Journal of Physical Chemistry B,* vol. 116, pp. 9424-9431, 2012.

[8] A. D. MacKerell Jr, J. Wiorkiewicz-Kuczera and . M. Karplus, "All-Atom Empirical Potential for Molecular Modeling and Dynamics Studies of Proteins," *J. Phys. Chem. B,* vol. 102, pp. 3586-3616, 1998.

[9] S. W. d. Leeuw, J. W. Perram and E. R. Smith, "Simulation of electrostatic systems in periodic boundary conditions. I. Lattice sums and dielectric constants," *Proc R Soc Lond A,* vol. 373, pp. 27-56, 1980.

[10] H. Andersen, "Molecular dynamics simulations at constant pressure and/or temperature," *The Journal of chemical physics,* vol. 72, p. 2384, 1980.

[11] W. Hoover, "Canonical dynamics: equilibrium phase-space distributions," *Physical Review A,* vol. 31, p. 1695 , 1985.

[12] G. J. Martyna, D. J. Tobias and M. L. Klein, "Constant pressure molecular dynamics algorithms," *J. Chem. Phys,* vol. 101, pp. 4177-4189, 1994.

[13] S. E. Feller, Y. Zhang and R. W. Pastor, "Constant pressure molecular dynamics simulation: The Langevin piston method," *The Journal of Chemical Physics,* vol. 103, p. 4613, 1995.

[14] A. P. Lyubartsev and A. L. Rabinovich, "Recent Development in Computer Simulations of Lipid Bilayers," *Soft Matte,* vol. 7, no. 1, pp. 25-39, 2011.

[15] M. Schlenkrich, J. Brickmann, A. D. MacKerell Jr and M. Karplus, "An empirical potential energy function for phospholipids: criteria for parameter optimization and applications," in *Biological Membranes*, Boston, Birkhäuser, 1996, pp. 31-81.

[16] S. E. Feller, R. M. Venable and R. W. Pastor, "Computer simulation of a DPPC phospholipid bilayer: structural changes as a function of molecular surface area," *Langmuir,* vol. 13, no. 24, pp. 6555-6561, 1997.

[17] S. E. Feller, D. Yin, R. W. Pastor and A. D. MacKerell, "Molecular dynamics simulation of unsaturated lipid bilayers at low hydration: parameterization and comparison with diffraction studies," *Biophysical journal,* vol. 73, no. 5, pp. 2269-2279, 1997.

[18] S. E. Feller and A. D. MacKerell, "An improved empirical potential energy function for molecular simulations of phospholipids," *The Journal of Physical Chemistry B,* vol. 104, no. 31, pp. 7510-7515, 2000.

[19] R. W. Pastor and A. D. MacKerell Jr, "Development of the CHARMM force field for lipids," *The journal of physical chemistry letters,* vol. 2, no. 13, pp. 1526-1532, 2011.

[20] T. M. Ferreira, F. Coreta-Gomes, O. S. Ollila, M. J. Moreno, W. L. Vaz and D. Topgaard, "Cholesterol and POPC segmental order parameters in lipid membranes: solid state 1 H–13 C NMR and MD simulation studies," *Physical Chemistry Chemical Physics,* vol. 15, no. 6, pp. 1976-1989, 2013.

[21] C. Hofsäß, E. Lindahl and O. Edholm, "Molecular dynamics simulations of phospholipid bilayers with cholesterol," *Biophysical journal,* vol. 84, no. 4, pp. 2192-2206, 2003.

[22] S. S. Qin, Z. W. Yu and Y. X. Yu, "Structural and kinetic properties of α-tocopherol in phospholipid bilayers, a molecular dynamics simulation study," *The Journal of Physical Chemistry B,* vol. 113, no. 52, pp. 16537-16546, 2009.

[23] S. S. Qin and Z. W. Yu, "Molecular dynamics simulations of α-tocopherol in model biomembranes," *Acta Physico-Chimica Sinica,* vol. 27, no. 1, pp. 213-227, 2011.

[24] S. E. Feller, K. Gawrisch and A. D. MacKerell, "Polyunsaturated fatty acids in lipid bilayers: intrinsic and environmental contributions to their unique physical properties," *Journal of the American Chemical Society,* vol. 124, no. 2, pp. 318-326, 2002.

[25] J. Kirkwood, "Statistical mechanics of fluid mixtures," *J. Chem. Phys.,* vol. 3, p. 300, 1935.

[26] G. M. Torrie and J. P. Valleau, "Nonphysical sampling distributions in Monte Carlo free-energy estimation - Umbrella sampling," *Journal of Computational Physics,* vol. 23, pp. 187-199, 1977.

[27] F. Zhu and G. Hummer, "Convergence and Error Estimation in Free Energy Calculations Using the Weighted Histogram Analysis Method," *Journal of Computational Chemistry,* pp. 453-465, 2011.

[28] C. Neale and R. Pomès, "Sampling errors in free energy simulations of small molecules in lipid bilayers," *Biochimica et Biophysica Acta (BBA)-Biomembranes,* vol. 1858, no. 10, pp. 2539-2548, 2016.

[29] F. Meng, "MOLECULAR SIMULATION OF α-TOCOPHEROL PASSING ACROSS DPPC LIPID USING POTENTIAL OF MEAN FORCE AND ACCELERATED MOLECULAR DYNAMICS METHOD," *Theoretical and Computational Chemistry,* vol. 12, no. 8, p. 1341011, 2013.

[30] Z. Zhang, L. Lu and M. L. Berkowitz, "Energetics of Cholesterol Transfer between Lipid Bilayers," *The Journal of Physical Chemistry B,* vol. 112, no. 12, pp. 3807-3811, 2008.

[31] W. D. Bennett, J. L. MacCallum, M. J. Hinner, S. J. Marrink and D. P. Tieleman, "Molecular View of Cholesterol Flip-Flop and Chemical Potential in Different Membrane Environments," *Journal of the American Chemical Society,* vol. 131, no. 35, pp. 12714-12720., 2009.

[32] W. D. Bennett and D. P. Tieleman, "Molecular simulation of rapid translocation of cholesterol, diacylglycerol, and ceramide in model raft and nonraft membranes," *Journal of lipid research,* vol. 53, no. 3, pp. 421-429, 2012.

[33] X. Leng, J. J. Kinnun, D. Marquardt, M. Ghefli, N. Kučerka, J. Katsaras, ... and S. R. Wassall, "α-Tocopherol Is Well Designed to Protect Polyunsaturated Phospholipids: MD Simulations," *Biophysical journal,* vol. 109, no. 8, pp. 1608-1618, 2015.

[34] R. Kjellander and S. Marčelja, "Perturbation of hydrogen bonding in water near polar surfaces," *Chemical physics letters,* vol. 120, no. 4-5, pp. 393-396, 1985.

[35] P. Van der Ploeg and H. J. C. Berendsen, "Molecular dynamics simulation of a bilayer membrane," *The Journal of Chemical Physics,* vol. 76, no. 6, pp. 3271-3276, 1982.

[36] J. B. Klauda, V. Monje, T. Kim and W. Im, "Improving the CHARMM force field for polyunsaturated fatty acid chains," *The journal of physical chemistry B,* vol. 116, no. 31, pp. 9424-9431, 2012.

[37] N. V. Eldho, S. E. Feller, S. Tristram-Nagle, I. V. Polozov and K. Gawrisch, "Polyunsaturated docosahexaenoic vs docosapentaenoic acid differences in lipid matrix properties from the loss of one double bond," *Journal of the American Chemical Society,* vol. 125, no. 21, pp. 6409-6421, 2003.

[38] C. Hofsäß, E. Lindahl and O. Edholm, "Molecular dynamics simulations of phospholipid bilayers with cholesterol," *Biophysical journal,* vol. 84, no. 4, pp. 2192-2206, 2003.

[39] A. Vogel, H. A. Scheidt, D. J. Baek, R. Bittman and D. Huster, "Structure and dynamics of the aliphatic cholesterol side chain in membranes as studied by 2 H NMR spectroscopy and molecular dynamics simulation," *Physical Chemistry Chemical Physics,* vol. 18, no. 5, pp. 3730-3738, 2016.

[40] T. M. Ferreira, F. Coreta-Gomes, O. S. Ollila, M. J. Moreno, W. L. Vaz and D. Topgaard, "Cholesterol and POPC segmental order parameters in lipid membranes: solid state 1 H–13 C NMR and MD simulation studies," *Physical Chemistry Chemical Physics,* vol. 15, no. 6, pp. 1976-1989, 2013.

[41] H. Martinez-Seara, T. Róg, M. Karttunen, I. Vattulainen and R. Reigada, "Cholesterol induces specific spatial and orientational order in cholesterol/phospholipid membranes," *PloS one,* vol. 5, no. 6, p. e11162, 2010.

[42] S. S. Qin and Z. W. Yu, "Molecular dynamics simulations of α-tocopherol in model biomembranes," *Acta Physico-Chimica Sinica,* vol. 27, no. 1, pp. 213-227, 2011.

[43] S. S. Qin, Z. W. Yu and Y. X. Yu, "Structural and kinetic properties of α-tocopherol in phospholipid bilayers, a molecular dynamics simulation study," *The Journal of Physical Chemistry B,* vol. 113, no. 52, pp. 16537-16546, 2009.

[44] M. C. Pitman, F. Suits, A. D. MacKerell and S. E. Feller, "Molecular-level organization of saturated and polyunsaturated fatty acids in a phosphatidylcholine bilayer containing cholesterol," *Biochemistry,* vol. 43, no. 49, pp. 15318-15328, 2004.

Table 2.1

Examples of PMF profile of cholesterol in different lipid membranes, obtained by all atom USMD simulations. Unit for the free energy is kcal/mol. Care should be taken when comparing the ΔG from simulations with different conditions (temperature, force field, and so on).

Lipid	Zhang et al. [30] (319K)	Bennett et al. [31] (323K)	Bennett et al. [32] (323K)
POPC	12.1		18.6
18:0 SM	14.5		
DPPC		19.1	
DAPC		16	
POPC+PSM (16:0 SM)+Cholesterol 1:1:1			31.5

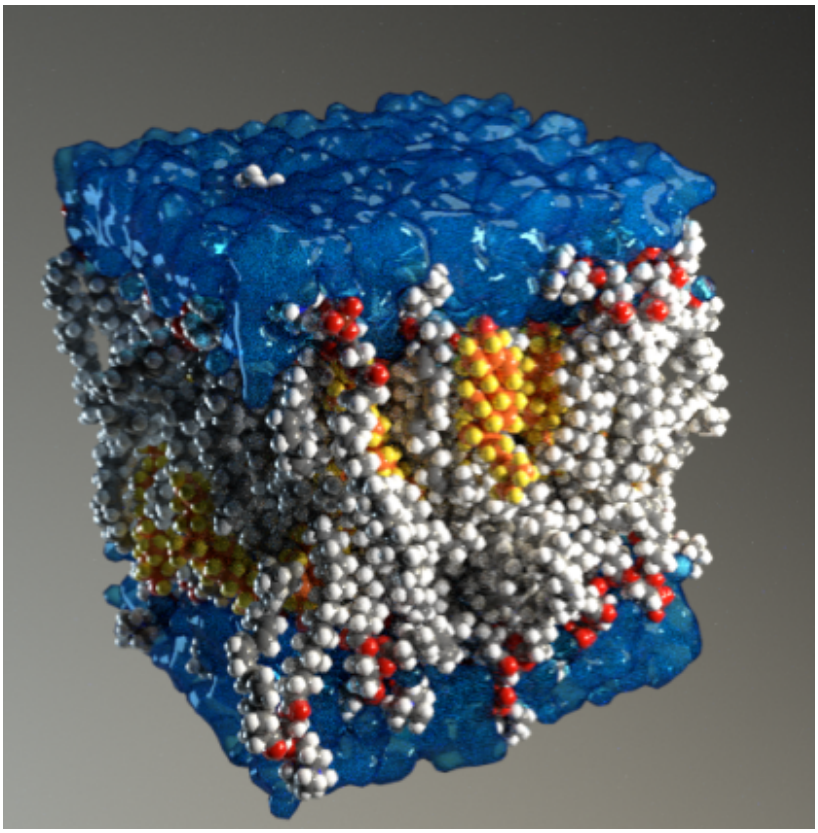

Figure 2.1

Snapshot of all atom model of lipid bilayer with explicit water. Lipid atoms are represented as van der Waals spheres, and water molecules are shown as contour surfaces.

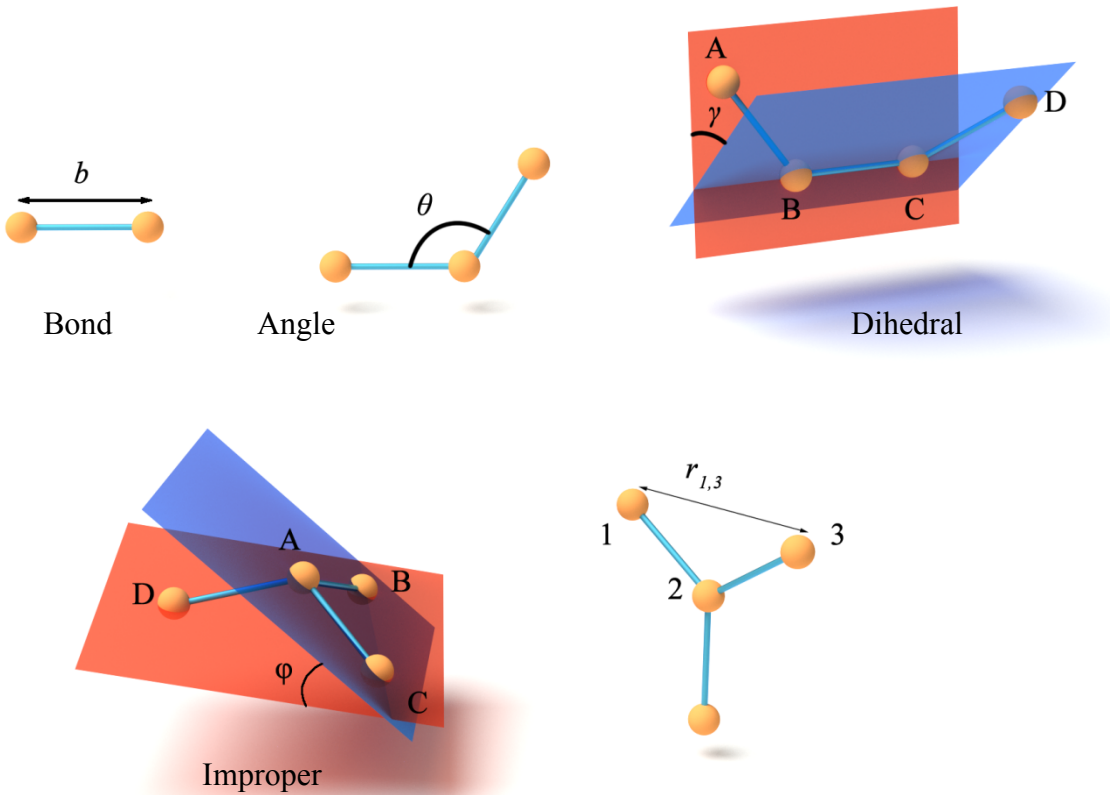

Figure 2.2

Illustration of CHARMM C36 bond energy terms.

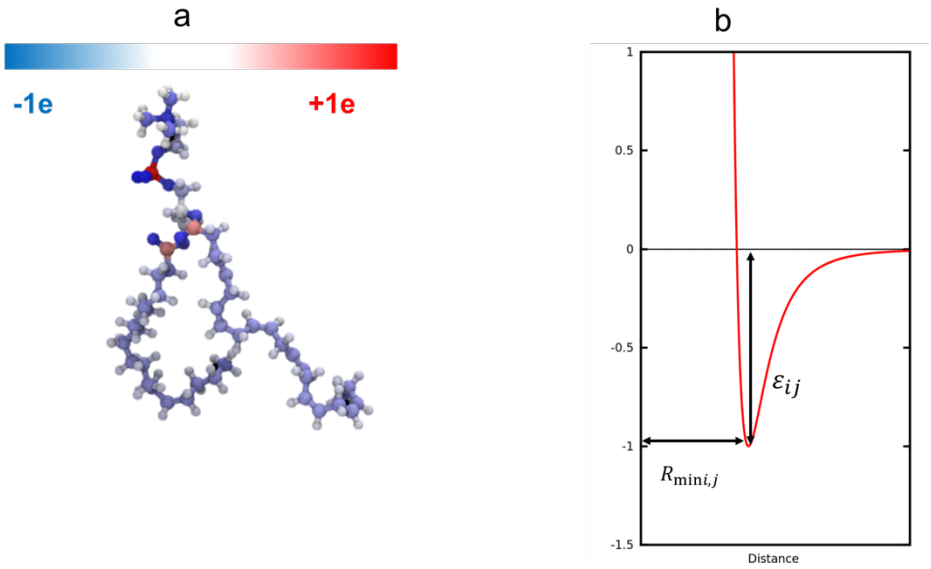

Figure 2.3

a). Partial charge distribution for the atoms in a PC lipid molecule due to the uneven charge distribution on the covalent bond and ion.

b). Lennard-Jones potential, $R_{\min i,j}$ and ε_{ij}.

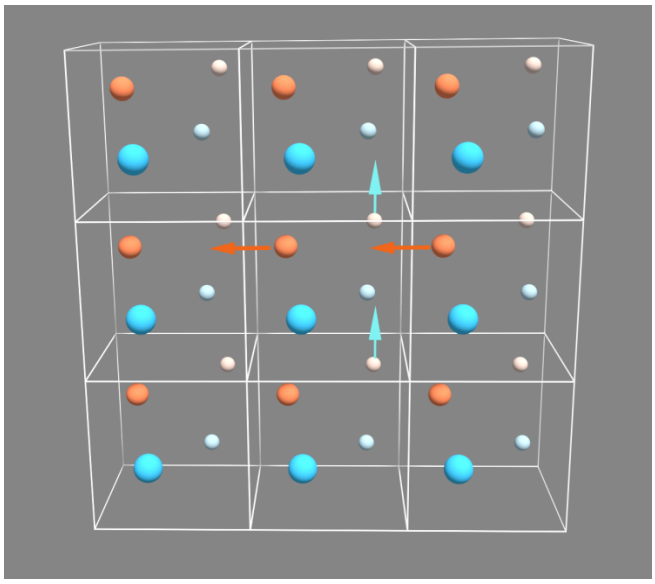

Figure 2.4

Illustration of periodic boundary condition with simulation box in the center, surrounded by its image.

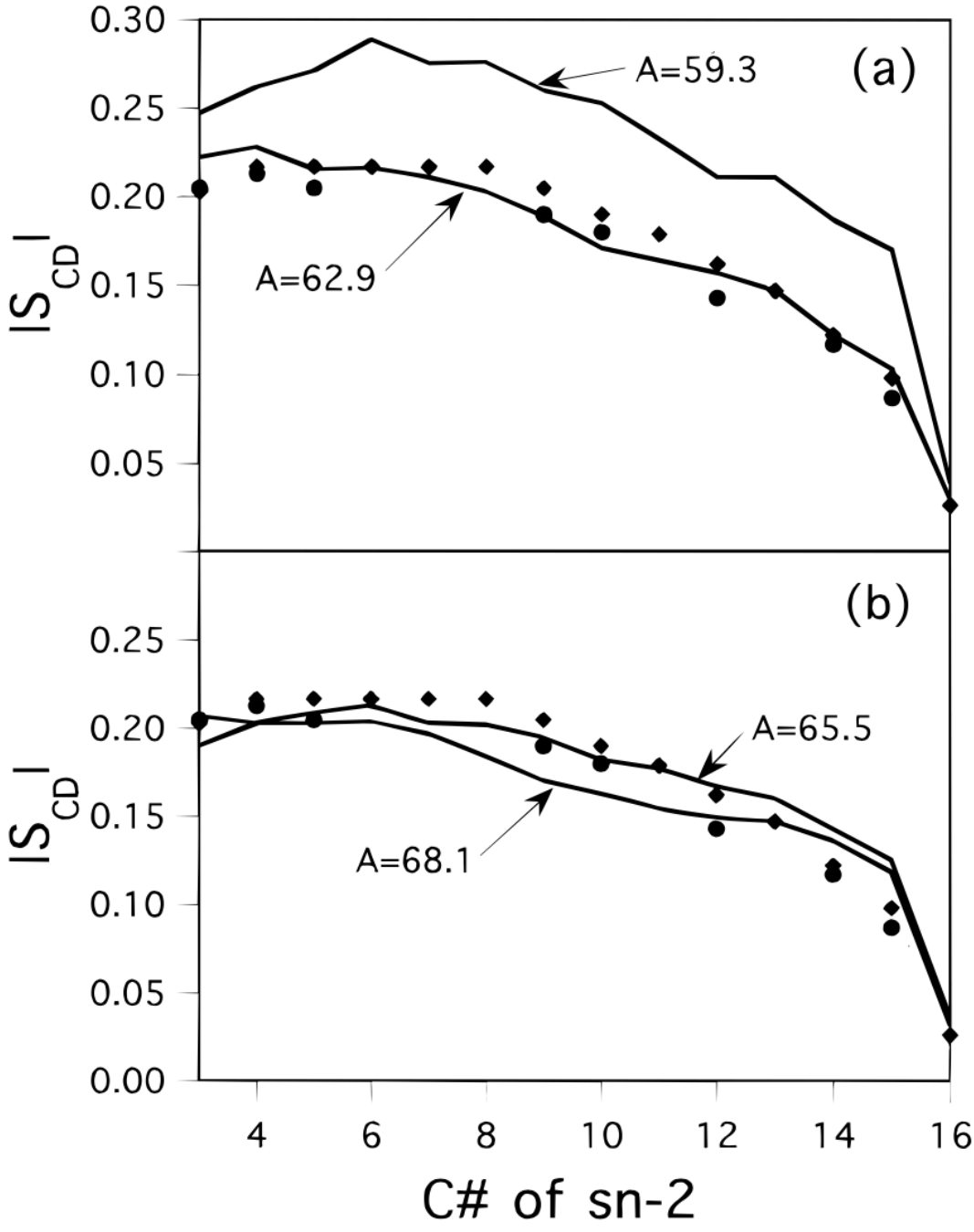

Figure 2.5

S_{CD} for the sn-2 chain of DPPC from MD simulation using NPAT ensemble with different are per lipid: a) 59.3 and 62.9 $Å^2$; b) 65.5 and 68.1 $Å^2$. NMR experimental data are denoted by symbols in both figures.

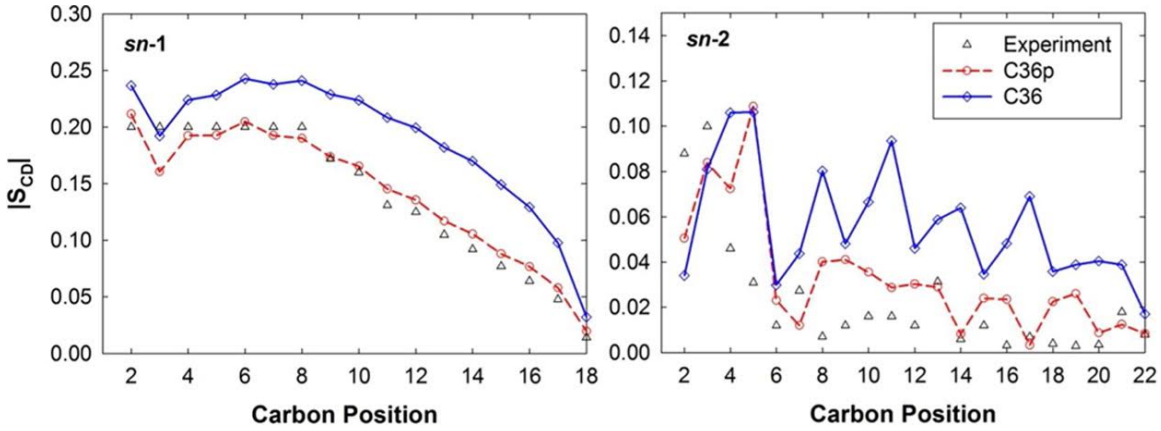

Figure 2.6

S_{CD} for the sn-1 (left) and sn-2 (right) chain of SDPC bilayers, obtained from MD simulations using CHARMM force field C36 and C36p, compared with experiment.

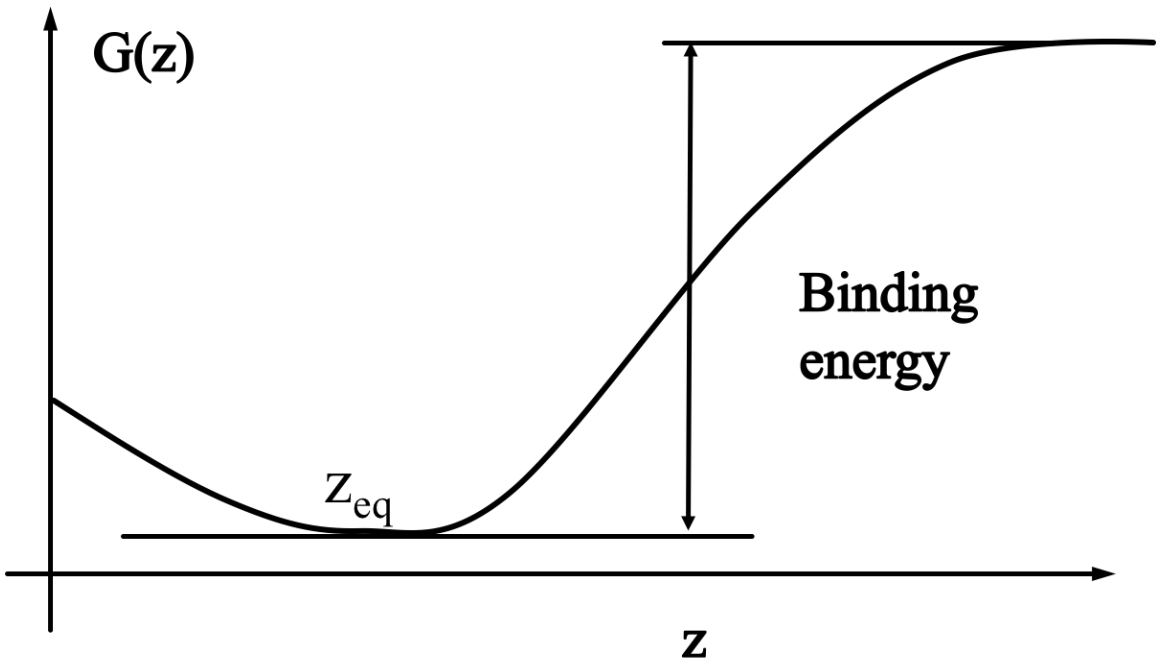

Figure 2.7

Schematic illustration of the potential of mean force (PMF, or G(z)) profile of αtoc in a lipid bilayer. The reaction coordinate z represent the membrane normal distace between the center of mass of the chromanol group and the center of the bilayer.

Acknowledgements

Figure 2.5 is reprinted from Langmuir, 13(24), 6555-6561, Feller, S. E., Venable, R. M., & Pastor, R. W. (1997), Computer simulation of a DPPC phospholipid bilayer: structural changes as a function of molecular surface area, with permission from American Chemical Society.

Figure 2.6 is reprinted from The journal of physical chemistry B, 116(31), Klauda, J. B., Monje, V., Kim, T., & Im, W. (2012), Improving the CHARMM force field for polyunsaturated fatty acid chains, , 9424-9431, with permission from American Chemical Society.

CHAPTER 3. ALPHA-TOCOPHEROL IS WELL-DESIGNED TO PROTECT POLYUNSATURATED PHOSPHOLIPIDS: MD SIMULATIONS

3.1 Introduction

α-Tocopherol (αtoc) is the form retained by the human body of a structurally related group of phenolic compounds that make up vitamin E [1,2]. It is a lipid soluble antioxidant that is an essential micronutrient. Symptoms of deficiency include, for example, neuromuscular abnormities [3]. There is overall consensus that a major function of αtoc is to prevent the oxidation of polyunsaturated lipids that are particularly vulnerable to free radical attack in subcellular and plasma membranes [2,4-6]. The chemistry is well established [7,8], but it remains to be seen whether a structural component exists in support of this role [5,9-11]. Here we present MD simulations that reveal αtoc is well designed to protect polyunsaturated lipids.

The molecular structure of αtoc consists of a chromanol head group that is methylated at all three of the available positions on a benzene ring and to which a 16-carbon saturated phytyl chain is attached at the opposite end (Fig. 3.1). A hydroxyl group on the benzene ring is responsible for antioxidant activity [7,8]. This hydrophilic group usually sits near the aqueous interface, anchored to a membrane by the hydrophobic chain that extends towards the center [12,13]. There it scavenges lipid peroxyl radicals that rise up ("snorkel") to the surface from the interior of the membrane via conformational isomerization, terminating the chain reaction by which lipid peroxidation proceeds. The same location provides easy access to polar reducing agents that regenerate αtoc. Polyunsaturated fatty acids (PUFA), notably docosahexaenoic acid (DHA, 22:6) with 6 double bonds, are an influential membrane constituent [14]. Their incorporation into phospholipids in plasma membranes has been proposed to be responsible for a vast array of health benefits attributed to dietary consumption of fish oils rich in PUFA [15-17], while they are abundant in the phospholipids of neural membranes and depletion from these specialized membranes results in functional impairment [18,19]. Extremely high disorder is the unique property that PUFA possess and by which polyunsaturated phospholipids modulate membrane

organization and protein activity [20-22]. The origin of the disorder is the presence of a repeating =CH-CH_2-CH= unit within which the energy barrier to rotation about C-C bonds is shallow [23]. Because the central methylene group in this recurring motif is readily attacked by free radicals [24], polyunsaturated phospholipids are prone to peroxidation and αtoc is thought to inhibit the process.

The amount of αtoc in membranes is extremely small. Reported levels are generally <1 mol% of the total lipid [25]. Thus, polyunsaturated phospholipid molecules grossly outnumber the molecule that is meant to defend them from oxidation by a mechanism necessitating intimate contact. How αtoc can effectively do so in an encompassing milieu of lipids and proteins is unclear and has led to proposals, as yet unproven, that it preferentially interacts with PUFA [9-11]. Atomistic MD simulations have been integral in developing a detailed picture of polyunsaturated phospholipid bilayers in which PUFA chains rapidly isomerize between conformational states [26-28]. In the current study, we applied this computational approach to compare the molecular organization of αtoc in 1-stearoyl-2-docosahexaenoylphosphatidylcholine (SDPC, 18:0-22-6PC) and 1-stearoyl-2-oleoylphosphatidylcholine (SOPC, 18:0-18:1PC) bilayers. SDPC with saturated stearic acid (SA, 18:0) for the *sn*-1 chain and DHA for the *sn*-2 chain is representative of a polyunsaturated phospholipid, while SOPC with oleic acid (OA, 18:1) containing a single double bond instead for the *sn*-2 chain serves as a monounsaturated control (Fig. 3.1). Solid state ^{2}H NMR and neutron diffraction measurements (done by Drew Marquardt at Chalk River Laboratories) were also performed to complement the MD simulations.

3.2 Materials and methods

3.2.1 MD simulations

MD simulations were performed for neat bilayers of SDPC and SOPC and of SDPC and SOPC containing 20 mol% αtoc. They were run in the constant particle number, pressure and temperature (NPT) ensemble. Each simulation has 100 lipid molecules and 2000 water molecules. The initial structures were assembled with the CHARMM-GUI Membrane Builder [29,30], and in presence of αtoc were prepared from the lipid-cholesterol structure built with CHARMM-GUI by replacing cholesterol with αtoc. Simulations were run using

the CHARMM C36 [31] and C36p [32] force fields for SOPC and SDPC, respectively, with the customary cut-offs. Non-bonded (pairwise van der Waals and short range electrostatic) interactions were smoothly turned off at 10 Å, while the particle-mesh Ewald method was employed to calculate long range electrostatic interactions [33]. The equilibration of bilayers was achieved using the standard CHARMM-GUI six-step process that gradually turns off restraints on lipids over 200 ps [30].

Production runs were over a minimum of 200 ns using a time step of 2 fs and the first 20 ns were considered as equilibration. The simulations were maintained in a rectangular box with equal x and y dimension (in the plane of the bilayer) and z varied independently in the NPT ensemble. The temperature was kept at 37 °C by the Hoover thermostat [34] while the Nosé-Hoover piston was applied to keep the pressure at 1 atm [35]. Analyses of simulations included the calculation of order parameters and neutron scattering length density (NSLD) profiles. The Lightweight Object-Oriented Structure (LOOS) library was employed to construct maps of the lateral distribution of lipid chains relative to αtoc [36]. Snapshots of bilayers and plots of the maps of lateral distribution were created with the Visual Molecular Dynamics (VMD) program [37].

3.2.2 Solid state 2H NMR

Samples were aqueous multilamellar dispersions of 50 wt% lipid in 50 mM Tris buffer (pH 7.5). The lipids comprised 1-[$^2H_{35}$]stearoyl-2-docosahexaenoylphosphatidyl-choline (SDPC-d_{35}), SDPC-d_{35}/20 mol% αtoc, 1-[$^2H_{35}$]stearoyl-2-oleoylphosphatidyl-choline (SOPC-d_{35}) and SOPC-d_{35}/20 mol% αtoc. In each sample there was 25 mg SDPC-d_{35} or SOPC-d_{35}. Avanti Polar Lipids (Alabaster, AL) was the source for the deuterated analogs of phospholipids, while deuterium depleted water was purchased from ISOTEC (Sigma-Aldrich Corporation, St. Louis, MO). αToc was obtained from commercial α-tocopheryl acetate by hydrolysis (K_2CO_3 in methanol for 5 h) and purification of the crude product via silica gel column chromatography using a step gradient of hexane:ether (95:5 to 9:1) as the eluting solvents. Preparation of the samples was as previously described [38], with additional precautions outlined in earlier work taken due to the susceptibility of PUFA to oxidation [39].

^2H NMR spectra were acquired on a homebuilt spectrometer operating at 46.0 MHz with a

7.05 T superconducting magnet (Oxford Instruments, Osney Mead, UK) [40] implementing a phase alternated quadrupolar echo sequence $(90^{o}_{x}\text{-}\tau\text{-}90^{o}_{y}\text{-acquire-delay})_{n}$ [41]. Data acquisition parameters were 90° pulse width = 3.8 μs; separation between pulses τ = 50 μs; delay between pulse sequences = 1.0 s; sweep width = ±100 kHz; dataset = 2 K; and number of transients = 10,000. The first moment M_1 was calculated from powder patterns obtained by conventional FFT and related to an average order parameter $\overline{S}_{CD}$ with standard equations [42]. The FFT depaking algorithm was applied to produce the corresponding aligned spectra characteristic of a planar membrane [43]. Exploiting the enhanced resolution of depaked spectra, profiles of order parameter S_{CD} were then constructed assuming the value of S_{CD} decreases smoothly along a lipid chain from the more ordered methylene groups near the membrane surface towards the disordered terminal methyl group in the middle of the membrane [44].

3.2.3 Neutron diffraction

Neutron diffraction of aligned multilayers prepared on a silicon single crystal substrate was employed to map the density distribution of lipid components along the membrane normal (z) direction. The methods have been documented before [12]. The samples were comprised of a total of 12 mg of SDPC or SOPC (Avanti Polar Lipids) with 20 mol% αtoc or a labeled analog, α-[5-$^{2}H_3$]tocopherol (αtoc-d_3), having a deuterated methyl group at the 5-position on the chromanol group (Fig. 3.1). Preparation of the labeled analog was by a previously cited protocol (12). The bilayers were hydrated at fixed humidity using a saturated salt solution of KNO_3 (94 % RH) with 70, 40, 16, and 8% $^{2}H_2O$. Care was taken throughout sample manipulation and experimentation to minimize exposure to the atmosphere and light. Samples were kept at room temperature during initial equilibration and controlled at 37±0.5 °C during data collection.

Diffraction data were taken on the D3 beam-line at the Canadian Neutron Beam Center (CNBC, Chalk River, Ontario, Canada). A wavelength of 2.37 Å was selected for the neutrons with a single crystal monochromator of pyrolytic graphite. Higher order (i.e., λ/2, etc.) reflections were eliminated using a pyrolytic graphite filter. Data correction and reconstruction of the bilayer profile proceeded as outlined in earlier work [12]. Briefly,

scattering form factors F_h were obtained from the integrated intensity of each of the quasi-Bragg peaks, typically 4-8, that were collected. The NSLD profile along the bilayer normal z was derived with the cosine transformation of the form factors. The difference between the profiles for labeled and unlabeled samples was calculated from the transformation of the difference in their respective structure factors. Data were placed on an arbitrary scale for comparison with MD simulations.

3.3 Results

3.3.1 Membrane organization and structure

3.3.1.1 Phospholipid acyl chain order

The order parameter is defined according to

$$S_{CD} = \frac{1}{2}\left\langle 3\cos^2\beta - 1 \right\rangle \tag{3.1}$$

In this equation β is the instantaneous angle between a C-H bond and the bilayer normal, about which lipid molecules reorient with axial symmetry, and the angular brackets designate a time average [45]. The value of S_{CD} for a methylene or methyl group in a lipid chain is determined by the degree of anisotropy of the motion for the group and the profile of order parameter along a lipid chain is a sensitive indicator of membrane organization [46]. From the MD simulations performed in the current study we calculated order parameter profiles for the *sn*-1 and -2 chains in SDPC and SOPC both in the absence and presence of 20 mol% αtoc. We also determined smoothed order parameter profiles for the *sn*-1 chain from the ^{2}H NMR spectra collected with SDPC-d_{35} and SOPC-d_{35}. Measurements made in ^{2}H NMR experiments are widely employed in validating MD simulations [47]. Comparison between the two approaches, however, is not straightforward. NMR work is typically, as in this study, conducted at higher water content and in the presence of a buffer that can impact bilayer properties [48,49]. Additionally, order parameters obtained experimentally are subject to instrumental factors that can distort the shape of the spectra from which they are evaluated [50,51].

Order parameter profiles along the *sn*-1 chain derived from MD simulations run on SDPC and SOPC bilayers at 37 ºC are plotted in Figure 3.2 (open squares in lower left and right panels, respectively). The corresponding surface areas per lipid, together with the values in the presence of αtoc, are listed in the Supporting Material (Table S1). In each case, the profile has the characteristic shape that is universally seen for a saturated chain esterified at the *sn*-1 position of phospholipids in the lamellar liquid crystalline phase. There is a plateau region of largely constant order parameter ($S_{CD} \sim 0.2$) in the upper half of the chain near the bilayer surface followed by a progressive fall-off in value in the lower half of the chain towards the disordered middle of the bilayer [46]. Reflecting the much greater disorder possessed by DHA relative to OA in the adjacent *sn*-2 chain, order parameters are 10% lower on average in the SA chain of SDPC ($\overline{S}_{CD}$ = 0.137±0.003) than SOPC ($\overline{S}_{CD}$ = 0.153±0.003). When 20 mol% αtoc is added, the response is to increase order while maintaining the same overall shape for the profile along the SA chain in both SDPC ($\overline{S}_{CD}$ = 0.010) and SOPC ($\overline{S}_{CD}$ = 0.008) (open squares in upper left and right panels, respectively, in Fig. 2). This behavior is consistent with results published in earlier ^{2}H NMR studies on saturated and monounsaturated PC systems [38,52,53]. The condensing effect of αtoc is, not surprisingly, more modest than seen with cholesterol [54,55]. Although both molecules are comprised of rigid rings with a hydroxyl group at one end and a branched chain at the other, the chromanol group on αtoc is about half the size of the steroid moiety on cholesterol.

The general trends seen in the profiles calculated from the MD simulations are corroborated by the order parameter profiles along the *sn*-1 chain constructed from ^{2}H NMR spectra collected using SDPC-d_{35} and SOPC-d_{35} (continuous line in the left and right panels, respectively) that are included in Figure 3.2. SDPC-d_{35} ($\overline{S}_{CD}$ = 0.130±0.003) is appreciably more disordered than SOPC-d_{35} ($\overline{S}_{CD}$ = 0.143±0.003), and adding αtoc increases order in SDPC-d_{35} ($\overline{S}_{CD}$ = 0.011) and SOPC-d_{35} ($\overline{S}_{CD}$ = 0.015). Because the profiles generated by NMR data are smoothed, it should be noted that subtleties in variation within the plateau region are not discerned. Copies of the depaked spectra from which the profiles were obtained can be found in Figure A1.1 in the Supporting Material.

Order parameters calculated from the MD simulations along the *sn*-2 chain of SDPC and SOPC are shown in Figure 3.3. In agreement with results from experiment [56], order parameters throughout almost all of the DHA chain in SDPC are very small (S_{CD} < 0.05) due to the high degree of flexibility associated with the multiple double bonds (open circles in left panel, Fig. 3). The S_{CD} values are comparable to the lowermost disordered portion of the SA chain at the *sn*-1 position. The profile for the OA chain in SOPC, by contrast, resembles that for the SA chain except there is a precipitous dip in the value of S_{CD} in the vicinity of the double bond (open circles in right panel, Fig. 3). Such a discontinuity is a feature of the order parameters obtained for an OA chain in phospholipid bilayers from ^{2}H NMR spectra [57] and computer simulations [58]. A most probable orientation that results in intrinsically low S_{CD} values, not local segmental motion of large amplitude, is responsible [57,59]. Deviation from monotonic variation for the order parameter is evident, as well, at the C2 position where the values of S_{CD} for the two C-H bonds on the methylene group are depressed and unequal. It is attributed to constraints imposed by the glycerol backbone upon the initial orientation of the *sn*-2 chain [60].

An increase that is barely perceptible is revealed by the order parameters presented for the DHA chain in SDPC upon the introduction of 20 mol% αtoc in Figure 3.3 (crosses in left panel). The change in average value determined for order parameter ($\overline{S}_{CD}$ = 0.004) is correspondingly very small. Minimal interference with the rapid transition between torsional states adopted by the polyunsaturated *sn*-2 chain due to αtoc is implied. Among the myriad of conformations formed, as identified in pioneering MD simulations on DHA-containing phospholipids [61], are bent arrangements that bring much of the chain up to the membrane surface. How the OA chain in SOPC is affected by the addition of αtoc has more in common with the situation for the SA chain. Like the SA chain, order parameters in the OA chain are elevated ($\overline{S}_{CD}$ = 0.013) in a profile that retains the shape observed in the absence of αtoc (crosses) in right panel, Fig. 3).

3.3.1.2 Location of α-tocopherol

Figure 3.4 displays NSLD profiles for SDPC (left) and SOPC (right) bilayers containing

20 mol% αtoc computed from our MD simulations (upper panel). By assigning a neutron scattering length to each atom, they were generated with

$$NSLD = \sum_i b_i n_i(z) \tag{3.2}$$

Here z is the distance from the center of the membrane, b_i is the neutron scattering length for an atom of type i and $n_i(z)$ is the number of atoms of type i in slices that are 0.2 Å thick. This format reveals structural information in a manner that is directly comparable to experiment. The distribution of the atoms on all the lipids (phospholipid and αtoc) about the midpoint of the bilayer ($z = 0$) has a negative dip at the middle that is due to the disordered methyl groups at the end of the lipid chains (dashed line). Scattering from the phosphate and glycero-ester regions is responsible for the symmetrically located maxima on each side. The separation of these maxima roughly represents the hydrocarbon thickness of the bilayer [62], which is 34.1±0.3 Å for SDPC (left upper panel) and 35.6±0.4 Å for SOPC (right upper panel). Consistent with the larger cross-sectional molecular area that accompanies higher disorder (Table S1 in Supporting Material), the bilayer is thinner for SDPC than SOPC. The scattering profile for only the deuterons, isotopic substituting for hydrogen, on the methyl group at the C5 position of the chromanol group in αtoc consists of a pair of peaks (continuous line). The peaks are ±13.7 and ±14.0 Å from the center of the bilayer in SDPC and SOPC, respectively. They are ~3-4 Å (3.3±0.4 Å in SDPC and 3.8±0.5 Å in SOPC) inside the maxima due to all atoms on the lipids in each case, which situates the chromanol group just below the membrane surface in SDPC and SOPC and is consistent with hydrogen bonding to the carbonyl groups on the phospholipids. This location falls within a range of sites in the vicinity of the aqueous interface that has been identified for a number of phospholipids by a variety of experimental techniques as well as computer modeling [12,13,25,63].

The MD simulations reproduce the chief features of the results from neutron diffraction measurements on aligned multilayers of SDPC (left, lower panel) and SOPC (right, lower panel) with 20 mol% αtoc that are also reported in Figure 3.4. That a reduced level of hydration applies to the experiments (~11-15 water molecules/lipid) relative to the simulations (~20 water molecules/lipid) should be borne in mind. A separation of 35.0±1.6

Å in SDPC and 38.8±0.2 Å in SOPC applies to the maxima that flank the negative dip at the center of the NSLD profiles for the whole bilayer (dashed line) obtained by analyzing the neutron diffraction peaks (Fig. A1.3 in Supporting Material). In these profiles the contribution from water was suppressed by conducting the experiments with water that contained 8% ^2H_2O [62]. The pair of peaks identified from the difference between NSLD profiles evaluated with bilayers prepared with labeled (αtoc-5d_3) and unlabeled αtoc (Fig. A1.4 and Table S2 in Supplementary Material), places the C5 position on αtoc at ±19.0 and ±21.0 Å with respect to the center of the bilayer in SDPC and SOPC, respectively (continuous line). They lay ~2 Å (1.5±2.0 Å in SDPC and 1.6±1.0 Å in SOPC) outside the maxima due to the entire lipid in both cases, such that the chromanol group slightly protrudes into the phospholipid head group region which suggests that there is hydrogen bonding to the phosphate group. Like the data from the MD simulations, although differences in detail exist, the experimental observations confirm that the chromanol group resides near the aqueous surface in SDPC and SOPC and imply that there is no appreciable disparity between the depth of αtoc in the polyunsaturated and monounsaturated systems.

The reason for the apparent discrepancy in position within the bilayer determined for αtoc from the analyses of our computational and experimental results is not entirely evident. Both approaches have inherent limitations, in common with NMR and other methods, and probe a system under conditions that are not identical. The MD simulations, the accuracy of which fundamentally depends on the reliability of the force field employed, were run on a patch containing 100 lipid molecules in a single bilayer. The neutron diffraction experiments, which rely crucially on the precise scaling of measurements made on two independent samples that differ only in isotopic replacement of deuterium for hydrogen at a specific molecular site, were performed on aligned multilayers on a silicon crystal substrate prepared, as noted above, at lower hydration. Exactly where αtoc sits, moreover, cannot be surmised from the literature that has been published to date. Three basic models, which were comprehensively discussed in a subsequent review [25], have been proposed [64]. They have the chromanol group poking into the head group region, recessed within the interfacial region and submerged into the bilayer. Each one has experimental support [25]. The majority of the earlier reports, albeit often somewhat qualitative and/or subject

to perturbation problems associated with the use of an extrinsic probe molecule, favor the latter two models. A location at the surface or within the bilayer was concluded on the basis of the quenching of the intrinsic fluorescence of αtoc produced by nitroxyl or anthroyloxyl stearic acids incorporated into 1,2-dipalmotoylphosphatidylcholine (DPPC, 16:0-16:0PC) and egg phosphatidylcholine (PC) vesicles [65,66], the time course of the loss in intensity for ^{19}F NMR signals from ^{19}F-labeled analogs of αtoc in egg PC vesicles following the addition of Pr^{3+} [67] and the chemical shift-polarity correlation of ^{13}C NMR resonances for αtoc in 1,2-dimyristoylphsphatidylchholine (DMPC, 14:0-14:0PC) vesicles [68]. Close to the phosphate, the dissenting view that has the chromanol group in the polar region of the phospholipid head groups, was deduced from lanthanide induced shifts of ^{13}C NMR spectra observed for a ^{13}C-enriched analog of αtoc in egg PC vesicles [69].

Although providing more quantitative information, the MD simulations and neutron scattering work that have been described more recently only compound the debate. Like in the current investigation, the tendency is for the respective methods to place the chromanol group on opposite sides of the lipid-water interface. Just beneath the interface was indicated in the computer simulations conducted on saturated and monounsaturated phosphatidylcholine (PC) bilayers [63,70]. Above and within the interfacial region was found in the neutron diffraction experiments done on saturated, monounsaturated and polyunsaturated PC multilayers [12], although a dependence upon head group causing deeper penetration in 1-palmitoyl-2-oleoylphosphatidylserine (POPS) was observed as well [13]. That quite different water contents were employed should again be recognized when comparing the two types of result. It is impossible, additionally, to discern a pattern in the variation in placement determined for the chromanol group by the neutron scattering measurements. As an example, substantially above vs. slightly below the lipid-water interface was seen in 1-palmitoyl-2-oleoylphosphatidylcholine (POPC, 16:0-18:1PC) and 1,2-dioleoylphosphatidylcholine (DOPC, 18:1-18:1PC), which is the reverse of the trend seen in 1-palmitoyl-2-arachidonylphosphatidylcholine (PAPC, 16:0-20:4PC) and its more disordered, homo-acid counterpart 1,2-diarachidonylphosphatidylcholine (DAPC, 20:4-20:4PC) [12]. Neutron scattering data that has also been reported showing αtoc sequesters at the center of DMPC bilayers further illustrate how poorly the situation is understood

[38]. A systematic attack on this problem will clearly be necessary in the future to resolve the issue.

3.3.2 Interaction of α-tocopherol with phospholipid acyl chains

To probe the relative affinity of αtoc for SDPC vs. SOPC, the van der Waals (vdW) interaction energy between αtoc and phospholipid acyl chains and the density of each chain surrounding αtoc molecules were determined from the MD simulations.

3.3.2.1 van der Waals interaction energy

The vdW interaction energy was calculated in CHARMM by summing over pairs of non-bonded atoms using the standard Lennard-Jones potential

$$U_{vdW} = \sum_{ij} \varepsilon_{ij} \left[\left(\frac{R_{\min,ij}}{r_{ij}} \right)^{12} - \left(\frac{R_{\min,ij}}{r_{ij}} \right)^{6} \right] \tag{3.3}$$

where ε_{ij} and $R_{\min,ij}$ are the energy and separation between pairs of atoms ij at equilibrium, respectively, and r_{ij} is the distance between the atoms [31]. Figure 3.5 shows the results for αtoc in SDPC (upper) and SOPC (lower) in the form of a bar graph. Separate values of U_{vdW} describing the interaction with the *sn*-1 and -2 chains are plotted. They reveal that the vdW interaction energy of αtoc with the saturated SA chain at the *sn*-1 position is less in SDPC (-20.3 kcal/mol) than SOPC (-23.4 kcal/mol), which we ascribe to the enhanced disorder, and hence loose packing, within the polyunsaturated bilayer. The opposite situation applies to the interaction of αtoc with the unsaturated chains at the *sn*-2 position. The vdW energy for the DHA chain in SDPC (23.2 kcal/mol) exceeds that for the OA chain in SOPC (21.4 kcal/mol). Moreover, the value of U_{vdW} for DHA is larger than SA in SDPC whereas it is smaller for OA than SA in SOPC. We attribute the greater proximity to αtoc implied for the polyunsaturated chain, paradoxically, to the tremendously high conformational freedom it possesses compared to a monounsaturated chain. Maps of the density of each chain around αtoc molecules constructed from the simulations provide insight into our explanation.

3.3.2.2 Spatial distribution of sn-1 and -2 chains

To better understand the interaction with the different chains in SDPC and SOPC, maps of the density of carbon atoms on the *sn*-1 and -2 chains surrounding αtoc molecules were generated utilizing the LOOS analysis library [36]. In our examination the rigid chromanol group serves as the molecular frame of reference and a vector extending from positions C4-6 specifies the orientation relative to the bilayer normal. The population distributions for this vector calculated from our simulations possess a maximum, representing the most probable orientation, at 39° in SDPC and 35.5° in SOPC. A state for an αtoc molecule closely matching the most probable orientation in a bilayer was then selected from our simulations and for each αtoc molecule in every frame of trajectory, the entire system was translated and rotated so that all of the chromanol groups were aligned with this reference. Next, summing over the realigned trajectories, we mapped the probability density for the *sn*-1 and -2 chains of either SDPC or SOPC separately within a cube of $30 \cdot 30 \cdot 30$ Å^3 lying in the plane of the bilayer in the reference system with an origin at the center of mass of the chromanol group. The cube was divided into $1 \cdot 1 \cdot 1$ Å^3 bins, and the probability density ρ is proportional to the number of times the carbon atoms in each chain appear in a bin during the 180 ns of simulation time.

In Figure 3.6, the difference in spatial distribution of the *sn*-1 and -2 chains in SDPC (left column) and SOPC (right column) relative to αtoc is explored. For this purpose we have defined the parameter

$$\Delta\rho = \rho_2 - \rho_1 \tag{3.4}$$

where the subscripts specify the probability density for the respective chains. Two slices separated by about 10 Å in depth coinciding with the chromanol group (slice A) and well below within the phytyl side chain (slice B) are shown. They are color-coded contour maps in which $\Delta\rho > 0$ indicates a higher probability density for the *sn*-2 chain whereas $\Delta\rho < 0$ indicates a higher probability density for the *sn*-1 chain. There is a small central region where $\Delta\rho = 0$ that corresponds to the location of the chromanol group in slice A. Such a region is absent in slice B which does not intersect with the chromanol group. In the case of SDPC, it is clear from slice A that around the chromanol group the probability of finding DHA (*sn*-2 chain) substantially exceeds SA (*sn*-1 chain). Lower down in the bilayer at slice

B, the probability of more DHA than SA is no longer found and a largely uniform probability distribution exists across the entire slice. The situation differs in SOPC. Only a small differential exists between the probability of finding OA (*sn*-2 chain) and SA (*sn*-1 chain) around the chromanol group in slice A. In slice B, there is more SA than OA throughout.

The higher probability that DHA will be near the chromanol group can be explained in terms of the tremendous flexibility of the polyunsaturated chain, which leads to very low order parameters (S_{CD} < 0.05) throughout the entire DHA chain that are minimally perturbed by the presence of αtoc in SDPC (Fig. 3.3). With the exception of the very top portion, the DHA chain in SDPC moves through all conformational space in 50 ns [71]. A greater density for DHA near the membrane surface, as opposed to the more rigid SA chain that has greater density in the middle of the membrane, is the result [72]. This arrangement ensures that all parts of the DHA chain frequently approach the hydroxyl group on the chromanol group that is responsible for the antioxidant function of αtoc.

3.3.3 Flip-flop of α-tocopherol

Figure 3.7 uncovers another aspect of the behavior of αtoc in a polyunsaturated environment with potential significance for the role of vitamin E as an antioxidant. In this figure the trajectory in the transbilayer (z) direction for the C5 position on the chromanol group of one of the αtoc molecules in the SDPC bilayer is plotted over 60 ns of simulation. The plot demonstrates that, although the chromanol group usually sits at its canonical depth near the aqueous interface, the αtoc molecule also undergoes flip-flop across the bilayer. At around 50 ns the C5 position jumps from one side of the bilayer to the other and subsequently back at around 75 ns. The "jumps" are abrupt, ~5 ns in duration. During them, as illustrated in 3 snapshots taken during the first "jump" (Fig. 7), the αtoc molecule adopts short-lived conformations that include lying in the middle of the bilayer approximately parallel to the plane. A total of 22 flip-flops were counted throughout 180 ns for all 20 αtoc molecules in the bilayer, from which a lifetime of 0.16 μs (equivalent to half-life $t_{1/2}$ = 0.11 μs) in SDPC was estimated. This rate is $>10\times$ faster than in SOPC where only 2 flip-

flops of αtoc molecules, corresponding to a lifetime of 1.8 μs ($t_{1/2}$ = 1.2 μs), transpired under the same circumstances.

Flip-flop of phospholipids across protein-free membranes has long been recognized to be extremely slow [73]. Passage through the hydrophobic interior is energetically unfavorable for the hydrophilic head groups. A timescale of hours applies to the half-lives that have been measured by a variety of techniques, with the values depending upon head group and chain composition [74,75]. Half-lives of 0.29 and 11.5 h describe the flip-flop of fluorescently labeled 7-nitrobenz-2-oxa-1,3-diazol-4-yl phosphatidylethanolamine in SDPC and SOPC bilayers, respectively, at 25 °C [75]. They represent an increase in rate by a factor of $40\times$ for the polyunsaturated membrane.

Very little attention has been paid to the flip-flop of αtoc. Estimates of the rate have been gleaned from only a sparse collection of MD simulations and experiments. There is an enormous discrepancy in the literature between the values according to these two approaches. Like in the current work, translocation of αtoc from one leaflet to the other was observed in recently published simulations run for ~200 ns on several phospholipid bilayers in a highly fluid state at 350 K [63,70]. A timescale of hours or longer, quite the reverse, was inferred in experimental studies conducted 3 decades ago monitoring the exchange of αtoc between the inner and outer layers of sonicated unilamellar vesicles (SUV) [76,77]. In our hands, however, assays of the oxidation of αtoc in PC vesicles showed complete loss of a fluorescence signal from αtoc on both sides of the bilayer in only a few minutes following the addition of potassium ferricyanide (unpublished data). There was no hint of long-term rate limitation brought about by flip-flop from the inner to outer leaflet. The very slow speed of transmembrane migration indicated for αtoc by the early work is difficult to understand. Methyl groups on either side (positions 5 and 7) shield the hydroxyl group in the chromanol moiety (Fig. 1), which should help overcome the energy barrier to movement through the hydrophobic core of the membrane. MD simulations on δ-tocopherol (δtoc), where neither position next to the hydroxyl group is methylated, in SDPC support this notion. There were only 2 flip-flops over 180 ns for δtoc in simulations that we ran under conditions identical to those on αtoc. Why flip-flop of αtoc should be much slower than cholesterol for which seconds characterize the process [78] is also a

mystery. Both molecules are structurally similar, composed of a rigid head group possessing a hydroxyl group at one end and a branched hydrocarbon chain at the opposite end.

3.4 Discussion

αToc is the form of vitamin E that is a required component in the human diet. The primary function of this lipophilic antioxidant is to protect lipids, especially polyunsaturated phospholipids, in membranes against oxidation [79,80]. To accomplish this purpose it traps a lipid peroxyl radical to break a chain of reactions that once initiated can oxidize many lipid molecules, and is subsequently restored by a water-soluble reducing agent such as ascorbate. Here we have, for the first time, performed atomistic MD simulations on the molecular organization of αtoc in a polyunsaturated phospholipid membrane. SDPC and SOPC bilayers in the absence and presence of 20 mol% αtoc were compared. SDPC is a polyunsaturated phospholipid that is representative of lipid species most susceptible to oxidative attack, while SOPC serves as a monounsaturated control that is much less vulnerable to such an assault.

The simulations capture the essence of the results from solid state ^{2}H NMR and neutron diffraction experiments that were carried out to provide validation. The same distinctive shape defines the variation of order parameter along the SA chain at the *sn*-1 position in SDPC and SOPC obtained from the simulations and by analysis of ^{2}H NMR spectra (Fig. 2). There is a plateau region of essentially uniform order in the upper portion of the chain and then in the lower portion order drops off progressively more quickly towards the terminal methyl group. In line with the NMR derived data, the profiles generated in silico demonstrated that SDPC is much more disordered than SOPC while the introduction of αtoc increases order by comparable amounts in both SDPC and SOPC. In accordance with the neutron diffraction measurements, the location of maxima attributable to the phosphate and glycerol-ester regions in the NSLD profile calculated from MD simulations showed that the thickness of the bilayer for SDPC is smaller than SOPC (Fig. 4). Both methods also placed the C5 position on the chromanol group of αtoc near the aqueous interface in the two membranes.

By comparing SDPC and SOPC bilayers, our simulations reveal aspects of molecular organization that help αtoc prevent the oxidation of polyunsaturated phospholipids. The extraordinary disorder possessed by PUFA chains, which promotes contact with the sacrificial hydroxyl group on the chromanol moiety, is key. The extremely low order parameters that characterize the profile of order along the DHA chain at the *sn*-2 position in SDPC (Fig. 3) are indicative of a rapidly varying conformation that redistributes the lower portion towards the bilayer surface [72,81]. There is consequently, as depicted in maps of acyl chain density generated from the simulated data (Fig. 6), increased likelihood that polyunsaturated chains reside in the immediate vicinity of the chomanol group on αtoc molecules. It is also apparent from plots of trajectories in the transbilayer direction that αtoc flip-flops across the bilayer in SDPC on a sub-microsecond timescale (Fig. 7), which is >10x more often than seen in SOPC. The frequent tunneling of αtoc through the fluid interior of an SDPC bilayer further enhances the chance that a chromanol group meets a polyunsaturated chain.

The findings from the MD simulations presented in this study, taken together, provide unprecedented structural insight into the molecular mechanism by which αtoc can efficiently inhibit the oxidation of polyunsaturated phospholipids in a membrane. They demonstrate how the hydroxyl group on the chromanol moiety, the reducing group in αtoc, is readily accessible to a lipophilic peroxyl radical formed anywhere within a PUFA chain and to water-soluble radicals that are necessary to restore antioxidant activity. The majority of the time the chromanol group sits near the membrane surface where water-soluble radicals easily reach it and intrinsic disorder brings even the lowest portion of polyunsaturated chains into close proximity on a regular basis. Flip-flop of αtoc, in addition, carries the chromanol group into the membrane interior and then back to the surface. This motion is made easier by loosely packed PUFA chains and by methyl groups at adjacent positions on the chromanol moiety that screen the hydroxyl group from the hydrophobic environment within a bilayer. It is emphasized that αtoc does not directly protect PUFA, but instead interacts with free radical intermediates formed during the series of reactions by which peroxidation proceeds. Our interpretation assumes that oxidized lipid chains retain high conformational mobility, which is implied by earlier work [82]. The situation is obviously more complex in a biological membrane. Because the concentration of αtoc is

small, typically in the range 0.1-1.0 mol% total phospholipid [25], lateral distribution relative to polyunsaturated phospholipids is another issue that affects its efficacy as an antioxidant. We have postulated that αtoc clusters together with polyunsaturated phospholipids in domains, thereby locally compensating for its overall scarcity (11,16). This arrangement would facilitate frequent encounters with lipid peroxyl radicals by the mechanisms identified here.

In summary, an understanding of the role molecular structure plays in αtoc stopping the oxidation of polyunsaturated phospholipids in membranes emerges from our MD simulations. The simulations on SDPC show that the chromanol group lies in wait to meet DHA chains that move up to the surface of the bilayer and, remarkably, travels down into the inside of the bilayer as well. Thus, mechanisms by which αtoc not only can intercept lipid peroxyl radicals at the surface of a membrane but can also patrol the inside of the membrane are identified. By predominantly sitting with the chromanol group near the membrane surface, moreover, access to water soluble reducing agents that recycle α-tocopheroxyl radicals formed when lipid peroxyl radicals are trapped is assured. We conclude from our results that αtoc is a lipid-soluble antioxidant that is well designed to protect polyunsaturated phospholipids in cell membranes.

3.5 References

[1] Zingg, J.M. 2007. Vitamin E: an overview of major research directions. *Mol. Aspects Med.* 28:400-422.

[2] Niki, E. and M.G. Traber. 2012. A history of vitamin E. *Ann. Nutr. Metab.* 61:207-212.

[3] Ulatowski, l. and D. Manor. 2013. Vitamin E trafficking in neurologic health and disease. *Ann. Rev. Nutr.* 33:87-103.

[4] Packer, L. 1994. Vitamin E is nature's master antioxidant. *Sci. Am. Sci. Med.* 1:54-63.

[5] Wang, X. and P.J. Quinn. 1999. Vitamin E and its function in membranes. *Prog. Lipid Res.* 38:309-336.

[6] Traber, M.G. and J. Atkinson. 2007. Vitamin E, antioxidant and nothing more. *Free Rad. Biol. Med.* 43:4-15.

[7] Burton, G.W. and K.U. Ingold. 1986. Vitamin E: application of the principles of physical organic chemistry to the exploration of its structure and function. *Acc. Chem. Res.* 19:194-201.

[8] Alessi, M., T. Paul, J.C. Scaiano and K.U. Ingold. 2002. The contrasting kinetics of peroxidation of vitamin E-containing phospholipid unilamellar vesicles and human low-density lipoprotein. *J. Amer. Chem. Soc.* 124:6957-6965.

[9] Diplock, A.T. and J.A. Lucy. 1973. The biochemical modes of action of vitamin E: a hypothesis. *FEBS Lett.* 29:205-210.

[10] Kagan, V.E. 1989. Tocopherol stabilizes membranes against phospholipase A, free fatty acids, and lysophospholipids. *Annals. NY Acad. Sci.* 570:121-135.

[11] Atkinson, J., T. Harroun, S.R. Wasssall, W. Stillwell and J. Katsaras. 2010. The location and behavior of α-tocopherol in membranes. *Mol. Nutr. Food Res.* 54:641-651.

[12] Marquardt, D., J.A. Williams, N. Kučerka, J. Atkinson, S.R. Wassall, J. Katsaras and T.A. Harroun. 2013. Tocopherol activity correlates with its location in a membrane: a new perspective on the anti-oxidant vitamin E. *J. Amer. Chem. Soc.* 135:7523–7533.

[13] Marquardt, D., N. Kučerka, J. Katsaras and T.A. Harroun. 2015. α-Tocopherol's location in membranes is not affected by their composition. *Langmuir* 31:4464-4472.

[14] Stillwell, W. and S.R. Wassall. 2003. Docosahexaenoic acid: membrane properties of a unique fatty acid. 2003. *Chem. Phys. Lipids* 126:1-27.

[15] Salem, N., Jr., H-Y. Kim and J.A. Yergey. 1986. Docosahexaenoic acid: membrane function and metabolism. *In* Health Effects of Polyunsaturated Fatty Acids in Seafoods. A.P. Simopoulos, R.R. Kifer and R.E. Martin, editors. Academic Press, New York. 263-317.

[16] Wassall, S.R., and W. Stillwell. 2009. Polyunsaturated fatty acid–cholesterol interactions: Domain formation in membranes. *Biochim. Biophys. Acta* 1788:24-32.

[17] Shaikh, S.R. 2012. Biophysical and biochemical mechanisms by which dietary N-3 polyunsaturated fatty acids from fish oil disrupt membrane lipid rafts. *J. Nutr. Biochem.* 23:101-105.

[18] Salem, N., Jr., B. Litman, H-Y. Kim and K. Gawrisch. 2001. Mechanisms of action of docosahexaenoic acid in the nervous system. *Lipids* 36:845-959.

[19] Niu, S-L., D.C. Mitchell, S-Y. Lim, Z-M. Wen, N. Salem Jr. and B.J. Litman. 2004. Reduced G protein-coupled signaling efficiency in retinal rod outer segments in response to *n*-3 fatty acid deficiency. *J. Biol. Chem.* 279:31098-31104.

[20] Brown, M.F. 1994. Modulation of rhodopsin function by properties of the membrane bilayer. *Chem. Phys. Lipids* 73:159-180.

[21] Gawrisch, K., O. Soubias and M. Mihailescu. 2008. Insights from biophysical studies on the role of polyunsaturated fatty acids for function of G-protein coupled membrane receptors. *Prost. Leuk. Essent. Fatty Acids* 79:131-134.

[22] Shaikh S.R., J.J. Kinnun, X. Leng, J.A. Williams and S.R. Wassall. 2015. How polyunsaturated fatty acids modify molecular organization in membranes: insight from NMR studies of model systems. *Biochim. Biophys. Acta* 1848:211-219.

[23] Feller, S.E. 2008. Acyl chain conformations in phospholipid bilayers: a comparative study of docosahexaenoic acid and saturated fatty acids, *Chem. Phys. Lipids* 153:76-80.

[24] Ingold, K.U., V.W. Bowry, R. Stocker and C. Walling. 1993. Autoxidation of lipids and antioxidation by α-tocopherol and ubiquinol in homogeneous solution and in aqueous dispersions of lipids: unrecognized consequences of lipid particle size as exemplified by oxidation of human low density lipoprotein. *Proc. Natl. Acad. Sci. USA* 90:45-49.

[25] Atkinson, J., R.F. Epand and R.M. Epand 2008. Tocopherols and tocotrienols in membranes: a critical review. *Free Rad. Biol. Med.* 44:739-764.

[26] Saiz, L. and M.L. Klein. 2001. Structural properties of a highly polyunsaturated lipid bilayer form molecular dynamics simulations. *Biophys. J.* 81:201-216.

[27] Feller, S.E., K. Gawrisch and A.D. MacKerell Jr. 2002. Polyunsaturated fatty acids in lipid bilayers: intrinsic and environmental contributions to their unique physical properties. *J. Amer. Chem. Soc.* 124:318-326.

[28] Huber, T., K. Rajamoorthi, V.F. Kurze, K. Beyer and M.F. Brown. 2002. Structure of docosahexaenoic acid-containing phospholipid bilayers as studied by ^{2}H NMR and molecular dynamics simulations. *J. Amer. Chem. Soc.* 124:298-309.

[29] Jo, S., T. Kim, V.G. Iyer and W. Im. 2008. CHARMM-GUI: a web-based graphical user interface for CHARMM. *J. Comput. Chem.* 29:1859-1865.

[30] Jo, S., J.B. Lim, J.B. Klauda and W. Im. 2009. CHARMM-GUI Membrane Builder for mixed bilayers and its application to yeast membranes. *Biophys. J.* 97:50-58.

[31] Klauda, J.B., R.M. Venable, J.A. Freites, J.W. O'Connor, D.J. Tobias, C. Mondragon-Ramirez, I. Vorobyov, A.D. MacKerell, Jr. and R.W. Pastor. 2010. Update of the CHARMM all-atom additive force field for lipids: validation on six lipid types. *J. Phys. Chem. B.* 114:7830-7843.

[32] Klauda, J.B., V. Monje, T. Kim and W. Im. 2012. Improving the CHARMM force field for polyunsaturated fatty acid chains. *J. Phys. Chem. B* 116:9424−9431.

[33] Darden, T., D. York and L. Pedersen. 1993. Particle mesh Ewald: an *N*-log(*N*) method for Ewald sums in large systems. *J. Chem. Phys.* 98:10089-10092.

[34] Hoover, W.G. 1985. Canonical dynamics: equilibrium phase-space distributions. *Phys. Rev. A* 31:1695-1697.

[35] Nosé, S. and M.L. Klein. 1983. A study of solid and liquid carbon tetrafluoride using the constant pressure molecular dynamics technique. *J. Chem. Phys.* 72:6928-6939.

[36] Romo, T.D. and A. Grossfield. 2009. LOOS: an extensible platform for the structural analysis of simulations. *Proc. Int. IEEE EMBS Conf., 31st*. 2332-2335.

[37] Humphrey, W., A. Dalke and K. Schulten. 1996. VMD: visual molecular dynamics. *J. Mol. Graphics.* 14:33-38.

[38] Marquardt, D., J.A. Williams, J.J. Kinnun, N. Kučerka, J. Atkinson, S.R. Wassall, J. Katsaras and T.A. Harroun. 2014. Dimyristoyl phosphatidylcholine: A remarkable exception to α-tocopherol's membrane presence. *J. Amer. Chem. Soc.* 136:203-210.

[39] Brzustowicz, M.R., V. Cherezov, M. Caffrey, W. Stillwell and S.R. Wassall. 2002. Molecular organization of cholesterol in polyunsaturated membranes: microdomain formation. *Biophys. J.* 82:285-298 (2002).

[40] Williams, J.A., S.E. Batten, M. Harris, B.D. Rockett, S.R. Shaikh, W Stillwell and S.R. Wassall. 2013. Docosahexaenoic and eicosapentaenoic acids segregate differently between raft and nonraft domains. *Biophys. J.* 103:228-237.

[41] Davis, J.H., K,R. Jeffrey, M. Bloom, M.I. Valic and T.P. Higgs. 1976. Quadrupolar echo deuteron magnetic resonance spectroscopy in ordered hydrocarbon chains. *Chem. Phys. Lett.* 42:390-394.

[42] Davis, J.H. 1983. The description of membrane lipid conformation, order and dynamics by ^{2}H NMR. *Biochim. Biophys. Acta* 737:117-171.

[43] McCabe, M.A. and S.R. Wassall. 1997. Rapid deconvolution of NMR powder spectra by weighted fast Fourier transformation. *Solid State Nucl. Magn. Reson.* 10:53-61.

[44] Lafleur, M., B. Fine, E. Sternin, P.R. Cullis and M. Bloom 1989. Smoothed orientational order profile of lipid bilayers by ^{2}H-nuclear magnetic resonance. *Biophys. J.* 56:1037-1041.

[45] Seelig, J. 1977. Deuterium magnetic resonance theory and application to lipid membranes. *Q. Rev. Biophys.*10:353-418.

[46] Holte, L.L., Separovic, F. and Gawrisch, K. 1996. Nuclear magnetic resonance investigation of hydrocarbon chain packing in polyunsaturated phospholpids. Lipids 31:S199-S203.

[47] Vermeer, L.S., B.L. de Groot, V. Réat, A. Milon and J. Czaplicki. 2007. Acyl chain order parameter profiles in phospholpid bilayers: computation from molecular dynamics simulations and comparison with ^{2}H NMR experiments. *Eur. Biophys. J.* 36:919-931.

[48] Mallikarjunaiah, K.J., A. Leftin, J.J. Kinnun, M.J. Justice, A.L. Rogozea, H.I. Petrache and M.F. Brown. 2011. Solid-state ^{2}H NMR shows equivalence of dehydration and osmotic pressures in lipid membrane deformation. *Biophys. J.* 100:98-107.

[49] Koerner, M.M., L.A. Palacio, J.W. Wright, K.S. Schweitzer, B.D. Ray and H.I. Petrache. 2011. Electrodynamics of lipid membrane interactions in the presence of zwitterionic buffers. *Biophys. J.* 101:362-369.

[50] Bloom, M., J.H. Davis and M.I. Valic. 1980. Spectral distortion effects due to finite pulse widths in deuterium nuclear magnetic resonance spectroscopy. *Can. J. Phys.* 58:1510-1517.

[51] Schäfer, H., B. Mädler and E. Sternin. 1998. Determination of orientational order parameters from ^{2}H NMR spectra of magnetically partially oriented lipid bilayers. *Biophys. J.* 74:1007-1014.

[52] Wassall, S.R., J.L. Thewalt, L. Wong, H. Gorrissen and R.J. Cushley 1986. Deuterium NMR study of the interaction of alpha-tocopherol with a phospholipid model membrane. *Biochemistry* 25:319-326.

[53] Suzuki, Y.J., M. Tsuchiya, S.R. Wassall, Y.M. Choo, G. Govil, V.E. Kagan and L. Packer. 1993. Structural and dynamic membrane properties of α-tocopherol and α-tocotrienol: implication to the molecular mechanism of their antioxidant potency. *Biochemistry* 32:10692-10699.

[54] Polozov, I., and K. Gawrisch. 2007. NMR detection of lipid domains. *Methods Mol. Biol.* 398:107-126.

[55] Mihailescu, M., O. Soubias, D. Worcester, S. H. White and K. Gawrisch. 2011. Structure and dynamics of cholesterol-containing polyunsaturated lipid membranes studied by neutron diffraction and NMR. *J. Membrane Biol.* 239:63-71.

[56] Gawrisch, K. and O. Soubias. 2008. Structure and dynamics of polyunsaturated hydrocarbon chains in lipid bilayers – significance for GPCR function. *Chem. Phys. Lipids* 153:64-75.

[57] Seelig, J. and N. Waespe-Sarcevic. 1978. Molecular order in cis and trans unsaturated phospholipid bilayers. *Biochemistry* 17:3310-3315.

[58] Wassall, S.R., M.A. McCabe, C.D. Wassall, R.O. Adlof and S.E. Feller. 2010. Solid state ^{2}H NMR and MD simulations of positional isomers of a monounsaturated phospholipid membrane: Structural implications of double bond location. *J. Phys. Chem. B* 114:11474-11483.

[59] Soni, S.P., J.A. Ward, S.E. Sen, S.E., Feller and S.R. Wassall. 2009. Effect of *trans* unsaturation on molecular organization in a phospholipid membrane. *Biochemistry* 48:11097-11107.

[60] Engel, A.K. and D. Cowburn. 1981. The origin of multiple quadrupole couplings in the deuterium NMR spectra of the 2 chain of 1,2 dipalmitoyl-sn-glycero-3-phosphorylcholine. *FEBS Lett.* 126:169-171.

[61] Feller, S.E., K. Gawrisch and A.D. MacKerell. 2002. Polyunsaturated fatty acids in lipid bilayers: intrinsic and environmental contributions to their unique physical properties. *J. Amer. Chem. Soc.* 124:318-326.

[62] Harroun, T.A., J. Katsaras and S.R. Wassall. 2006. Cholesterol hydroxyl group is found to reside in the center of a polyunsaturated lipid membrane. *Biochemistry* 45:1227-1233.

[63] Qin, S-S. and Z-W. Yu. 2011. Molecular dynamics simulations of α-tocopherol in model membranes. *Acta Phys. –Chim. Sin.* 27:213-227.

[64] Fukuzawa, K., W. Ikebata, A. Shibata, T. Sakanaka and S. Urano. 1993. Location of α-tocopherol in phospholipid vesicles and its dynamics in inhibiting lipid peroxidation. *In* Vitamin E: its Usefulness in Health and in Curing Diseases. M. Mino, H. Nakamura, A.T. Diplock and H.J. Kayden, editors. Japan Scientific Societies Press, Tokyo, Japan, 31-40.

[65] Bisby, R.H. and S. Ahmed, S. 1989. Transverse distribution of α-tocopherol in bilayer membranes studied by fluorescence quenching. *Free Rad. Biol. Med*. 6:231-239.

[66] Gomez-Fernandez, J.C., J. Villalain, F.J. Aranda, A. Ortiz, V. Micol, A. Coutinho, N.M. Berberan-Santos and J.E. Prieto. 1989. Location of α-tocopherol in membranes. *Ann. NY Acad. Sci.* 570:109-120.

[67] Urano, S., M. Matsuo, T. Sakanaka, I. Uemura, M. Koyama, I. Kumadaki and K. Fukuzawa. 1993. Mobility and molecular orientation of vitamin E in liposomal membranes as determined by ^{19}F NMR and fluorescence polarization techniques. *Arch. Biochem. Biophys.* 303:10-14.

[68] Afri, M., B. Ehrenberg, Y. Talmon, J. Schmidt, Y. Cohen and A.A. Frimer. 2004. Active oxygen chemistry within the liposomal bilayer. Part III: Locating vitamin E, ubiquinol and ubiquinone and their derivatives in the lipid bilayer. *Chem. Phys. Lipids* 131:107–121.

[69] Perly, B., I.C.P. Smith, L. Hughes, G.W. Burton and K.U. Ingold. 1985. Estimation of the location of natural α-tocopherol in lipid bilayers by ^{13}C-NMR spectroscopy. *Biochim. Biophys. Acta* 819:131-135.

[70] Qin, S-S., Z-W. Yu and Y-X. Yu. 2009. Structural and kinetic properties of α-tocopherol in phospholipid bilayers, a molecular dynamics simulation study. *J. Phys. Chem. B* 113:16537-16546.

[71] Soubias, O., K. Gawrisch. 2007. Docosahexaenoyl chains isomerize on the sub-nanosecond time scale. *J. Am. Chem. Soc.* 129:6678-6679.

[72] Mihailescu, M. and K. Gawrisch. 2005. The structure of polyunsaturated lipid bilayers important for rhodopsin function: a neutron diffraction study. *Biophys. J.* 90:L4-L6.

[73] Contreras, F.-X., L. Sánchez-Magraner, A. Alonso and F.M. Goni. 2010. Transbilayer (*flip-flop*) lipid motion and lipid scrambling in membranes. *FEBS Lett.* 584:1779-1786.

[74] Homan, R. and H.J. Pownall. 1988. Transbilayer diffusion of phospholipids: dependence on headgroup structure and acyl chain length. *Biochim. Biophys. Acta* 938:155-166.

[75] Armstrong, V.T., M.R. Brzustowicz, S.R. Wassall, L.J. Jenski and W. Stillwell. 2003. Rapid flip-flop in polyunsaturated (docosahexaenoate) phospholipid membranes. *Arch. Biochem. Biophys.* 414:74-82.

[76] Bellemare, F. and M. Fragata. 1981. Transmembrane distribution of α-tocopherol in single-lamellar mixed lipid vesicles. *J. Membrane Biol.* 58:67-74.

[77] Tyurin, V.A., V.E. Kagan, E.A. Serbinova, N.V. Gorbunov, A.N. Erin, L.L. Prilipko and Ts.S. Stoichev, 1986. Interaction of α-tocopherol with phospholipid liposomes: absence of transbilayer mobility. *Bull. Exp. Biol. Med.* 102:1677–1680.

[78] Hamilton, J.A. 2003. Fast flip-flop of cholesterol and fatty acids in membranes: Implications for membrane transport proteins. *Curr. Opin. Lipidol.* 14:263-271.

[79] Niki, E. 2014. Role of vitamin E as a lipid-soluble peroxyl radical scavenger: in vitro and in vivo evidence. *Free Rad. Biol. Med.* 66:3-12.

[80] Lebold, K.M. and M. Traber. 2014. Interactions between α-tocopherol, polyunsaturated fatty acids, and lipoxygenases during embryogenesis. *Free Rad. Biol. Med.* 66:13-19.

[81] Eldho, N.V., S.E. Feller, S.Tristram-Nagle, I.V. Polozov and K. Gawrisch. 2003. Polyunsaturated docosahexaenoic vs. docosapentaenoic acid-differences in lipid matrix properties from the loss of one double bond. *J. Amer. Chem. Soc*. 25:6409–6421.

[82] Garrec, A., A. Monari, X. Assfeld, L.M. Mir and M. Tarek. 2014. Lipid peroxidation in membranes: The peroxyl radical does not “float”. *J. Phys. Chem. Lett.* 5:1653-1658.

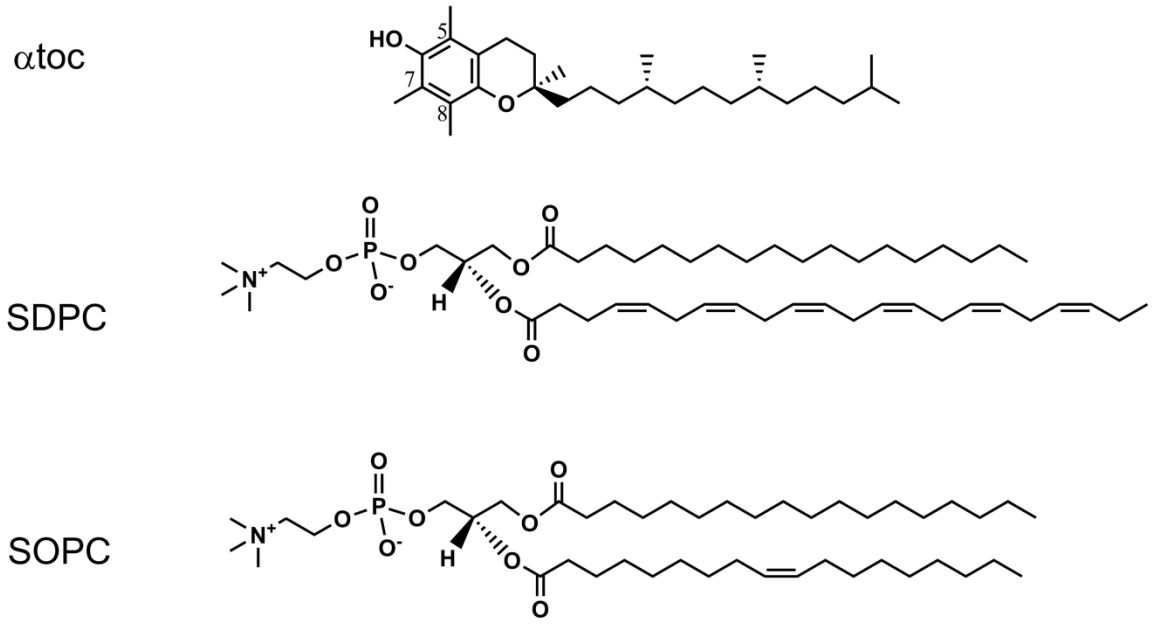

Figure 3.1

Molecular structure of αtoc, SDPC and SOPC.

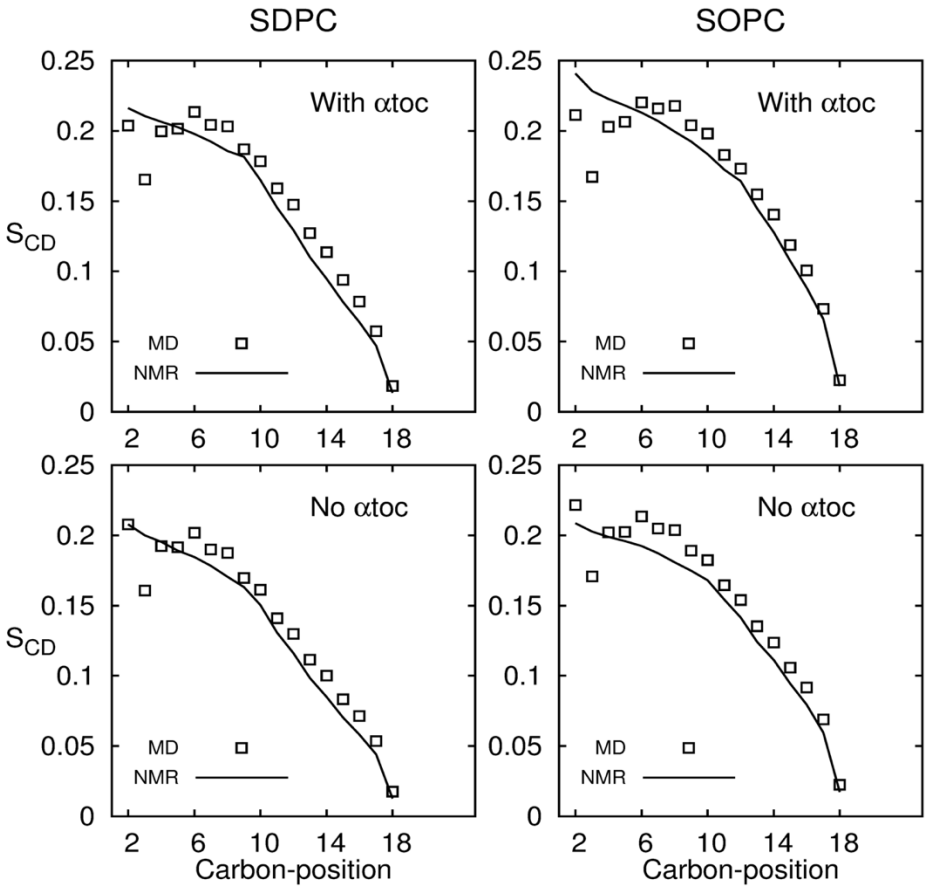

Figure 3.2

Order parameter profiles along the *sn*-1 chain in SDPC and SOPC at 37 ºC obtained from MD simulations (□) and FFT depaked ^{2}H NMR spectra (continuous line). The lower left panel is for SDPC and the upper left panel is for SDPC + 20 mol% αtoc, while the lower right panel is for SOPC and the upper right panel is for SOPC + 20 mol% αtoc. Figure A1.2 included in the Supporting Material shows the effect of αtoc on the order parameter profiles obtained from the MD simulations and ^{2}H NMR experiments separately. The uncertainty in the simulated data is ≤±2%, which was estimated from the standard error obtained treating each lipid molecule independently. A reproducibility of ±2% applies to the NMR data.

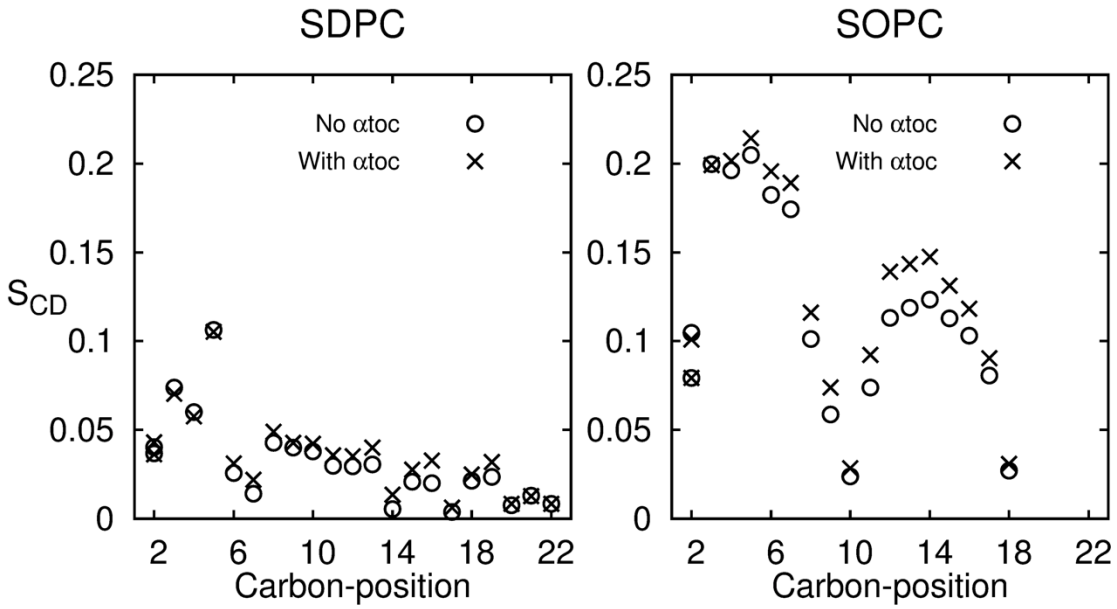

Figure 3.3

Order parameter profiles along the *sn*-2 chain in SDPC and SOPC at 37 ºC obtained from MD simulations. The left panel is for SDPC (○) and SDPC + 20 mol% αtoc (x), while the right panel is for SOPC (○) and SOPC + 20 mol% αtoc (x).

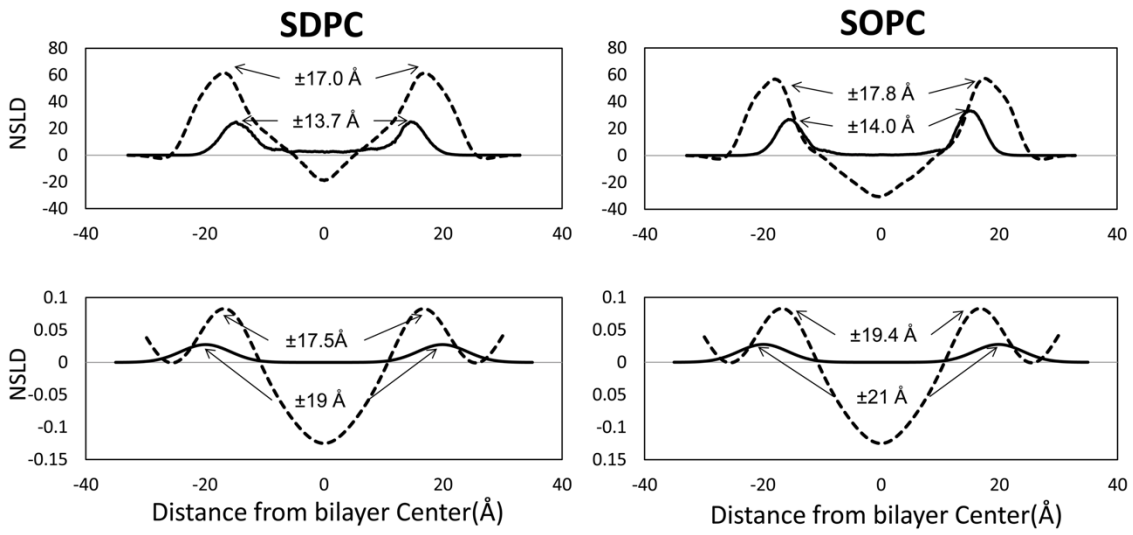

Figure 3.4

Neutron scattering length density (NSLD) profiles for SDPC+ 20 mol% αtoc (left) and SOPC + 20 mol% αtoc (right) at 37 ºC obtained from MD simulations (upper panel) and neutron diffraction experiments (lower panel). The dashed line is the profile for all lipids (phospholipid and αtoc), while the solid line is the profile for deuterium on the C5 position of the chromanol group in αtoc (amplified in intensity for comparison). The uncertainty in the location of the center of the peak for the C5 position is ±0.3 Å in SDPC and SOPC (MD simulations), and ±1.5 Å in SDPC and ±1.0 Å in SOPC (neutron diffraction experiments).

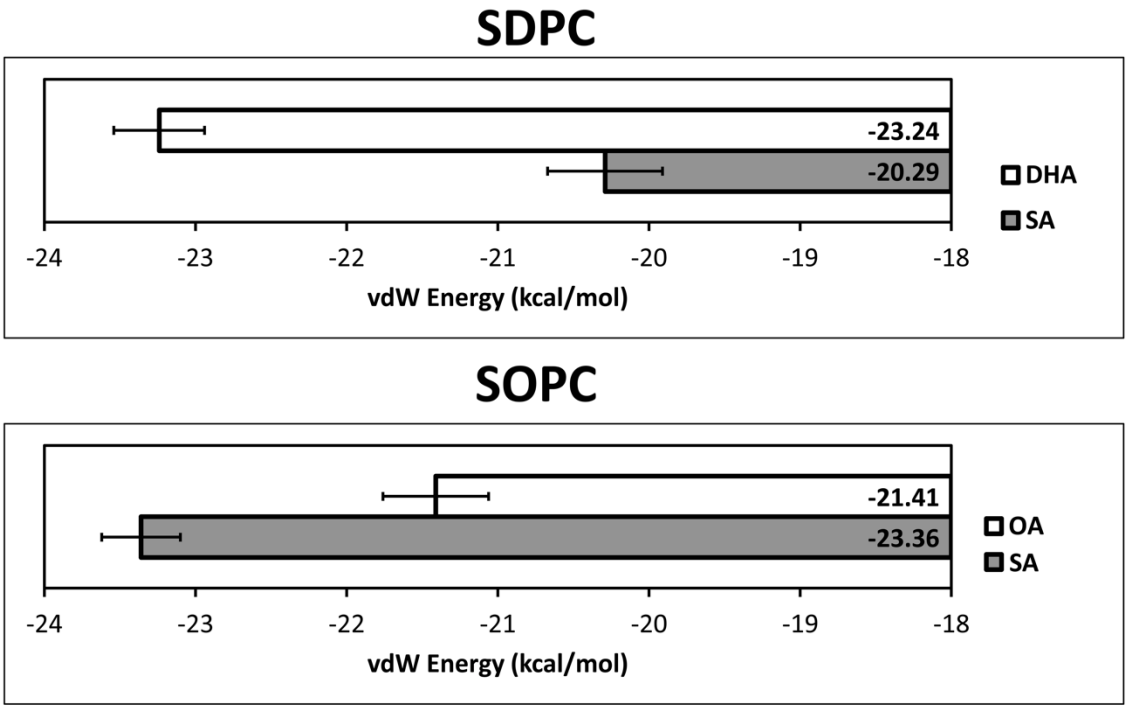

Figure 3.5

van de Waals (vdW) energy for the interaction of αtoc with the *sn*-1 chain (clear bar) and *sn*-2 chain (grey bar) of the phospholipid in SDPC + 20 mol% αtoc (upper panel) and SOPC + 20 mol% αtoc (lower panel). The values plotted are an average over time for all αtoc molecules, and the errors were calculated based on the values for each αtoc molecule.

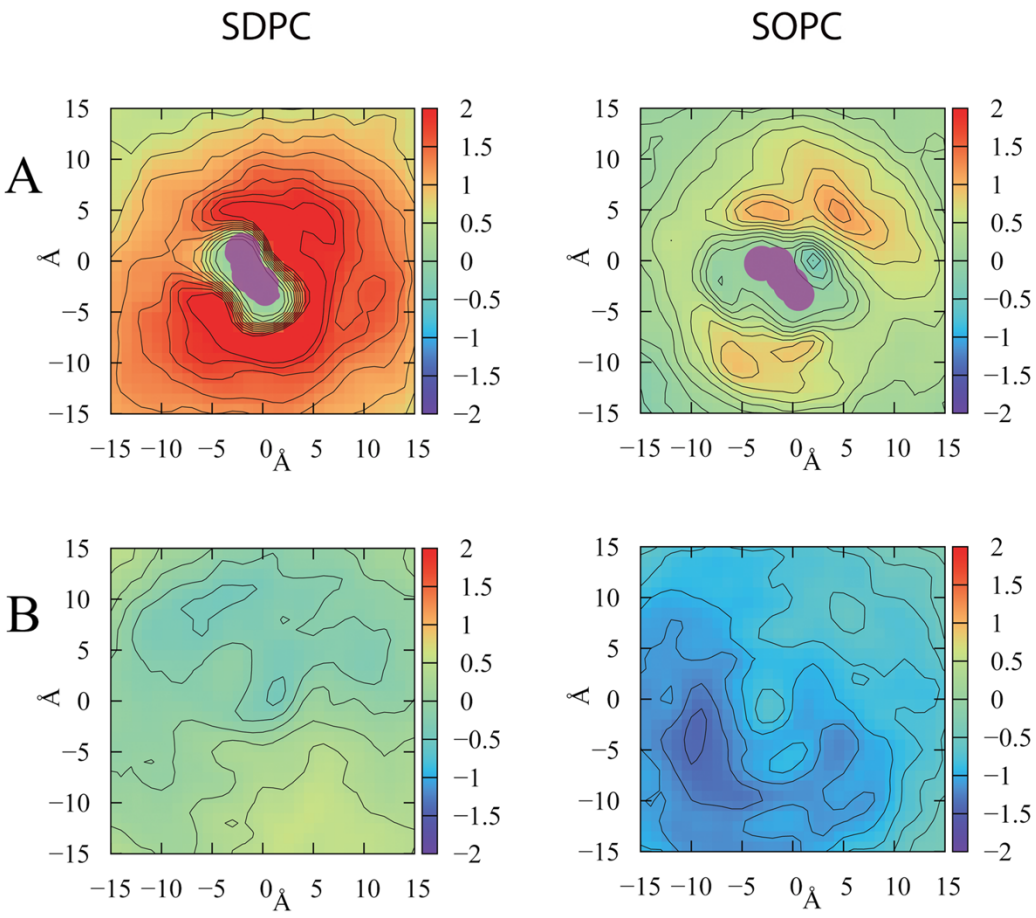

Figure 3.6

Color-coded contour maps of the difference in probability density ($\Delta\rho = \rho_2 - \rho_1$) for the carbons on the *sn*-1 and -2 chains in SDPC and SOPC around αtoc. The unit for ρ is the number of carbons counted in 1×1×1 Å^3 bins over 180 ns of simulation. The densities were generated in a 30×30×30 Å^3 cube centered on αtoc. Two representative slices lying in the xy plane (parallel to membrane surface) at different depth are shown. Slice A intersects the chromanol group while slice B lays approximately 10 Å below. To place the scales for $\Delta\rho$ in context the respective average values for ρ_1 and ρ_2 in slice A are 3.95 and 5.15 for SDPC and 3.97 and 4.35 for SOPC, and in slice B and are 4.74 and 4.79 for SDPC and 4.97 and 4.01 for SOPC.

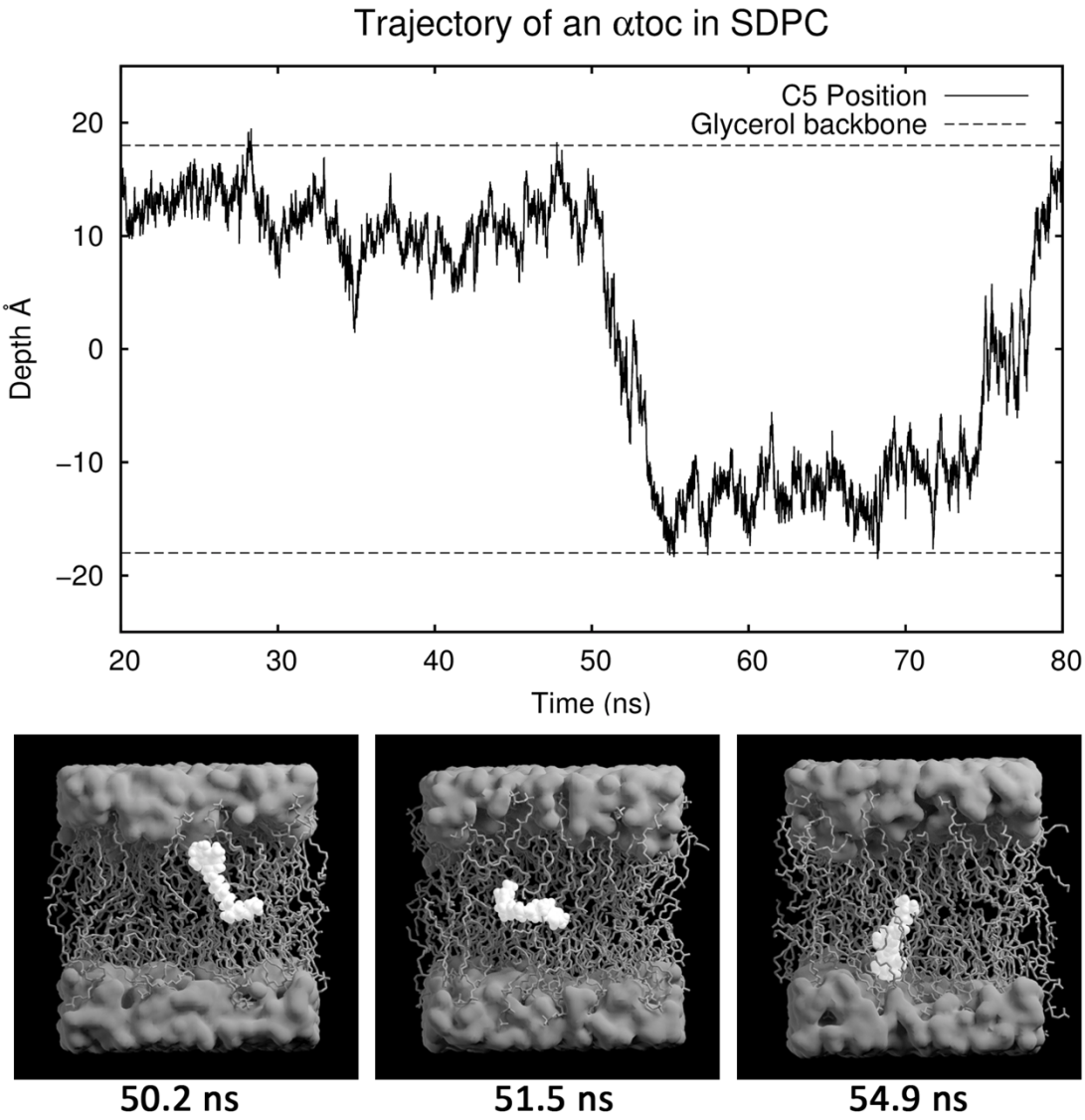

Figure 3.7

Trajectory in the transbilayer (z) direction of a representative αtoc molecule (continuous line indicates depth of C5 position on chromanol group) in SDPC (dashed line signifies location of glycerol backbone). Flip-flop of αtoc back and forth across the bilayer occurs at 50 and 75 ns. The 3 snapshots illustrate how the flip-flop occurs in short time (~5 ns). An enlarged version of the snapshots may be found in the Supporting Material (Fig. A1.5).

Supplemental Material

Appendix A1 contains one table and four figures, and references.

Acknowledgement

This work is reprinted from Biophysical Journal, 109(8), X. Leng, J. J. Kinnun, D. Marquardt, M. Ghefli, N. Kučerka, J. Katsaras, ... and S. R. Wassall, α-Tocopherol Is Well Designed to Protect Polyunsaturated Phospholipids: MD Simulations, 1608-1618, Copyright (2015), with permission from Elsevier.

CHAPTER 4. BINDING OF VITAMIN E TO LIPID BILAYERS: UMBRELLA SAMPLING MD SIMULATIONS

4.1 Introduction

Vitamin E stands for the name of a group of naturally occurring, biologically active tocol (tocopherol and tocotrienol) compounds [1,2]. α-Tocopherol (αtoc) is the form that is retained in the human body. This lipid soluble antioxidant is an essential micronutrient, neurological problems being among the symptoms of its deficiency [3]. There is general agreement that the primary function for αtoc is to protect polyunsaturated lipids that are extremely susceptible to attack from free radicals in membranes [2,4-6]. The growing consumption of fish oil supplements rich in omega-3 polyunsaturated fatty acids (n-3 PUFA) that are taken up into membrane phospholipids underscores the importance of this role [7-9]. Although the chemistry by which αtoc inhibits the peroxidation of lipid chains is known [10.11], an open question is whether preferential interaction with polyunsaturated lipids exists [12-14].

The αtoc molecule is composed of a chromanol head group with a hydroxyl group at one end and a phytyl chain at the other end (Figure 4.1). It usually resides in a membrane with the hydroxyl group near the aqueous interface while the phytyl chain extends towards the center [15, 16]. In this arrangement the sacrificial hydroxyl group traps lipid peroxyl radicals when they rise up to the surface of the membrane and subsequently is recycled by a water-soluble reducing agent such as ascorbate [17]. The general features of the location and orientation of αtoc in phospholipid bilayers are reproduced in the few atomistic MD simulations that have been published to date [18-20]. Our simulations demonstrated how efficiently αtoc is able to fulfill its antioxidant role in a polyunsaturated phospholipid bilayer [20]. They revealed that high disorder enhances the probability that a polyunsaturated chain comes into close proximity with the hydroxyl group on a chromanol group that resides at the surface of the bilayer. Additionally, we observed flip-flop for αtoc is fast, which suggests the hydroxyl group can also easily penetrate into the interior of a polyunsaturated membrane to intercept lipid peroxyl radicals.

Here we follow up on our earlier simulations with an umbrella sampling molecular dynamics (USMD) simulation study that compares the binding of αtoc to 1-stearoyl-2-docosahexaenoylphosphatidylcholine (SDPC, 18:0-22-6PC) and 1-stearoyl-2-oleoylphosphatidylcholine (SOPC, 18:0-18:1PC) bilayers. The molecular structure of SDPC with saturated stearic acid (SA, 18:0) for the *sn*-1 chain and docosahexaenoic acid (DHA, 22:6) containing 6 double bonds for the *sn*-2 chain is representative of a polyunsaturated phospholipid. SOPC where the *sn*-2 chain is replaced by oleic acid (OA, 18:1) that has a single double bond serves as a monounsaturated control (Figure 4.1). Does αtoc have a preference for polyunsaturated phospholipids, as has been hypothesized [12,14], is the question that we address.

4.2 Methods

4.2.1 MD simulations

We prepared two lipid membrane systems: SDPC with αtoc and SOPC with αtoc. In each case there are in total 80 PC lipid molecules and 2 αtoc molecules, which are divided equally between the two leaflets. The initial structures of these lipid bilayers were taken from our earlier published simulations containing 20 mol% αtoc, which have been equilibrated and run for over 200 ns [20]. We deleted the extra αtoc molecules, leaving two of them - one in each leaflet - to get the bilayer content we needed. In order to ensure enough room to allow an αtoc molecule to be fully pulled out of the bilayer into the aqueous phase, the bilayers were hydrated with 8562 water molecules that made a water layer of approximately 45 Å on each side. A harmonic constraint was applied to the two αtoc molecules to keep them 35 Å apart in the *xy* plane, which is approximately ½ the diagonal length of the bilayer, to minimize interactions between them during the umbrella sampling process. We used the CHARMM C36p force field for all simulations [21]. Non-bonded (van der Waals and short-range electrostatic) interactions were gradually switched off at 10 Å, and the long-range electrostatic interactions were calculated using the particle-mesh Ewald method [22]. Periodic boundary conditions were applied to a rectangular box in which the *x* and *y* dimensions (in the plane of the membrane) were held equal while the *z* dimension (in the direction of the membrane normal) was varied independently. The

temperature was kept at 37 °C by the Hoover thermostat [23] and the Langevin piston method was applied to maintain the pressure at 1 atm [24].

4.2.2 Umbrella sampling

With USMD simulations we obtained the free energy, known as the potential of mean force (PMF), as a function of αtoc's distance from the bilayer center. Then the energy cost of pulling an αtoc molecule out from the bilayer, which we call the binding energy, was determined from the corresponding PMF profile. The procedure was briefly as follows.

The distance along the direction (z) of the membrane normal between the center of the bilayer and the center of mass of the rigid chromanol headgroup on each αtoc molecule was chosen to represent the location of αtoc - the reaction coordinate. The αtoc molecules in both leaflets were restrained symmetrically with respect to the center of bilayer, which maintains the compositional balance of the bilayer and doubles the sampling efficiency. 45 windows i were simulated with the value of z_i varying from 0 to 44 Å in increments of 1 Å. In each window i, the αtoc molecules were restrained by a harmonic potential

$$U_i = k(z - z_i)^2 \tag{4.1}$$

with a force constant k = 3.68 kcal/(mol·m^2) at the corresponding z_i value. The initial structures in the windows were generated by a series of simulations that pulled the αtoc molecules from the equilibrium position to z = 0 Å or z = 44 Å with a speed of 1 Å/ns. The replica exchange method was applied during umbrella sampling to optimize the process. Production runs were performed with NAMD [25] on the Big Red II super computer at Indiana University. Their duration was 200 ns in each window, with the last 100 ns of the trajectories employed to perform the PMF calculation using the weighted histogram analysis method (WHAM) [26]. Errors were estimated following a method that has been previously described [26].

4.3 Results

4.3.1 Potential of mean force

Figure 4.2 shows the PMF (G(z)) vs. position relative to the center of the bilayer calculated from our simulations for αtoc in SDPC and SOPC. As expected, the shape of the plots

resembles that reported for cholesterol [27] - like αtoc, the sterol consists of a rigid moiety (tetracyclic ring) with a hydroxyl group at one end and a branched chain at the opposite end [14]. The variation of G(z) is flat where αtoc becomes completely disengaged from the membrane ($z \geq 35$ Å) in the water, and the baseline (G=0) is set there. When αtoc is brought into contact with phospholipid, G(z) starts to drop as αtoc penetrates more deeply within the membrane until the equilibrium location is reached (where $G(z) = G(z_{eq})$ exhibits a minimum). Then there is small increase in G(z) towards the center of the bilayer (z=0) that represents a barrier to movement from one side of the bilayer to the other. We define the binding energy of αtoc in the membrane to be $\Delta G_{bind} = -G(z_{eq}G(0)\text{-}G_{min})$ and the free energy barrier for the flip-flop of αtoc between leaflets to be $\Delta G_{flip} = G(0) - G(z_{eq}G(0)\text{-}G_{min})$. Table 4.1 lists the magnitude of these quantities for SOPC and SDPC. Also included in the table are values for the equilibrium depth z_{eq} of αtoc in the two bilayers (10.1 Å in SDPC and 11.4 Å in SOPC), which qualitatively agree with estimates made from our previous standard all-atom MD simulations (11.3 Å in SDPC and 11.8 Å in SOPC) [20]. Exact agreement is not be expected in view of the increase in bilayer order and thickness that accompanies the higher concentration of the vitamin in the earlier work (20 vs. 2.5 mol%).

4.3.2 Binding energy

The binding energy ΔG_{bind} evaluated here for αtoc by UBSMD simulations in SDPC (16.7 kcal/mol) is lower than in SOPC (18.3 kcal/mol) (Table 4.1). From the plots of PMF (Fig. 4.2), we can see that the differential originates in the interfacial region ($z \approx 35$ Å) where αtoc starts to interact with the membrane. An abrupt change in the slope of the PMF curve occurs there in SOPC, from flat when αtoc is entirely in the aqueous phase to an approximately linear decline as the phytyl sidechain and then the chromanol group penetrate more deeply into the bilayer. In SDPC, the change in slope of the PMF curve is initially more gradual ($31 \leq z \leq 35$ Å) and only subsequently at greater depth within the bilayer does the curve become approximately linear in slope. We attribute this behavior to the more loosely packed nature of the polyunsaturated bilayer. The PMF curve in SDPC consequently lies a bit above that in SOPC, resulting in a correspondingly smaller binding energy.

4.3.3 Membrane deformation

Insight into the effect of desorption of αtoc on membrane structure may be gleaned from inspection of the simulations obtained during umbrella sampling. Deformation of the SDPC and SOPC membrane is observed in the windows where αtoc has been partly pulled out from the membrane. Figure 4.3A shows this deformation as a plot of z(r), which is the average z coordinate (relative to the center of then bilayer) of the phosphorus atoms located on the PC head groups, against their lateral distance from αtoc in different windows – i.e. held at different depths in the membrane. The curves are mostly flat from window 0, where the αtoc molecule is at the middle of the bilayer, to widow 10, which is its equilibrium position. For windows 20 and 30, when αtoc is in the interfacial region, nearby ($r \leq 15$ Å) there is an increase in z(r). This indicates the head groups on the lipids located near αtoc extend into water more than on ones farther away - in other words, the pulling of αtoc out of the bilayer deforms the membrane. The snapshot presented in Figure 4.3B gives an illustration of the deformation. Once αtoc is completely in water, the membrane returns to normal as shown in window 35 where no deformation is apparent. We take the difference in z(r) between the window ($r = 5$ Å) where it is greatest in magnitude and where αtoc is at its equilibrium depth as a measure of how much the membrane is deformed when αtoc is removed. The difference is 4.7 Å (between windows 30 and 10) in SDPC, which is less than the difference of 5.6 Å in SOPC (between windows 31 and 11).

4.3.4 Behavior at aqueous interface

In the replica exchange method, it is possible that neighboring windows swap their replicas and cause them to take a random walk between the windows [28]. In our simulations, we found examples of replicas that migrate through the interface between a window with αtoc entirely in water and a window with αtoc in contact with the membrane. The snapshots in Figure 4.4 give an illustration of the two states. With the trajectories of such replicas, we can take a close look at how αtoc leaves the membrane into the water and, vice versa, enters the membrane from water. When αtoc leaves the membrane, it begins from a state that has the chromanol head in the water and the phytyl tail is still inside the membrane and extended down into the interior (Fig. 4.4A). When αtoc becomes fully pulled into the water

(by replica exchange), the orientation of chromanol and the whole molecule including the phytyl tail quickly becomes random and surrounded by water (Fig. 4.4B). On the other hand, when αtoc enters the membrane from water, the phytyl chain encounters the membrane first. We did not find that water molecules penetrate into the membrane with the phytyl chain in this process.

4.3.5 Flip-flop

Between the equilibrium position (z_{eq}) and the center of membrane (z=0), there is an increase in the PMF which denotes a barrier to the transverse movement of αtoc (Fig. 4.2). The barrier reflects that insertion of the hydrophilic OH group on the chromanol head group into the hydrophobic interior of the bilayer is energetically unfavorable. That the barrier in SDPC (ΔG_{flip} = 1.9 kcal/mol) is lower than in SOPC (ΔG_{flip} = 2.5 kcal/mol) indicates that flip-flop of αtoc from one side of the bilayer to the other is easier in the polyunsaturated than monounsaturated case (Table 4.1). This assessment is qualitatively consistent with the greater number of flip-flop events observed in SDPC compared to SOPC during our earlier conventional all-atom MD simulations [20]. A calculation of the rate of flip-flop now follows.

To estimate the rate of flip-flop for αtoc, we adopt an approach applied to cholesterol in the past [27]. A complete flip-flop is defined as αtoc moving from z_{eq} (equilibrium position) in one leaflet to z_{eq} in the other leaflet. In this process the molecule moves from z_{eq} to the membrane center (z = 0) and then to z_{eq} on the other side of the bilayer. The respective rate constants k_f and k_d that characterize these motions are related via

$$k_f = k_d e^{-\frac{\Delta G_{flip}}{RT}}, \tag{4.2}$$

and equate to the rate of flip-flop

$$k_{flip} = \frac{1}{\left(k_f^{-1} + k_d^{-1}\right)} \times \frac{1}{2}. \tag{4.3}$$

The factor of ½ is included in eq. 3 to take into account the possibility that an αtoc molecule that has reached the center of the membrane can return to its original leaflet as well as cross over to the other leaflet. An estimate of k_d, was obtained by performing 10 standard MD

simulations with αtoc initially located at the center of membrane, and measuring the time (t_d) it takes to move back to z_{eq} without harmonic restraint.

Table 4.2 lists the results of our calculations. They reveal that the average rate of flip-flop rate $\bar{k}_{flip}$ is approximately 3 times greater in SDPC than in SOPC.

4.3.6 Chromanol orientation

To investigate how the orientation of the chromanol group on αtoc changes with depth in the membrane, we made two-dimensional probability histograms of $\rho(z,\theta)$ defined according to

$$\rho(z,\theta) = \frac{n(z,\theta)}{N(z)\sin\theta}. \quad (4.4)$$

In this equation z is the distance from the center of the bilayer and θ is the angle that the C3-C6 vector on the chromanol group makes with the bilayer normal (Fig. 4.5A). To calculate the histogram, z and θ are divided into bins that are 0.5 Å and 1° in respective size. $n(z,\theta)$ is the incidence of being found in bin z and θ, $N(z)$ is the total incidence of being found in bin z, which is used to normalize the total probability density at different z, and $\sin\theta$ in the denominator accounts for the change of bin size with respect to θ.

The two-dimensional histograms of orientation for the chromanol group obtained in SDPC and SOPC are plotted in Figure 4.5B. They are similar in the two membranes. As would be expected, the chromanol group has no preferred direction when the whole of the αtoc molecule is in water (z >35 Å). When the phytyl chain penetrates the bilayer (z <35 Å), it packs parallel to the surrounding phospholipid chains and the orientation of the chromanol group becomes constrained in a distribution that tends to line up with the bilayer normal (θ = 0°). Near the disordered center of the bilayer (z ~ 0 Å), however, the situation changes and the distribution is almost uniform. It indicates that αtoc undergoes significant reorientation there, and that our simulations have a good sampling of the orientation of the chromanol.

4.4 Discussion

The role of αtoc in the plasma membrane is to protect polyunsaturated phospholipids from oxidation, an activity that requires close contact with the lipid peroxyl radicals formed during the chain reaction by which oxidation proceeds. However, the global concentration of αtoc is small (< 1 mol% of all lipids) [15]. How αtoc can effectively protect the comparatively larger amount of polyunsaturated phospholipid remains a question. The answer might rely on the unique membrane properties of PUFA chains that contain multiple -C-C=C-C- units. The C-C bonds next to each C=C bond have a shallow rotational energy barrier, so that PUFA chains are tremendously disordered [29]. This disorder provides membrane environment necessary for the function of specific proteins [30]. It also produces an aversion for cholesterol that drives the formation of PUFA-rich domains [31], leading to the hypothesis that αtoc preferentially co-localizes with PUFA in such domains to increase the local concentration of αtoc around the lipid species most in need of protection from oxidation [14]. This hypothesized mechanism is analogous to the co-localization of cholesterol with saturated sphingolipids in lipid rafts [32].

Our simulations reveal that there is higher binding energy for αtoc associated with SOPC (18.3 kcal/mol) than SDPC (16.7 kcal/mol) (Table 4.1). These values are comparable to the only other report to date of a binding energy from UBSMD simulation for αtoc (12.4 kcal/mol in 1,2-dipalmitoylphosphatidylcholine(DPPC)) [33], although direct comparison is inappropriate given that the force field is not the same. The differential in value $\Delta\Delta G$ between the two lipids that we measure can be related to a relative partition coefficient K_{SDPC}^{SOPC} = 13.3 (SOPC with respect to SDPC) via

$$K_{SDPC}^{SOPC} = e^{-\frac{\Delta\Delta G}{RT}} \tag{4.5}$$

where R and T are the gas constant and temperature, respectively [34]. The trend is the same as seen for the binding of cholesterol between saturated and unsaturated lipids by both experiment and in UBSMD simulation [34,35]. Upon reflection, this observation is not too surprising given the similarity in molecular structure of cholesterol and αtoc. Like in the case of cholesterol, the more disordered lipid environment in the SDPC bilayer is responsible for the differences in binding energy for αtoc. The SDPC membrane is thinner and looser in the lipid packing (larger area per lipid) than the SOPC membrane. Thus, in

the PMF the change of G(z) is more gradual both near the center of membrane (from z_{eq} to z_0) and at the aqueous interface (z between 30-35 Å) in SDPC membrane compared to SOPC membrane (Fig. 4.2).

The argument used in the cholesterol umbrella sampling study is that the difference in desorption energy (binding energy) for cholesterol in different lipid membranes is equal to the free energy change for cholesterol to exchange between different domains [35]. With the same argument, it appears that αtoc would have greater affinity for a more saturated lipid environment than a polyunsaturated DHA environment in the plasma membrane. This assessment contradicts the hypothesis that PUFA and αtoc co-localize together. However, there are still possible mechanisms that could support the hypothesis. The high concentration of cholesterol in lipid rafts, driven by its high affinity for saturated lipids, may exclude αtoc into regions that are PUFA-rich/cholesterol-poor. We suggest two possible future ways to investigate this problem. First, we can perform UBSMD simulations to compare the binding energy of αtoc to membranes with different cholesterol concentrations and unsaturation. We would then learn whether the presence of cholesterol reduces the affinity of αtoc to a more saturated environment. Second, we could try to investigate the partition of αtoc in different lipid domains directly, using larger scale simulation like coarse graining that can reproduce lipid domain formation in a bilayer [36].

In the windows where αtoc is sticking out from the membrane, we noticed deformation of the membrane (Fig. 4.3). It indicates that not only αtoc-PC interactions, but also PC-PC interactions, contribute to the binding energy ΔG. This issue has previously been ignored. In an USMD simulation study on cholesterol, for instance, the enthalpic contribution to the change in free energy is only represented by the interaction energy between cholesterol and water/PC [37]. We suggest that PC-PC interactions should be included as well. Replica exchange reveals the strongly hydrophobic nature of the behavior of αtoc near the aqueous interface (Fig. 4.4). The water layer that surrounds atoc molecule when it is in water does not follow it in to the bilayer hydrophobic interior. This avoids the possibility that a water pore forms during the simulation, which might affect the accuracy of the PMF by perturbing membrane order [38].

The smaller energy barrier at the center of the bilayer identified in the profile of PMF in SDPC and SOPC (Fig. 4.2) and the corresponding rate of flip-flop calculated (Table 4.2)

show that it is easier for αtoc to translocate across a highly disordered membrane interior. This difference qualitatively agrees with the greater number of flip-flop events observed for αtoc in SDPC than SOPC during the 200 ns over which our previous standard simulations were run [20]. The same trend of faster flip-flop in more unsaturated, disordered membranes was seen for cholesterol in MD simulations [35,37,39]. Fast flip-flop for αtoc in SDPC implies the vitamin could easily penetrate the interior of a polyunsaturated bilayer to intercept lipid peroxyl radicals, which would help in the protection against oxidation [20]. Our simulations also provide insight on the path that the flip-flop of αtoc takes. The orientation of the chromanol group remains upright and lined up with the bilayer normal until the center of the bilayer is reached in both SDPC and SOPC (Fig. 4.5B). In the vicinity bilayer, the orientation becomes random so that the chromanol group can invert and place the OH group towards the aqueous interface on the opposite side of the membrane. This scenario is similar to that envisaged for the flip-flop of cholesterol in lipid membranes studied by the USMD method [37,39].

In summary, our findings do not support the proposal that vitamin E binds preferentially to polyunsaturated phospholipids. The dynamics and organization of vitamin E in many respects resemble that of structurally similar cholesterol.

4.5 References

[1] Zingg, J.M. 2007. Vitamin E: an overview of major research directions. *Mol. Aspects Med.* 28:400-422.

[2] Niki, E. and M.G. Traber. 2012. A history of vitamin E. *Ann. Nutr. Metab.* 61:207-212.

[3] Ulatowski, l. and D. Manor. 2013. Vitamin E trafficking in neurologic health and disease. *Ann. Rev. Nutr.* 33:87-103.

[4] Packer, L. 1994. Vitamin E is nature's master antioxidant. *Sci. Am. Sci. Med.* 1:54-63.

[5] Wang, X. and P.J. Quinn. 1999. Vitamin E and its function in membranes. *Prog. Lipid Res.* 38:309-336.

[6] Traber, M.G. and J. Atkinson. 2007. Vitamin E, antioxidant and nothing more. *Free Rad. Biol. Med.* 43:4-15.

[7] Calder, P.C. 2015. Marine omega-3 fatty acids and inflammatory processes: Effects, mechanisms and clinical relevance. *Biochim. Biophys. Acta* 1851:469–484.

[8] Hou, T.Y., D.N. McMurray and R.S. Chapkin. 2016. Omega-3 fatty acids, lipid rafts, and T cell signaling. *Eur. J. Pharmacol.* 785:2-9.

[9] Shaikh, S.R. 2012. Biophysical and biochemical mechanisms by which dietary N-3 polyunsaturated fatty acids from fish oil disrupt membrane lipid rafts. *J. Nutr. Biochem.* 23:101-105.

[10] Burton, G.W. and K.U. Ingold. 1986. Vitamin E: application of the principles of physical organic chemistry to the exploration of its structure and function. *Acc. Chem. Res.* 19:194-201.

[11] Alessi, M., T. Paul, J.C. Scaiano and K.U. Ingold. 2002. The contrasting kinetics of peroxidation of vitamin E-containing phospholipid unilamellar vesicles and human low-density lipoprotein. *J. Amer. Chem. Soc.* 124:6957-6965.

[12] Diplock, A.T. and J.A. Lucy. 1973. The biochemical modes of action of vitamin E: a hypothesis. *FEBS Lett.* 29:205-210.

[13] Kagan, V.E. 1989. Tocopherol stabilizes membranes against phospholipase A, free fatty acids, and lysophospholipids. *Annals. NY Acad. Sci.* 570:121-135.

[14] Atkinson, J., T. Harroun, S.R. Wasssall, W. Stillwell and J. Katsaras. 2010. The location and behavior of α-tocopherol in membranes. *Mol. Nutr. Food Res.* 54:641-651.

[15] Atkinson, J., R.F. Epand and R.M. Epand 2008. Tocopherols and tocotrienols in membranes: a critical review. *Free Rad. Biol. Med.* 44:739-764.

[16] Marquardt, D., N. Kučerka, J. Katsaras and T.A. Harroun. 2015. α-Tocopherol's location in membranes is not affected by their composition. *Langmuir* 31:4464-4472.

[17] Marquardt, D., J.A. Williams, N. Kučerka, J. Atkinson, S.R. Wassall, J. Katsaras and T.A. Harroun. 2013. Tocopherol activity correlates with its location in a membrane: a new perspective on the anti-oxidant vitamin E. *J. Amer. Chem. Soc.* 135:7523–7533.

[18] Qin, S-S., Z-W. Yu and Y-X. Yu. 2009. Structural and kinetic properties of α-tocopherol in phospholipid bilayers, a molecular dynamics simulation study. *J. Phys. Chem. B* 113:16537-16546.

[19] Qin, S-S. and Z-W. Yu. 2011. Molecular dynamics simulations of α-tocopherol in model membranes. *Acta Phys. – Chim. Sin.* 27:213-227.

[20] Leng, X., J.J. Kinnun, D. Marquardt, M. Ghefli, N. Kucerka, J. Katsaras, J. Atkinson, T.A. Harroun, S.E. Feller and S.R. Wassall. 2015. α-Tocopherol is well designed to protect polyunsaturated phospholipids: MD simulations. *Biophys. J.* 109:1608-1618.

[21] Klauda, J.B., V. Monje, T. Kim and W. Im. 202. Improving the CHARMM force field for polyunsaturated fatty acid chains. *J. Phys Chem. B* 116:9424-9431.

[22] Darden, T., D. York and L. Pedersen. 1993. Particle mesh Ewald: an $n \cdot \log(n)$ method for Ewald sums in large systems. *J. Chem. Phys.* 98:10089-10092.

[23] Hoover, W.G. 1985. Canonical dynamics: equilibrium phase-space distributions. *Phys. Rev. A* vol. 31:1695-1697.

[24] Feller, S.E., Y. Zhang, R.W. Pastor and B.R. Brooks. 1995. Constant pressure molecular dynamics simulation: the Langevin piston method. *J. Chem. Phys.* 103:4613-4621.

[25] Phillips, J.C., R. Braun, W. Wang, J. Gumbart, E. Tajkhorshid, E. Villa, C. Chipot, R.D. Skeel, L. Kalé and K. Schulten. 2005. Scalable molecular dynamics with NAMD. *J. Comp. Chem.* 26:1781-1802.

[26] Zhu, F., and G. Hummer. 2012. Convergence and error estimation in free energy calculations using the weighted histogram analysis method. *J. Comp. Chem.* 33:453-465.

[27] Bennett, W.D., J.L. MacCallum, M.J. Hinner, S.J. Marrink and D.P. Tieleman. 2009. Molecular view of cholesterol flip-flop and chemical potential in different membrane environments. *J. Amer. Chem. Soc.* 131:12714-12720.

[28] Sugita, Y., A. Kitao and Y. Okamoto. 2000. Multidimensional replica-exchange method for free-energy calculations. *J. Chem. Phys.* 113:6042-6051.

[29] Feller, S.E. 2008. Acyl chain conformations in phospholipid bilayers: a comparative study of docosahexaenoic acid and saturated fatty acids. *Chem. Phys.* Lipids 153, 76-80.

[30] Grossfield, A., S.E. Feller and M.C. Pitman. 2006. Contribution of omega-3 fatty acids to the thermodynamics of membrane protein solvation. *J. Phys. Chem.* B 110, 8907-8909.

[31] Wassall, S.R. and W. Stillwell 2009. Polyunsaturated fatty acid–cholesterol interactions: domain formation in membranes. *Biochim. Biophys. Acta* 1788, 24-32.

[32] Silvius, J.R. 2003. Role of cholesterol in lipid raft formation: lessons from lipid model systems. *Biochim. Biophys.* Acta 1610, 174-183.

[33] Meng, F. 2013. Molecular simulation of α-tocopherol passing across DPPC lipid using potential of mean force and accelerated molecular dynamics method. *J. Theor. Comput. Chem.* 12, 1341011-1-1341011-16.

[34] Williams, J.A., C.D. Wassall, M.D. Kemple and S.R. Wassall. 2013. An EPR method for measuring the affinity of a spin labeled analog of cholesterol for phospholipids. *J. Membrane Biol.* 246, 689-696.

[35] Bennett, W.F.D. and D. P. Tieleman. 2012. Molecular simulation of rapid translocation of cholesterol, diacylglycerol, and ceramide in model raft and nonraft membranes. *J. Lipid Res.* 53, 421-429.

[36] Risselada, H.J. and S.J. Marrink. 2008. The molecular face of lipid rafts in model membranes. *Proc. Natl. Acad. Sci.* 105, 17367-17372.

[37] Jo, S., H. Rui, J.B. Lim, J.B. Klauda and W. Im. 2010. Cholesterol flip-flop: insights from free energy simulation studies. *J. Phys. Chem.* B 114, 13342-13348.

[38] Neale, C., C. Madill, S. Rauscher and R. Pomès. 2013. Accelerating convergence in molecular dynamics simulations of solutes in lipid membranes by conducting a random walk along the bilayer normal. *J. Chem. Theor. Comput.* 9, 3686-3703.

[39] Bennett, W.D., J.L. MacCallum, M.J. Hinner, S.J. Marrink and D.P. Tieleman. 2009. Molecular view of cholesterol flip-flop and chemical potential in different membrane environments. *J. Amer. Chem. Soc.* 131, 12714-12720.

Table 4.1

Energetic terms derived from the PMF profile of αtoc.

	Binding Energy (kcal/mol)	Flip-flop barrier (kcal/mol)	Equilibrium depth (Å)
SDPC	16.7±0.2	1.9±0.2	10.1
SOPC	18.3±0.2	2.5±0.2	11.4

Table 4.2

Kinetic properties of αtoc flip-flop in SDPC and SOPC at 310K. Data are taken from the average of 20 cases (2 αtoc in 10 standard MD simulations) - 16/20 cases in SDPC and 15/20 cases in SOPC (αtoc did not reach equilibrium within 60 ns in the rest of the cases). The range of t_d and derived rate constants are shown for reference, as well as the average rate of flip-flop.

	t_d (ns)	k_d (s^{-1})	k_f (s^{-1})	k_{flip} (s^{-1})	$\bar{k}_{flip}$ (s^{-1})
SDPC	8 to 55	1.3×10^{8} to 1.8×10^{7}	5.7×10^{6} to 8.3×10^{5}	2.7×10^{6} to 4.0×10^{5}	7.5×10^{5}
SOPC	8 to 60	1.3×10^{8} to 1.7×10^{7}	2.2×10^{6} to 2.9×10^{5}	1.1×10^{6} to 1.4×10^{5}	2.5×10^{5}

αtoc

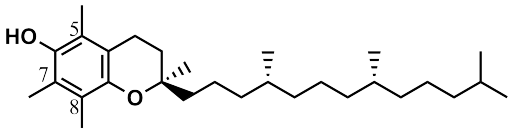

SDPC

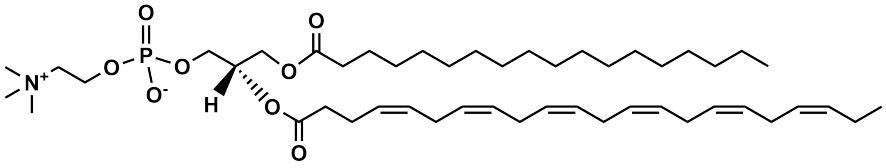

SOPC

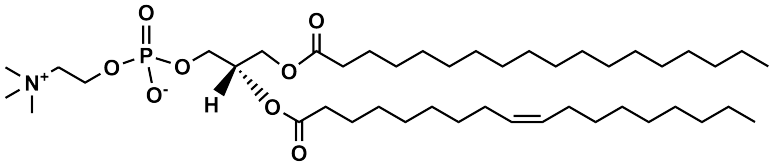

Figure 4.1

Molecular structure of αtoc, SDPC and SOPC.

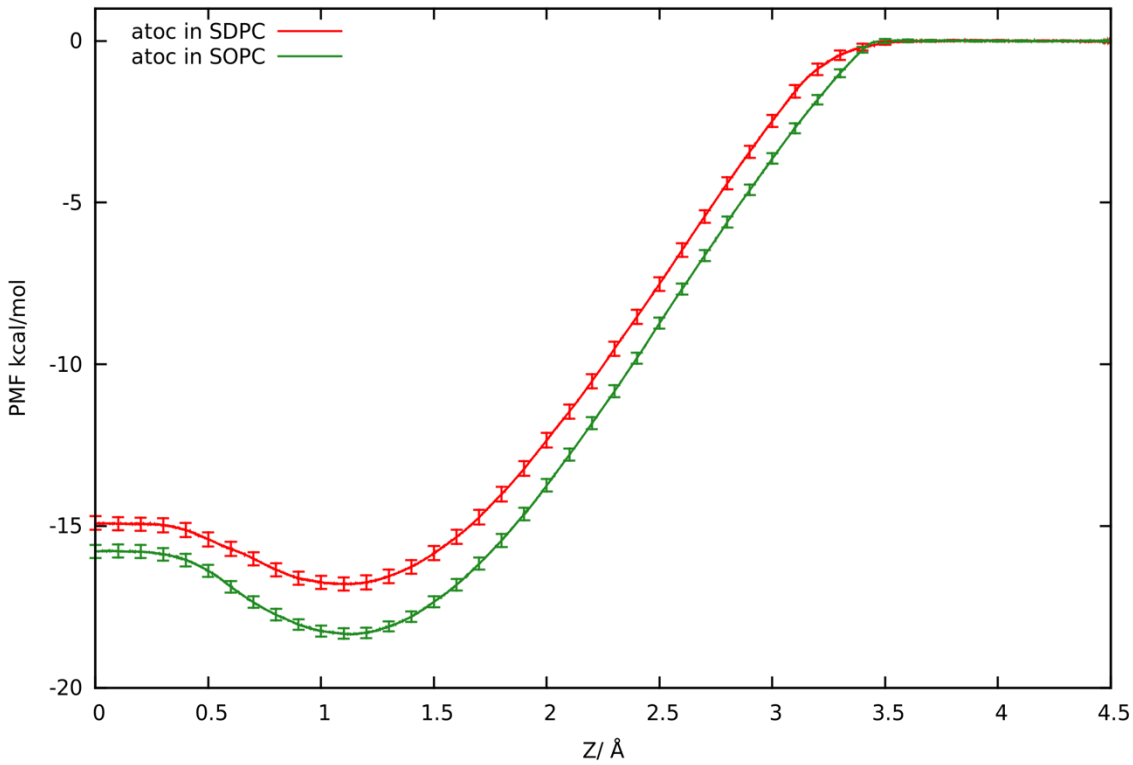

Figure 4.2

PMF for αtoc partitioning from water to the center of the bilayer in SDPC (red) and SOPC (green). The PMF was set to zero in the aqueous phase. Error bars are the standard error calculated using block averaging. The length of the time block is 10 ns.

A

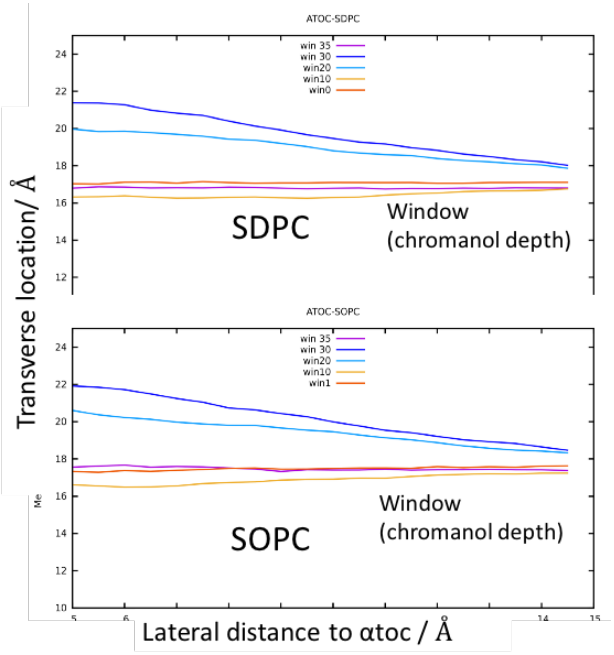

B

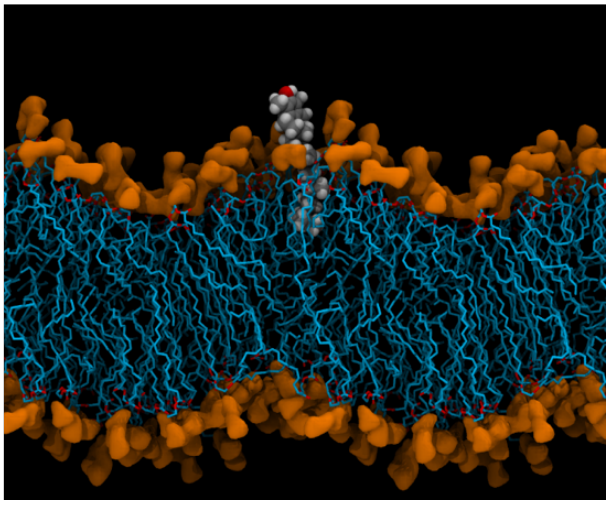

Figure 4.3

A) Average z coordinate of the phosphate atom on PC lipids as a function of lateral distance r from the αtoc at in different windows (different depths of the chromanol group).

B) Snapshot of the system when αtoc has been half-pulled out from the membrane (SDPC). αToc is shown as a space-filling model, the head groups of PC lipid are shown in an orange surface representation and the acyl chains of PC lipids are shown as blue lines.

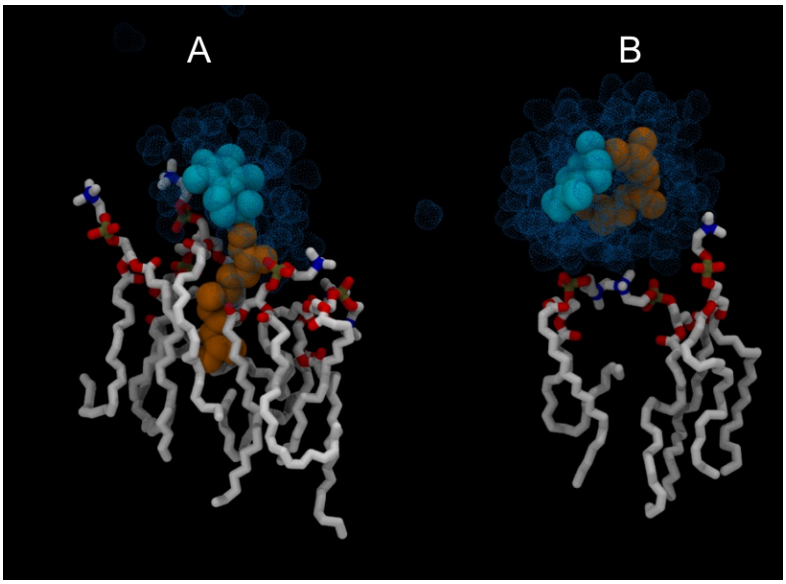

Figure 4.4

Snapshots from the trajectory of one replica that swaps between the windows of αtoc in and out of the membrane - αtoc with the chromanol group restrained in the water and the phytyl chain inside the membrane (A), and with the whole molecule completely in water (B). αToc is shown as a space-filling model (chromanol group colored in light blue and phytyl chain colored in orange), water molecules within a distance of 5 Å from αtoc are shown as blue balls, and PC lipids with their head group within a lateral distance of 10 Å from αtoc are shown in licorice representation.

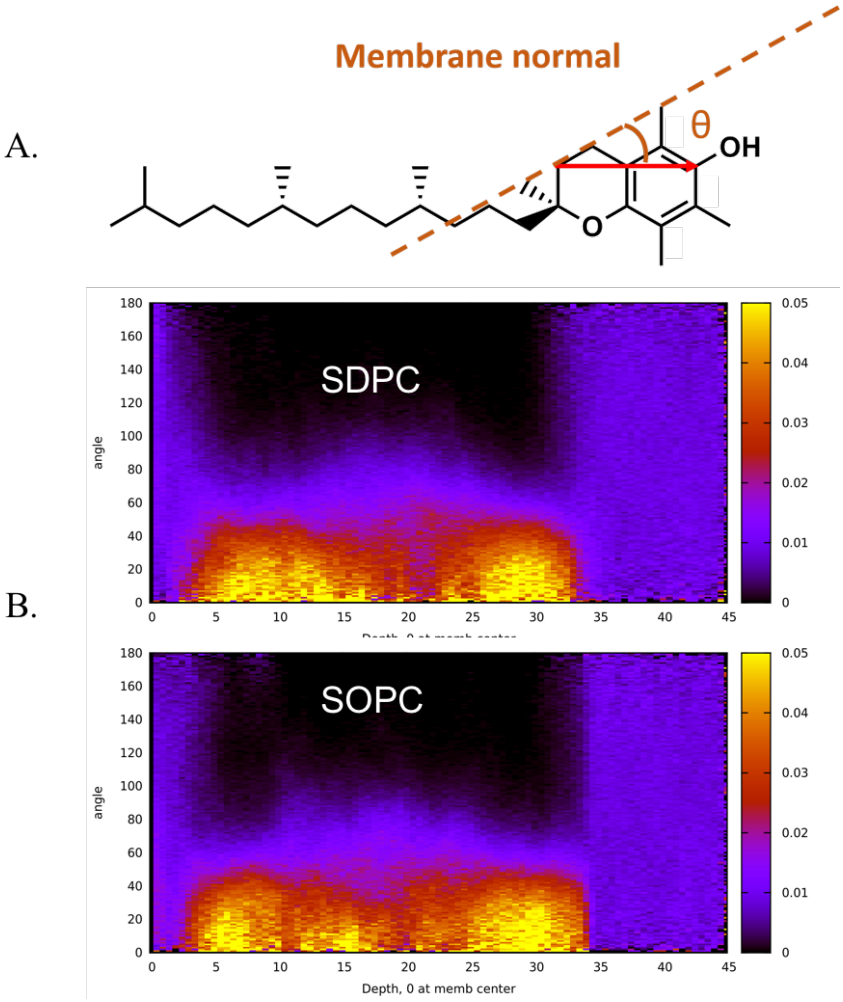

Figure 4.5

Probability distribution for the orientation of the chromanol group on αtoc (A) as a function of depth in SDPC and SOPC (B).

CHAPTER 5. ARE ALL N-3 PUFA THE SAME? A COMPARISON OF EPA, DHA AND DPA BY MD SIMULATIONS

5.1 Introduction

Long chain omega-3 polyunsaturated fatty acids (n-3 PUFA) are a distinct class of fatty acids that have multiple double bonds, with the last double bond being located 3 carbons from the terminal methyl (n or ω) end of the chain [1]. They began to attract attention in the 1970's when a low incidence of cardiovascular disease was noted in the Inuit population who consumed a diet rich in oily fish that contain an abundance of n-3 PUFA [2]. Since then many more health benefits have been discovered including in the treatment of neurological problems [3], relief of the symptoms of inflammatory disorders [4] and prevention of the progress of certain cancers [5]. The major source of n-3 PUFA in the diet is fish and extracted oil supplements [1]. Eicosapentaenoic acid (EPA, 20:5) with 20 carbons and 5 double bonds at the 5, 8, 11, 14 and 17 positions and docosahexaenoic acid (DHA, 22:6) with 22 carbons and 6 double bonds at the 4, 7, 10, 13, 16 and 19 positions are the primary ones. Present in smaller concentration, and to which EPA often converts, is docosapentaenoic acid (DPA, 22:5) with 22 carbons and 5 double bonds at the 7, 10, 13, 16 and 19 positions. DPA has only recently begun to be the subject of research, in contrast to EPA ad DHA that have been widely studied [6]. Although all three n-PUFA are similar in chemical structure, whether they have similar, unique or complementary impact upon health remains a matter of debate [7].

A complete explanation of the mode of action for n-3 PUFA currently does not exist. Modulation of the organization of plasma membranes following the uptake of n-3 PUFA into phospholipids is among the potential mechanisms that have been identified [8-10]. The basic idea is a variation on the lipid raft concept [11]. According to this concept, predominantly saturated sphingolipids and cholesterol segregate into tightly packed nanodomains that coalesce into functional microdomains (rafts) within a surrounding sea of phospholipids that are less ordered. By incorporating into membrane phospholipids, highly disordered n-3 PUFA that have an aversion for cholesterol are then proposed to manipulate the composition and structure of the domains. One example of a scenario

envisaged, for instance, has the introduction of n-3 PUFA-containing phospholipids into a raft displacing cholesterol and breaking apart the domain [10]. Detergent extraction assays and imaging studies performed on cells treated with n-3 PUFA support the general premise [12,13]. Changes in the levels of other fatty acids due to cellular metabolism, however, complicate interpretation. A series of studies on model membranes of controlled composition carried out in our laboratories have started to provide insight [14-17]. They established that the partitioning of an n-3 PUFA-containing phospholipid between more ordered raft-like and less ordered non-raft environments is sensitive to molecular structure. A much greater tendency for DHA- than EPA-containing phosphatidylcholine (PC) to infiltrate raft-like domains was revealed, which we attribute to a differential in the disorder associated with DHA relative to EPA and speculate may indicate a variance in bioactivity. To better understand this behavior and the possible role that the structure of an individual n-3 PUFA plays in determining biological activity, we have run atomistic MD simulations to make a direct comparison of EPA, DHA and DPA and their interaction with cholesterol. All atom MD simulation opens up a perspective on molecular structure and dynamics within lipid membranes that is unprecedented in detail [18]. The reliability of this computational method has been ascertained in tests on well-characterized systems that successfully reproduce experimental measurements. It is an approach that has been tremendously influential in developing a comprehension of the physical properties of PUFA-containing phospholipids. Simulations published for DHA-containing PC bilayers more than a decade ago were instrumental in showing that the polyunsaturated chain is highly flexible, rapidly undergoing isomerization between conformations that include extended and bent configurations [19-21]. A reduced energy barrier for rotation about the single bonds in the recurring =C-C-C= unit possessed by PUFA is responsible, debunking an alternative view that the rigidity of multiple bonds would produce low flexibility. Subsequent analysis of simulations on a 1-stearoyl-2-docosahexaenoylphosphatidylcholine (DHA-PC) bilayer in the presence of cholesterol showed that the steroid moiety prefers close proximity to the saturated stearic acid (SA) chain over the polyunsaturated DHA chain [22]. This finding corroborates an arrangement inferred from experimental measurements of the orientation of cholesterol and its solubility in polyunsaturated membranes [23]. Phenomenal disorder that pushes cholesterol away is

what distinguishes PUFA and renders membrane architecture particularly responsive to their presence.

An investigation of how molecular organization in lipid bilayers is affected by differences in the structure of EPA, DHA and DPA is presented here. To this end, we performed atomistic MD simulations comparing 1-stearoyl-2-eicosapentaenoylphosphatidylcholine (EPA-PC), DHA-PC, 1-stearoyl-2-docosapentaenoylphosphatidylcholine (DPA-PC) and 1-stearoyl-2-oleoylphosphatidylcholine (OA-PC) bilayers. Their molecular structure, together with cholesterol, is shown Figure 5.1. With a saturated chain at the *sn*-1 position and a polyunsaturated chain at the *sn*-2 position, DHA-PC, EPA-PC and DPA-PC are representative of a phospholipid into which n-3 PUFA have been taken up in the plasma membrane [24]. OA-PC serves as a monounsaturated control. The simulations were run on single component membranes and in the presence of 20 mol% cholesterol to characterize interaction with the sterol for each n-3 PUFA. Supplementary solid state ^{2}H NMR experiments employing analogs of the phospholipids perdeuterated in the *sn*-1 chain were conducted for validation.

5.2 Materials and methods

5.2.1 MD simulations

Atomistic MD simulations were performed on DHA-PC, EPA-PC, DPA-PC and OA-PC bilayers in the absence and presence of 20 mol% cholesterol. They run in the constant particle, pressure and temperature (NPT) ensemble. There were 98 PC molecules in the single component membrane simulations, and 80 PC molecules and 20 cholesterol molecules in the two-component membrane simulations. In each case, the membrane was hydrated with 2000 water molecules. The initial structure of OA-PC, OA-PC + cholesterol, DHA-PC and DHA-PC + cholesterol bilayers was assembled with the CHARMM-GUI Membrane Builder [25]. Then, by modifying the DHA chain on DHA-PC molecules, the initial structure of EPA-PC + cholesterol and DPA-PC + cholesterol bilayers was generated from our assembled DHA-PC + cholesterol bilayer. The initial structure of EPA-PC and DPA-PC bilayers was created by locating the corresponding lipid molecule into a bilayer grid with a customized script. This approach avoided atom/chain conflicts that appear in

the initial structure when it is directly modified from the assembled DHA-PC bilayer. All simulations were run using the CHARMM C36p force field [26]. Non-bonded (van der Waals and short-range electrostatic) interactions were gradually switched off at 10 Å, and the long-range electro static interactions were calculated using the particle-mesh Ewald method [27]. The membranes were equilibrated with the standard CHARMM-GUI six-step process over 200 ps [25] during which constraints on lipids were gradually released CHARMM [28].

Production runs of our simulations were performed with NAMD [29] on the Big Red II super computer at Indiana University. Each one was run over 200 ns using a time step of 2 fs, with the first 20 ns considered to be equilibration. In all simulations, periodic boundary conditions were applied to a rectangular box on which the x and y dimensions (in the plane of the membrane) were kept equal while the z dimension (in the direction of the membrane normal) was varied independently. The temperature was kept at 37 °C by the Hoover thermostat [30] and the Langevin piston method was applied to keep the pressure at 1 atm [31]. Analyses of simulations, including calculating order parameters and densities of atoms in 1- and 3-dimensions were achieved with customized Tcl script executed in the VISUAL MOLECULAR DYNAMICS (VMD) program [32]. Snapshots of bilayers and illustrations were also created with VMD, and rendered by blender.

5.2.2 Solid state 2H NMR

Details of solid state ^{2}H NMR experiments are provided in Supporting Information.

5.3 Results and discussion

5.3.1 Molecular organization in single component membranes

From our simulations on EPA-PC, DHA-PC and DPA-PC bilayers, differences in how each n-3 PUFA affects acyl chain order within membranes and the thickness of a bilayer were identified.

5.3.1.1 Membrane order

The order parameter S_{CD} is a fundamental quantity describing the dynamics of acyl chain segments in a membrane that is accessible by MD simulations and solid state ^{2}H NMR spectroscopy [33]. It is a measure of the anisotropy of motion for the C-H (H is replaced by ^{2}H in ^{2}H NMR experiments) bond on a methylene or methyl group in an acyl chain. The definition of the order parameter is

$$S_{CD} = \tfrac{1}{2}\langle 3\,cos^2\,\beta - 1\rangle \tag{5.1}$$

where β is the angle between the C-H bond on a particular chain segment and the membrane normal about which the reorientation of the chain is axially symmetric [34]. The angular brackets signify a time average that is also taken over all the molecules in a simulation. In the case of methylene groups and the terminal methyl group, an average order parameter for the two and three C-H bonds in the respective segments is usually calculated. An exception is the two C-H bonds on the methylene group at the C2 position of the *sn*-2 chain for which constraints on orientation due to the glycerol backbone lead to order parameters that are unequal [35]. A range $0 \leq |S_{CD}| \leq 0.5$ typically applies to the value for S_{CD} [17]. The upper limit corresponds to a methylene group undergoing fast axial rotation in an all-trans chain (β= 90°) while the lower limit corresponds to isotropic motion (β takes all angles) for a methylene or methyl group.

Figure 5.2 (upper panel) shows the order parameter profiles obtained from simulation along the saturated SA chain at the *sn*-1 position in EPA-PC, DHA-PC, DPA-PC and OA-PC. They all display a form that is a signature for saturated phospholipid acyl chains in the lamellar liquid crystalline phase [34]. In the top half of the chain the S_{CD} values exhibit a plateau region of approximately constant order (S_{CD} ~ 0.2, C4-C8 positions), and then progressively decrease in the bottom half toward the terminal methyl group (S_{CD} ~ 0.02, C18 position) near the center of bilayer. Reorientation is constrained by tighter packing in the upper portion where the chain is anchored at the hydrophilic interface, while in the lower portion there is increasingly less restriction to motion towards the free end at the foot of the chain. Inspection of the profiles reveals the reduction in order expected to accompany the presence of a polyunsaturated *sn*-2 chain, which we quantify in terms of an average order parameter $\bar{S}_{CD}$ that represents the global effect on the entire *sn*-1 chain (Table 1).

Among the PUFA-containing phospholipids, EPA-PC ($\bar{S}_{CD}$ = 0.131 ± 0.003) is the most disordered while DPA-PC ($\bar{S}_{CD}$ = 0.139 ± 0.003) is the least disordered. DHA-PC ($\bar{S}_{CD}$ = 0.136 ± 0.003) lies in between, somewhat closer to DPA-PC. They are all ~10% less ordered than monounsaturated OA-PC ($\bar{S}_{CD}$ = 0.152 ± 0.003).

The trends seen here are consistent with those observed experimentally by ^{2}H NMR with analogs of PC deuterated in the *sn*-1 chain. Order parameter profiles published for the SA *sn*-1 chain in a series of PC membranes as a function of the level of unsaturation in the *sn*-2 chain demonstrated that increasing the number of double bonds from 1 to 3 substantially decreases order [36]. Thereafter the changes in order on increasing the number of double bonds from 3 to 6 are modest, like we saw in our simulations on n-3 PUFA-containing bilayers with 5 (EPA-PC and DPA-PC) and 6 (DHA-PC) double bonds. The hierarchy of disorder EPA-PC (most disordered) > DHA-PC > DPA-PC (least disordered) identified by simulation qualitatively reproduces the variation of the average order parameter previously measured by us using moment analysis [37] and of the smoothed order parameter profiles constructed from FFT depaked spectra in the current work (Fig. A3.1 and Table A3.1 in Supporting Information). To the best of our knowledge an order parameter profile has not been reported for DPA-PC before. DPA*-PC with DPA* (n-6 isomer) containing 20 carbons and 5 double bonds at 4, 7, 10, 13 and 16 positions, as opposed to DPA (n-3 isomer), for the *sn*-2 chain was compared with DHA-PC in earlier work [38]. As with DPA-PC, the SA *sn*-1 chain in DPA*-PC was found to be slightly less disordered than DHA-PC ($\Delta\bar{S}_{CD}$ = 0.008).

The order parameters that were calculated for the unsaturated *sn*-2 chain in EPA-PC, DHA-PC, DPA-PC and OA-PC are plotted as function of position in Figure 5.2 (lower panel). Not surprisingly, there is a big difference between the OA chain and PUFA chains. The OA chain in OA-PC has a profile that is similar to the SA *sn*-1 chain, apart from positions C8-C11 where there is big drop in the magnitude of S_{CD}. This phenomenon was first observed experimentally and is understood [39,40]. A localized region of enhanced segmental motion within the OA chain is not the reason for the reduced order parameters. The configuration of the chain around the rigid *cis* double bond, instead, produces a most probable orientation for which the order parameters of the C-H bonds on the chain

segments at (C9 and C10) and flanking (C8 and C11) the double bond are inherently low – i.e. β takes angles near the "magic" angle (54.7°) at which the second order Legendre polynomial in the definition of the order parameter (eq. 1) goes to zero.

Compared to the OA chain in OA-PC, the order parameters for the PUFA chain in EPA-PC, DHA-PC and DPA-PC are much lower. They are less than 0.05 throughout the bottom two-thirds of the chain (C7 to the end), which is comparable to the value of S_{CD} for the highly mobile methyl group at the free end of a chain. An almost uniform distribution from 0 to 180° for the value of the angle β that the C-H bonds make with the bilayer normal is responsible. The truly high disorder implied is the result of the shallow energy barrier to rotation about C-C bonds in the repeating =CH-CH_2-CH= motif that distinguish PUFA with their multiple double bonds from less unsaturated fatty acids [41]. This behavior is well documented by simulation and experiment in the case of DHA [26,42-44]. Higher order exists in the uppermost portion of the PUFA chains before the sequence of double bonds begins. The effect is most pronounced in DPA where the first double bond does not occur until carbon C7 (Fig. 5.1). The order parameter ($S_{CD} \sim 0.17$) at positions C3-5 of the DPA chain in DPA-PC approaches the value seen at the same positions for OA in OA-PC ($S_{CD} \sim 0.20$) (Fig. 5.3). A similar plateau-like region of elevated order is found in the profile for neither DHA in DHA-PC nor EPA in EPA-PC. We attribute its presence in DPA to the removal of the double bond at the C4 position relative to DHA and to the addition of two methylene groups prior to the first double bond relative to EPA (Fig. 5.1). In response, order parameters in the SA *sn*-1 chain are higher for DPA-PC than DHA-PC and, to greater extent, EPA-PC. The lower order of the SA chain in EPA-PC than DHA-PC indicates that, as we have previously surmised [37], the ordering associated with the loss of a double bond is more than compensated by the disordering associated with the shortening of the chain on replacing DHA by EPA.

5.3.1.2 Membrane thickness

Electron density profiles (EDP) across the membrane that were calculated for EPA-PC, DHA-PC, DPA-PC and OA-PC are shown in Figure 5.3 (upper panel). They were generated from histograms of the atoms in lipids along the bilayer normal (z direction) that were weighted by the number of electrons associated with each atom. Because the area of

membrane that was simulated is too small to undulate, the z direction in our system well represents the membrane normal [45]. In the EDP of each membrane, there is a dip in the middle (z = 0) of the bilayer reflecting where the highly disordered methyl groups at the end of acyl chains reside. The peaks on both sides correspond to the electron dense head group at the edge of the membrane and, as illustrated (Fig. 5.3, upper panel), approximate to the location of the phosphate group. Their separation is commonly taken to be the membrane thickness [46] and was used by us to determine the D_{HH} values listed in Table 2. The agreement with experimental data that exist in the literature for OA-PC (38.7 Å) [47] and DHA-PC (37.9 Å) [38] is good (within 1 Å). As far we know D_{HH} has not been measured for EPA-PC and DPA-PC, although in the latter case a thickness has been reported from X-ray work for its n-6 isomeric counterpart DPA*-PC (37.9 Å) [38].

It is generally recognized that introducing double bonds into a lipid chain causes a thinning of the bilayer [48]. A lipid chain with a double bond, and more markedly with multiple double bonds, is more disordered and occupies a larger cross-sectional than a saturated chain with same number of carbons. The result is a thinner bilayer. The measurements of membrane thickness obtained from our simulations conform to the gist of this view (Table 2). They demonstrate that DPA-PC, DHA-PC (22 carbons) and EPA-PC (20 carbons) with a polyunsaturated *sn*-2 chain are comparable in thickness or thinner than OA-PC (18 carbons) with a shorter monounsaturated *sn*-2 chain. As an aside, we point out that the values of D_{HH} measured from the EDP generated from our simulations underscore that care should be exercised when relating the average order parameter for the saturated *sn*-1 chain (Table 1) to membrane thickness. The basic idea connecting the two parameters is that a more ordered *sn*-1 chain has a bigger projected length, corresponding to greater bilayer thickness [49]. However, despite an average order parameter for the SA *sn*-1 chain in DPA-PC that is almost 10% lower than in OA-PC, the thickness of the n-3 PUFA containing bilayer is slightly bigger. The length of the *sn*-2 chain is clearly a factor.

5.3.2 Molecular organization in membranes containing cholesterol

From simulations run in the presence of 20 mol% cholesterol, we compared how acyl chain order within the membrane and the thickness of the bilayer were affected in EPA-PC, DHA-PC and DPA-PC. To further assess interaction with the sterol, the location and

orientation of cholesterol within the bilayers were determined and the distribution of each chain around the steroid moiety was mapped.

5.3.2.1 Membrane order

The addition of 20 mol% cholesterol to EPA-PC, DHA-PC and DPA-PC produces the anticipated increase in order within the bilayer [50]. Order parameters are elevated along the entire SA chain at *sn*-1 position in each case, reflecting the constraint upon reorientation imposed by the rigid sterol molecule (Fig. 5.4, upper panel). The shape of the profile remains largely unchanged. There is still a relatively flat region of approximately constant order parameter in the upper portion of the chain before order drops off in the lower portion towards the terminal methyl group. As judged by estimates of the average order parameter (Table 1), all three n-3 PUFA containing bilayers undergo essentially the same rise in order ($\Delta\bar{S}_{CD} \approx 0.040$) due to cholesterol so that the hierarchy of order between them is retained - DPA-PC ($\bar{S}_{CD} = 0.182 \pm 0.003$) > DHA-PC ($\bar{S}_{CD} = 0.178 \pm 0.003$) > EPA-PC ($\bar{S}_{CD} = 0.169 \pm 0.003$). The sterol-induced ordering is less than seen for the SA chain in OA-PC ($\Delta\bar{S}_{CD} = 0.061$), which results in the greater differential in order between the n-3 PUFA- and OA-containing bilayers that is apparent on inspection of the profiles obtained with (Fig. 5.4, upper panel) and without (Fig. 5.2, upper panel) cholesterol. It has similarly been surmised from experimental results presented in earlier studies there is a smaller increase in order due to cholesterol for polyunsaturated vs. monounsaturated bilayers [51,52].

A substantially more modest increase in order occurs for the n-3 PUFA chain at the *sn*-2 position in EPA-PC, DHA-PC and DPA-PC following the introduction of cholesterol than for the SA chain at the *sn*-1 position (Fig. 5.4, lower panel). The shift in average value for the order parameter ($\Delta\bar{S}_{CD} < 0.015$) is correspondingly smaller and comparable in each case (Table 1). There is little change in the overall shape of the profile. Despite the presence of the rigid steroid moiety, the n-3 PUFA chains are still highly disordered with order parameters that are low throughout much of their length ($S_{CD} < 0.08$ in the bottom two thirds). In contrast, the order of the OA *sn*-2 chain in OA-PC is elevated to a much greater extent by cholesterol. It increases by an amount ($\Delta\bar{S}_{CD} = 0.055$) approaching that undergone by the saturated SA *sn*-1 chain, retaining the form of the profile observed in the absence of the sterol. The effect of cholesterol on the order parameter profile for the DHA

sn-2 chain in DHA-PC derived from our simulations parallels the results obtained from NMR spectra [52]. Experimental measurements of the order parameter in the OA *sn*-2 chain of OA-PC are too sparse to make a meaningful comparison, while we are unaware that order parameters in either the EPA *sn*-2 chain of EPA-PC or DPA *sn*-2 chain of DPA-PC have been experimentally determined.

5.3.2.2 Membrane thickness

A thickening of EPA-PC, DHA-PC and DPA-PC, as well as of OA-PC, that follows the introduction of cholesterol is evident in the EDP constructed in Figure 5.3 (lower panel). It is a manifestation of the condensing effect of the sterol - the projected length of phospholipid chains ordered by cholesterol is greater and the bilayer becomes thicker [53]. All three of the n-3 PUFA-containing membranes undergo a comparable increase in thickness (ΔD_{HH} = 3.2-3.8 Å) that is less than the change undergone by the OA-containing membrane (ΔD_{HH} = 4.6 Å) (Table 2). As would be expected, the magnitude of these changes qualitatively parallels the elevation in molecular ordering due to cholesterol (Table 1). In agreement with these simulation-based findings, that the sterol produces a smaller increase in the width of DHA-PC compared to OA-PC bilayers may be gleaned from reports of neutron and x-ray scattering data [52,53].

5.3.2.3 Location of cholesterol

Cholesterol usually resides in a membrane with the hydroxyl group at one end of the tetracyclic ring near the aqueous interface while the short chain at the opposite end extends towards the center of the membrane [50]. An exception is bilayers that are thin (D_{HH} < 30 Å) in which hydrophobic mismatch drives the sterol into the interior of membrane where it straddles both leaflets [48]. This latter situation does not apply to the systems in the current study. The partial EDP generated from the simulated data for [2,3,4]- and [25,26,27]-carbons on cholesterol in EPA-PC, DHA-PC, DPA-PC and OA-PC conform to the canonical arrangement (Fig. 5.5, upper panel). They place the head and tail of the sterol, respectively, just below the surface and in the middle of the bilayer.

5.3.2.4 Orientation of cholesterol

The motion of cholesterol can be modeled as a fast rotation about the bilayer normal for the long molecular axis that in addition fluctuates in direction about a most probable orientation (tilt angle) offset from the normal [54]. Figure 5.5 (lower panel) shows the probability distribution calculated here for the angle a vector connecting the C13-C10 carbons, designating the alignment of the steroid moiety, makes with the bilayer normal in EPA-PC, DHA-PC, DPA-PC and OA-PC. A shift to larger angle and a broadening of the entire distribution accompanies the increase in disorder on replacing OA by each n-3 PUFA. It is clear, however, that there is little variation (< 2°) in the most probable orientation, denoted by the maximum in the distribution, between the various systems (Table 3). This observation is consistent with ^{2}H NMR work on [3α-$^2H_1$]cholesterol, an analog of the sterol labeled at the 3α position, incorporated at 50 mol% into PC bilayers with SA at the *sn*-1 position [55]. These experiments revealed the tilt angle is almost independent of the level of unsaturation for the *sn*-2 chain

5.3.2.5 Interaction of cholesterol with acyl chains

As a molecule that orders the membrane, cholesterol does so by interacting with the nearby fatty acid chains. The local lipid environment around the sterol molecule, thus, reflects how it interacts with the surrounding lipids. To analyze the packing around cholesterol of the fatty acyl chains in our study, a two-dimensional radial distribution function (RDF)

$$g(r_i) = \frac{N(r_i)}{2\pi r_i \rho(r_\infty)} \tag{5.2}$$

was generated [56]. In this equation r_i is the distance from a selected atom on the steroid moiety (defined as the central atom) to the carbon atom on an acyl chain (*sn*-1 or -2) of the phospholipid, and $N(r_i)$ is the number of acyl chain carbons inside a bin at distance r_i and at the same depth (±1 Å in the z direction) within the bilayer as the central atom. The term

$$\rho(r_\infty) = \frac{N(r_\infty)}{2\pi r_\infty} \tag{5.3}$$

represents the overall density of acyl chain atoms in the membrane, with r_∞ set to 25 Å in practice. C10 and C13 were chosen as the central atom. Of the series of peaks in the RDF

obtained (Fig. 5.6), we focus on the first one that reflects the arrangement of the chains closest to a cholesterol molecule.

Differences in the packing around cholesterol for the SA chain at the *sn*-1 position and for the OA and n-3 PUFA chains at the *sn*-2 position are immediately apparent in the RDF calculated with C10 for the central atom (Fig. 5.6, upper panel). The RDF for the SA *sn*-1 chain has a similar shape in each case. The first maximum at distance of about 6 Å is a well-defined single peak. By contrast, the RDF for the unsaturated *sn*-2 chain differs in each case. In OA-PC the first maximum for the OA chain is reduced in height compared to the SA chain and, suggesting the presence of two peaks that do not precisely overlap, there is a hint of asymmetry. The reduction in height of the first maximum for the DPA chain in DPA-PC is more marked, as is its asymmetry. There is further reduction in height and a better-defined separation into two peaks for the DHA chain in DHA-PC and the EPA chain in EPA-PC. These observations indicate that the PUFA, and to less extent OA, chains do not pack around cholesterol as tightly as the SA chain. The greater order of the saturated SA chain means that it adopts a more linear conformation that is able to lie parallel to the planar faces of the tetracyclic ring of the sterol. The higher disorder of the OA and, much more markedly, DPA, DHA and EPA chains produces an irregular configuration that is less compatible with close proximity, resulting in a distribution that is more spread out and uneven.

We also calculated RDF lower down the steroid moiety by choosing C13 to be the central atom (Fig. 5.6b). The first maximum for the *sn*-1 chain in all cases is less sharp than when C10 is the central atom. This change is due to the higher disorder that exists deeper in the bilayer where the C13 position is located. The same argument applies to the shape of the first maximum in the RDF for the *sn*-2 chains. The OA and DPA chains have a first maximum that is more clearly split into two peaks in the case of C13 position because the chains are more disordered. For DHA and EPA the difference between the C10 and C13 cases is less, which we attribute to near uniform high disorder that these chains possess throughout their entire length.

The sterol ring on cholesterol is not symmetric. It has a planar structure that is flat on one side (α face) and has two methyl groups poking out on the other bumpy side (β face) (Fig. 5.7, upper panel). Given this molecular structure, the surrounding phospholipid chains are

not expected to pack equally with respect to the two faces. To map the azimuthal distribution, and so elaborate upon the RDF described above (Fig. 5.6), we generated a number density profile (NDP) for the carbon atoms on the acyl chains with respect to an axis system (x',y',z') fixed in the cholesterol molecule. All 20 cholesterol molecules in our simulation were registered to a common frame of reference in which the C13 atom was chosen to be the origin, the C13-C18 vector was fixed on the x' direction and C13-C10 vector was kept in the $x'z'$ plane (Fig. 5.7, upper panel). The space around sterol molecules was then divided into bins $0.5\times0.5\times0.5$ Å^3 in size, and the number density of specified atoms on phospholipid molecules in each bin was counted through 180 ns of trajectory using a sampling rate of 50 frames per ns. Because of the consistent registration of coordinates, the NDP for all 20 cholesterol molecules could be simply added up. We computed in this way the NDP for the carbon atoms on the *sn*-1 or -2 chain of phospholipids within 1 nm distance from the origin on cholesterol in each system. A slice taken at $z' = 0$ (Fig. 5.7, lower panel) illustrates the set-up of the map of the spatial position of N(x',y') obtained.

Two ring-like structures around the cholesterol molecule can be discerned in the NDP for the *sn*-1 (Fig. 5.8, left column) and -2 chains (Fig. 5.8, right column) on OA-PC, DPA-PC, DHA-PC and EPA-PC in the slice taken at $z' = 0$. The first (inner) ring, which is 10-12 Å in diameter, maps the distribution of the chains closest to the sterol and follows the shape of the flat α face on the left and the bumpy β face on the right. The second ring, which is approximately 20 Å in diameter, maps the distribution of the chains in the next layer out and is fuzzier. The pattern for the NDP is unique in each case. For OA-PC, the inner ring for the SA and OA chains is thinner and better defined compared to the corresponding chains in the polyunsaturated systems. In addition, the gap between the first and second rings is clearer for the saturated *sn*-1 chain than for the monounsaturated and, more markedly, polyunsaturated *sn*-2 chains. These general features quantitatively agree with our assessment from the two-dimensional RDF plots - the packing of SA at the *sn*-1 position is tighter around cholesterol than OA and, even more so, DPA, DHA and EPA at the *sn*-2 position.

The NDP plots also probe how the density of the nearest neighbor chains in the first ring varies with orientation around the sterol (Figur. 5.8). Regions of highest density, which

indicate where a chain is most likely to be found, are apparent at the 1, 4, 9 and 11 o'clock positions for the SA chain and at the 4 and 7-10 o'clock positions for the OA chain in OA-PC. The region of high density for the latter chain at the 7-10 o'clock positions indicates that to some extent OA favors the flat surface of cholesterol. There is less heterogeneity in density for the more disordered chains in the n-3 PUFA containing membranes. In DPA-PC, the SA and DPA chains have highest density at the 1, 4 and 9 positions and the 4 and 11 positions, respectively. The regions of high density are less pronounced than in OA-PC and, in contrast to the OA chain, the DPA chain does not exhibit any preference for the flat face of the sterol. An almost homogenous distribution of density exists for the SA chain in DHA-PC, while regions of high density occur at the 1 and 9 o'clock positions for the DHA chain. As in DPA-PC, the regions of high density are not as distinct as in OA-PC. In EPA-PC, the ost disordered of the three n-3 PUFA-containing membranes, the distribution of both SA and EPA chains ultimately becomes homogenous.

The preference of the OA chain in OA-PC for the flat face of cholesterol exhibited in our NDP plots is contrary to the assessment made in simulations comparing RDF between the CH=CH on the phospholipid and CH_3 group at the C13 position on cholesterol in 1-palmitoyl-2-oleoylphosphatidycholine (POPC), which has saturated palmitic acid at the sn-1 position and OA at the sn-2 position, and 1,2-dioleoylphosphatidylcholine (DOPC), which has OA at sn-1 and -2 position, bilayers [27]. In this earlier work greater disparity in height between the first and second peaks in POPC compared to DOPC was attributed to OA preferring the bumpy face. It is an interpretation, however, made without the definitive insight into orientation provided by our NDP plots. The higher density for DHA than SA seen in the inner ring closest to cholesterol of our NDP plots with DHA-PC is another observation that contradicts previously published simulations [22]. Probability density distributions around the sterol were calculated showing a shell-like structure, similar to the rings in the NDP plots reported here, in which solvation by SA over DHA is preferred. Possible reasons for the discrepancy between findings include the use in the current simulations of an updated version of the force field (CHARMM36p vs. CHARMM27) and of the more physically realistic NPT ensemble (as opposed to the constant-energy, constant-volume ensemble (NVE)).

5.3.3 Biological implications

In conclusion, our MD simulations on DPA-PC, DHA-PC and EPA-PC confirmed that the n-3 PUFA increase disorder within a membrane and interact less favorably with cholesterol compared to monounsaturated OA in an OA-PC control. Differences between the molecular organization of the three n-3 PUFA and their interaction with cholesterol were revealed. EPA and DPA create most disorder and least disorder, respectively, while the effect of DHA lies between them. The differential in order between them is modest (~ 5%), as quantified by the average order parameter of the SA chain at the sn-1 position, yet affects their ability to pack close to cholesterol. It is, moreover, of potential significance in understanding the dietary impact of the n-3 PUFA found in fish oils.

The lipid raft concept offers an example of potential sensitivity to the amount of disorder produced by a particular n-3 PUFA. According to this concept, nano-sized domains enriched in sphingolipid and cholesterol that are liquid ordered (l_o) and contain signaling proteins float in a sea of surrounding bulk lipid that is liquid disordered (l_d) in the plasma membrane [58]. When the rafts coalesce together, they become functionalized. A variation on this scenario has incorporation of n-3 PUFA into the phospholipids of the bulk lipid fine tuning the clustering of rafts via the increased differential in order between within raft and non-raft environments that results [17,59]. In support of this proposal, we recorded solid state ^{2}H NMR spectra for deuterated analogs of EPA-, DHA and OA-containing PC in mixtures with SM and cholesterol (1:1:1 mol) that were analyzed in terms of segregation into SM-rich/cholesterol-rich (raft-like) and PC-rich/cholesterol-poor (non-raft) domains [16]. Two-component spectra indicating slow exchange between domains larger in size ($r > 35$ nm) were obtained with EPA, whereas single component spectra indicating fast exchange between domains smaller in size ($r < 45$ nm) were obtained with OA. Consistent with a smaller reduction in order, spectra indicative of intermediate exchange between domains that fall in size between the limits estimated for EPA and OA were obtained with DHA. Whether signaling proteins in rafts are turned on or off, thus, may depend upon the n-3 PUFA incorporated into membrane phospholipids.

The smaller reduction in order produced by DPA compared to EPA is also a factor that should be borne in mind when assessing the efficacy of EPA. Specifically, fatty acid

analyses of the composition of cells fed EPA have shown that substantial elongation to DPA can occur [6]. In such cases, the increase in disorder anticipated in response to uptake of EPA would be reduced. The similar effect on membrane order, for instance, was seen in B lymphoma cells treated with EPA and DHA was ascribed in part to elongation of EPA to DPA.

5.4 References

[1] Mozaffarian, D., and Wu, J.H.Y. (2011) Omega-3 fatty acids and cardiovascular disease: effects on risk factors, molecular pathways and clinical events, *J. Am. Coll. Cardiol.* 58, 2047-2067.

[2] Bang, H.O., Dyerberg, J., and Nielson, A. (1971) Plasma lipid and lipoprotein pattern in Greenlandic West-coast Eskimos, *Lancet* 297, 1143–1146.

[3] Dyall, S.C. (2015) Long-chain omega-3 fatty acids and the brain: a review of the independent and shared effects of EPA, DPA and DHA. *Front. Aging Neurosci.* 7, 52.

[4] Calder, P.C. (2013) Omega-3 polyunsaturated fatty acids and inflammatory processes: nutrition or pharmacology? *Br. J. Clin. Pharmacol.* 75, 645-662.

[5] Vaughan, V.C., Hassing, M-R. and Lewandowski, P.A. (2013) Marine polyunsaturated fatty acids and cancer therapy, *Br. J. Cancer* 108, 486–492.

[6] Kaur, G., Cameron-Smith, D., Garg, M., and Sinclair, A.J. (2011) Docosapentaenoic acid (22:5n-3): A review of its biological effects, *Prog. Lipid Res.* 50, 28–34.

[7] Mozaffarian, D., and Wu. J.H.Y. (2012) (n-3) Fatty acids and cardiovascular health: are effects of EPA and DHA shared or complementary? *J. Nutr.* 142, 614S–625S.

[8] Calder, P.C. (2015) Marine omega-3 fatty acids and inflammatory processes: Effects, mechanisms and clinical relevance, *Biochim. Biophys. Acta* 1851, 469–484.

[9] Hou, T.Y., McMurray D.N., and Chapkin, R.S. (2016) Omega-3 fatty acids, lipid rafts, and T cell signaling, *Eur. J. Pharmacol.* 785, 2-9.

[10] Shaikh, S.R. (2012) Biophysical and biochemical mechanisms by which dietary N-3 polyunsaturated fatty acids from fish oil disrupt membrane lipid rafts, *J. Nutr. Biochem.* 23, 101-105.

[11] Lingwood, D., and K. Simons, K. (2010) Lipid rafts as a membrane-organizing principle, *Science* 327, 46–50.

[12] Yaqoob, P., and Shaikh, S.R. (2010) The nutritional and clinical significance of lipid rafts, *Curr. Opin. Clin. Nutr. Metab.* 13, 156-166.

[13] Turk, H.F., and Chapkin, R.S. (2013) Membrane lipid raft organization is uniquely modified by n-3 polyunsaturated fatty acids, *Prost. Leuk. Essent. Fatty Acids* 88, 43–47.

[14] Shaikh, S.R., Dumaual, A.C., Castillo, A., LoCascio, D., Siddiqui, R.A., Stillwell, W., and Wassall, S.R. (2004) Oleic and docosahexaenoic acid differentially phase separate from lipid raft molecules: A comparative NMR, DSC, AFM, and detergent extraction study, *Biophys. J.* 87, 1752-1766.

[15] Soni, S.P., LoCascio, D.S., Liu, Y., Williams, J.A., Bittman, R., Stillwell, W., and Wassall, S.R. (2008) Docosahexaenoic acid enhances segregation of lipids between raft and non-raft domains: ^{2}H NMR study, *Biophys. J.* 95, 203-214.

[16] Williams, J.A., Batten, S.E., Harris, M., Rockett, B.D., Shaikh, S.R., Stillwell, W., and Wassall, S.R. (2012) Docosahexaenoic and eicosapentaenoic acids segregate differently between raft and non-raft domains, *Biophys. J.* 103, 228-237.

[17] Shaikh, S.R., Kinnun, J.J., eng, X., Williams, J.A., and Wassall, S.R. (2015) How polyunsaturated fatty acids modify molecular organization in membranes: insight from NMR studies of model systems, *Biochim. Biophys. Acta* 1848, 211-219.

[18] Pastor, R.W., and MacKerell Jr., A.D. (2012) Development of the CHARMM force field for lipids, *J. Phys. Chem. Lett.* 2, 1526-1532.

[19] Saiz, L., and Klein, M.L. 2001. Structural properties of a highly polyunsaturated lipid bilayer from molecular dynamics simulations, *Biophys. J.* 81, 201-216.

[20] Feller, S.E., Gawrisch K., and MacKerell Jr., A.D. (2002) Polyunsaturated fatty acids in lipid bilayers: intrinsic and environmental contributions to their unique physical properties, *J. Amer. Chem. Soc.* 124, 318-326.

[21] Huber, T., Rajamoorthi, K., Kurze, V.F., Beyer, K., and Brown, M.F. (2002) Structure of docosahexaenoic acid-containing phospholipid bilayers as studied by ^{2}H NMR and molecular dynamics simulations, *J. Amer. Chem. Soc.* 124, 298-309.

[22] Pitman, M.C., Suits, F., MacKerell Jr., A.D., and Feller, S.E. (2004) Molecular-level organization of saturated and polyunsaturated fatty acids in a phosphatidylcholine bilayer containing cholesterol, *Biochemistry* 43, 15318–15328.

[23] Shaikh, S.R., Cherezov, V., Caffrey, M., Soni, S.P., LoCascio, D., Stillwell, W., and Wassall, S.R. (2006) Molecular organization of cholesterol in unsaturated phosphatidylethanolamines: X-ray diffraction and solid state ^{2}H NMR reveal differences with phosphatidylcholines, *J. Amer. Chem. Soc.* 128, 5375-5383.

[24] Stillwell, W., and Wassall, S.R. (2003) Docosahexaenoic acid: membrane properties of a unique fatty acid, *Chem. Phys. Lipids* 126, 1–27.

[25] Jo, S., Lim, J.B., Klauda, J.B., and Im, W. (2009) CHARMM-GUI MEMBRANE BUILDER for mixed bilayers and its application to yeast membranes, *Biophys. J.* 97, 50-58.

[26] Klauda, J.B., Monje, V., Kim, T., and Im, W. (2012) Improving the CHARMM force field for polyunsaturated fatty acid chains, *J. Phys Chem. B* 116, 9424-9431.

[27] Darden, T., York, D., and Pedersen, L. (1993) Particle mesh Ewald: an $n \cdot \log(n)$ method for Ewald sums in large systems, *J. Chem. Phys.* 98, 10089-10092.

[28] Brooks, B.R., Brooks III, C.L., MacKerell Jr., A.D., Nilsson, L., Petrella, R.J., Roux, B., Won, Y., Archontis, G., Bartels, C., Boresch, S., Caflisch, A., Caves, L., Cui, Q., Dinner, A.R., Feig, M., Fischer, S., Gao, J., Hodoscek, M., Im, W., Kuczera, K., Lazaridis, T., Ma, J., Ovchinnikov, V., Paci, E., Pastor, R.W., Post, C.B., Pu, J.Z., Schaefer, M., Tidor, B., Venable, R.M., Woodcock, H.L., Wu, X., Yang, W., York, D.M., and Karplus, M. (2009) CHARMM: the biomolecular simulation program, *J. Comp. Chem.* 30, 1545-1614.

[29] Phillips, J.C., Braun, R., Wang, W., Gumbart, J., Tajkhorshid, E., Villa, E., Chipot, C., Skeel, R.D., Kalé, L., and Schulten, K. (2005) Scalable molecular dynamics with NAMD, *J. Comp. Chem.* 26, 1781-1802.

[30] Hoover, W.G. (1985) Canonical dynamics: equilibrium phase-space distributions, *Phys. Rev. A* 31, 1695-1697.

[31] Feller, S.E., Zhang, Y., Pastor, R.W., and Brooks, B.R. (1995) Constant pressure molecular dynamics simulation: the Langevin piston method, *J. Chem. Phys.* 103, 4613-4621.

[32] Humphrey, W., Dalke, A., and Schulten, K. (1996) VMD - Visual Molecular Dynamics, *J. Mol. Graph.* 14, 33-38.

[33] Vermeer L.S., De Groot, B.L., Réat, V., A. Milon, A., and Czaplicki, J. (2007) Acyl chain order parameter profiles in phospholipid bilayers: computation from molecular dynamics simulations and comparison with ^{2}H NMR experiments, *Eur. Biophys. J.* 36, 919-931.

[34] Seelig, J. (1977) Deuterium magnetic resonance theory and application to lipid membranes, *Q. Rev. Biophys.*10, 353-418.

[35] Engel, A.K., and Cowburn, D. (1981) The origin of multiple quadrupole couplings in the deuterium NMR spectra of the 2 chain of 1,2 dipalmitoyl-sn-glycero-3-phosphorylcholine, *FEBS Lett.* 126, 169-171.

[36] Holte, L.L., Peter, S.A., Sinnwell, T.M., and Gawrisch, K. (1995) ^{2}H nuclear magnetic resonance order parameter profiles suggest a change of molecular shape for phosphatidylcholines containing a polyunsaturated acyl chain, *Biophys. J.* 68, 2396-2403.

[37] Harris, M., Kinnun, J.J., Kosaraju, R., Leng, X., Wassall S.R., and Shaikh, S.R. (2016) Membrane disordering by eicosapentaenoic acid in B lymphomas is reduced by elongation to docosapentaenoic acid as revealed with solid-state nuclear magnetic resonance spectroscopy of model membranes, *J. Nutr.* 146, 1283-1289.

[38] Eldho, N.V., Feller, S.E., Tristram-Nagle, S., Polozov, I.V., and Gawrisch, K. (2003) Polyunsaturated docosahexaenoic vs. docosapentaenoic acid-differences in lipid matrix properties from the loss of one double bond, *J. Amer. Chem. Soc*. 25, 6409–6421.

[39] Seelig, J, and Waespe-Sarcevic, N. (1978) Molecular order in cis and trans unsaturated phospholipid bilayers, *Biochemistry* 17, 3310-3315.

[40] Soni, S.P., Ward, J.A, Sen, S.E., Feller, S.E., and Wassall, S.R. (2009) Effect of *trans* unsaturation on molecular organization in a phospholipid membrane, *Biochemistry* 48, 11097-11107.

[41] Feller, S.E. (2008) Acyl chain conformations in phospholipid bilayers: a comparative study of docosahexaenoic acid and saturated fatty acids, *Chem. Phys. Lipids* 153, 76-80.

[42] Soubias, O., and Gawrisch, K. (2007) Docosahexaenoyl chains isomerize on the sub-nanosecond timescale, *J. Am. Chem. Soc.* 129, 6678-6679.

[43] Gawrisch, K., and Soubias, O. (2008) Structure and dynamics of polyunsaturated hydrocarbon chains in lipid bilayers—significance for GPCR function, *Chem. Phys. Lipids* 153, 64-75.

[44] Leng, X., Kinnun, J.J., Marquardt, D., Ghefli, M., Kučerka, N., Katsaras, J., Atkinson, J., Harroun, T.A., Feller, S.E., and Wassall, S.R. (2015) α-Tocopherol is well designed to protect polyunsaturated phospholipids: MD simulations, *Biophys. J.* 109, 1608-1618.

[45] Braun, A.R., Brandt, E.G., Edholm, O., Nagle, J.F., and Sachs, J.N. (2011) Determination of electron density profiles and area from simulations of undulating membranes, *Biophys. J.* 100, 2112-2120.

[46] Kučerka, N., Heberle, F.A., Pan, J., and Katsaras, J. (2015) Structural significance of lipid diversity as studied by small angle neutron and X-ray scattering, *Membranes* 5, 454-472.

[47] Heftberger, P., Kollmitzer, B., Heberle, F.A., Pan, J., Rappolt, M., Amenitsch, H., N. Kučerka, N., Katsaras, J., and Pabst, G. (2014) Global small-angle X-ray scattering data analysis for multilamellar vesicles: the evolution of the scattering density profile model, *J. Appl. Cryst.* 47, 173-180.

[48] Marquardt, D., Heberle, F.A., Greathouse, D.V., Koeppe R.E., II, Standaert, R.F., Van Oosten, B.J., Harroun, T.A., Kinnun, J.J., Williams, J.A., Wassall, S.R., and Katsaras, J. (2016) Lipid bilayer thickness determines cholesterol's location in model membranes, *Soft Matter* 12, 9417-9428.

[49] Petrache, H.I., Dodd, S.W., and Brown, M.F. (2000) Area per lipid and acyl chain length distributions in fluid phosphatidylcholines determined by ^{2}H NMR spectroscopy. *Biophys. J.* 78, 3172–3192.

[50] Marquardt, D., Kučerka, N., Wassall, S.R., Harroun, T.A., and Katsaras, J. (2016) Cholesterol's location in lipid bilayers. *Chem. Phys. Lipids* 99, 17-25.

[51] Huster, D., Arnold, K., and Gawrisch, K. (1998) Influence of docosahexaenoic acid and cholesterol on lateral lipid organization in phospholipid mixtures. *Biochemistry* 37, 17299-17308.

[52] Mihailescu, M., Soubias, O., Worcester, D., White, S.H., and Gawrisch, K. (2011) Structure and dynamics of cholesterol-containing polyunsaturated lipid membranes studied by neutron diffraction and NMR. *J. Membrane Biol.* 239, 63-71.

[53] Hung, W-C., Lee, M-T., Chen, F-Y., and Huang, H.W. (2007) The condensing effect of cholesterol in lipid bilayers. *Biophys. J.* 92, 3960–3967.

[54] Oldfield, E., Meadows, M., Rice, D., and Jacobs, R. (1978) Spectroscopic studies specifically deuterium labeled membrane systems. Nuclear magnetic resonance investigation of the effects of cholesterol in model systems. *Biochemistry* 17, 2727-2740.

[55] Brzustowicz, M.R., Stillwell, W., and Wassall, S.R. (1999) Molecular organization of cholesterol in polyunsaturated phospholipid membranes: a solid state ^{2}H NMR investigation. *FEBS Lett.* 451, 197-202.

[56] Róg, T., Pasenkiewicz-Gierula, M., Vattulainen I., and Karttunen, M. (2007) What happens if cholesterol is made smoother: importance of methyl substituents in cholesterol ring structure on phosphatidylcholine–sterol interaction. *Biophys. J.* 92, 3346-3357.

[57] Pandit, S.A., Chiu, S.W., Jakobsson, E., Grama, A., and Scott, H.L. (2008) Cholesterol packing around lipids with saturated and unsaturated chains: a simulation study. *Langmuir* 24, 6858-6865.

[58] Lingwood, D., and Simons, K. (2010) Lipid rafts as a membrane-organizing principle. *Science 327*, 46–50.

[59] Levental, K.R., Lorent, J.H., Lin, X., Skinkle, A.D., Surma, M.A., Stockenbojer, E.A., Gorfe, A.A., Levental, I. (2016) Polyunsaturated lipids regulate membrane domain stability by tuning membrane order. *Biophys. J. 110*, 1800–1810.

Table 5.1

Membrane thickness (D_{HH}) measured by phosphate-phosphate distance (Å). The uncertainty is $\pm$0.09 Å, estimated from the standard error of the peak locations.

	OA-PC	DPA-PC	DHA-PC	EPA-PC
Pure	39.6	39.7	38.4	37.5
With cholesterol	44.2	42.9	42.2	40.7
Change	4.6	3.2	3.8	3.2

Table 5.2

Average order parameters of sn-1 chain and sn-2 chain from OA-PC, DPA-PC, DHA-PC and EPA-PC membranes without and with 20 mol% of cholesterol.

Lipids	$\bar{S}_{CD}$			
	Sn-1		Sn-2	
	Without Cholesterol	With cholesterol	Without Cholesterol	With cholesterol
OA-PC	0.152	0.214	0.114	0.170
DPA-PC	0.140	0.182	0.047	0.062
DHA-PC	0.136	0.178	0.031	0.041
EPA-PC	0.131	0.169	0.032	0.044

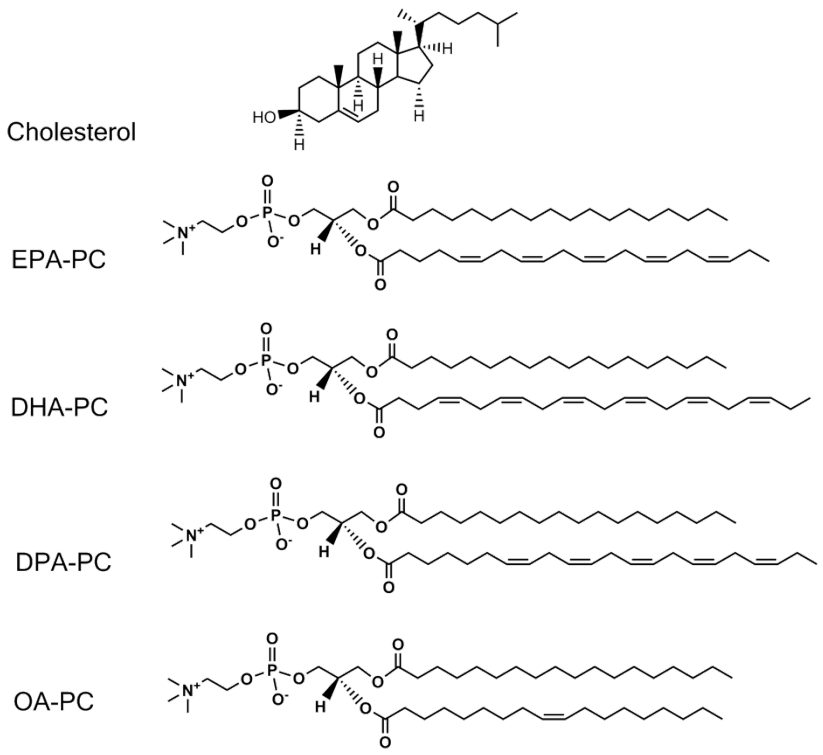

Figure 5.1

Molecular structure of OA-PC, DPA-PC, DHA-PC, EPA-PC and cholesterol.

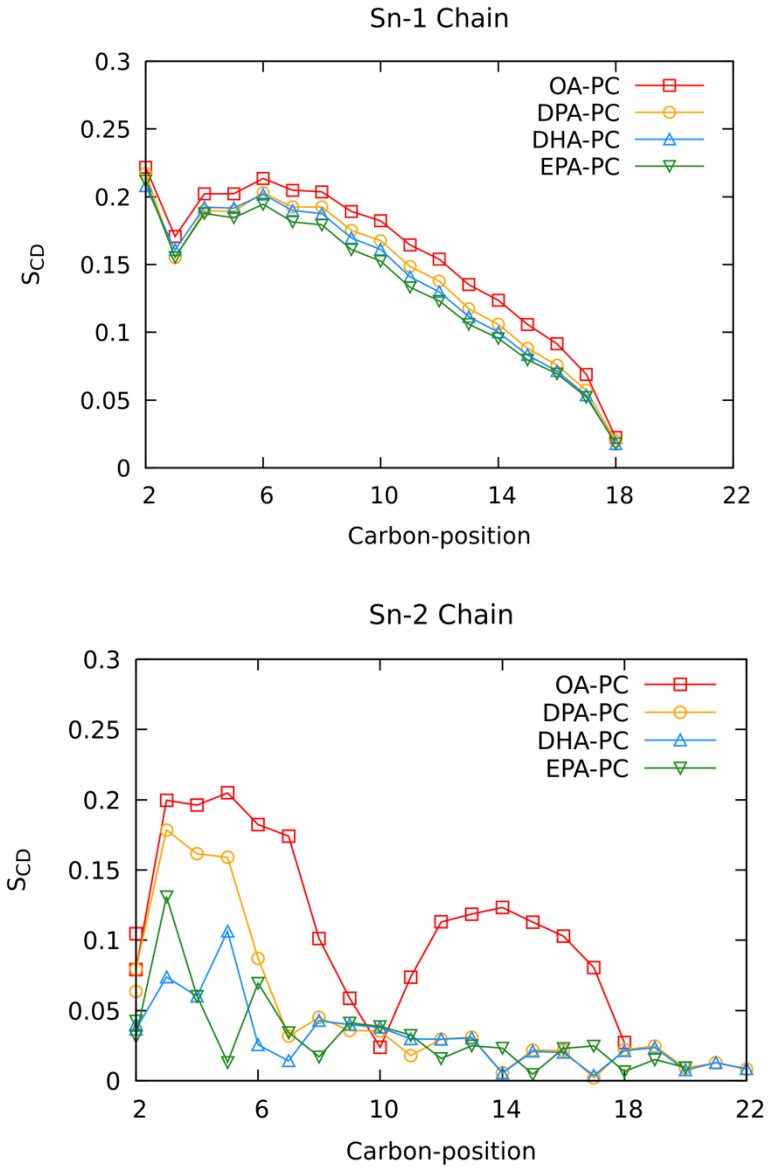

Figure 5.2

Order parameter profile along the *sn*-1 (upper panel) and -2 (lower panel) chains in OA-PC (red), DPA-PC (yellow), DHA-PC (blue) and EPA-PC (green) bilayers obtained from MD simulations at 37°C. The uncertainty in the simulated data is ≤±0.003 in sn-1 chain and ≤±0.002 in sn-2 chain, which was estimated from the standard error obtained treating each lipid molecule independently. The uncertainty is smaller in more disordered (lower S_{CD} value) carbon positions.

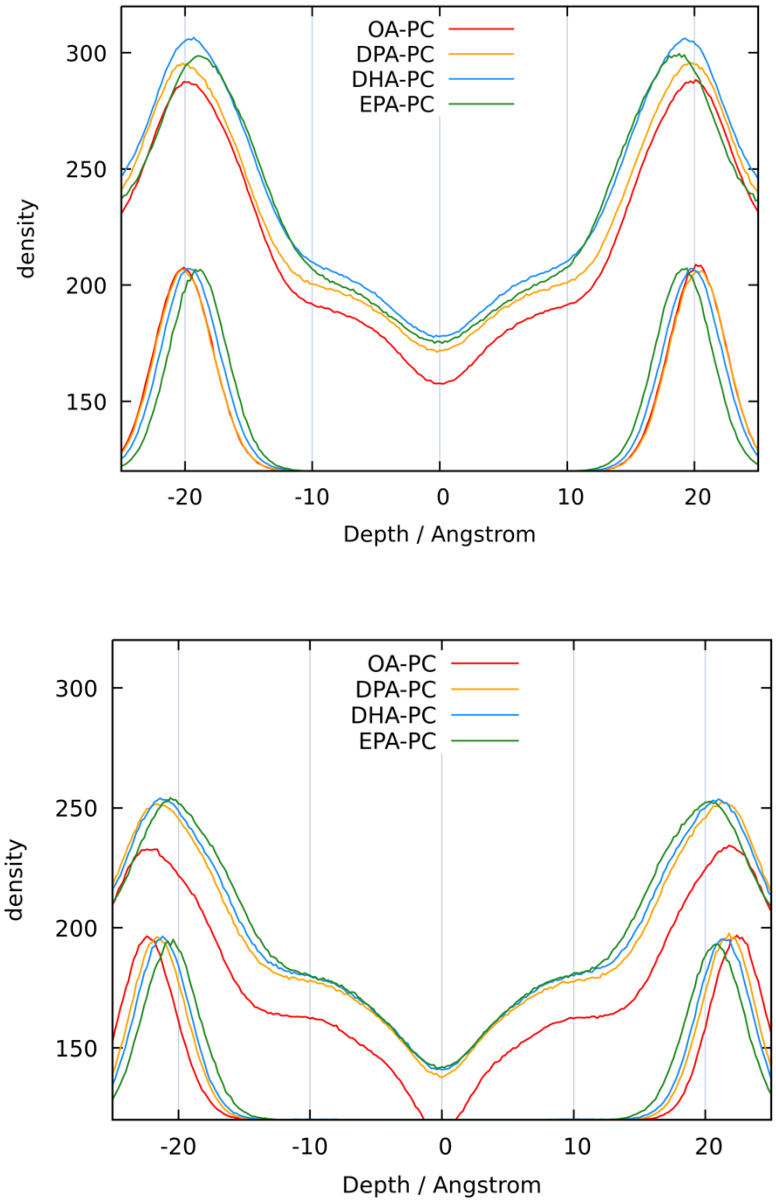

Figure 5.3

EDP for all atoms (above) and the number density profile of phosphorus atom (below) on the phospholipid in OA-PC, DPA-PC, DHA-PC and EPA-PC bilayers without cholesterol (upper panel) and with addition of 20 mol% cholesterol (lower panel). The phosphate curves are scaled and shifted for clarity.

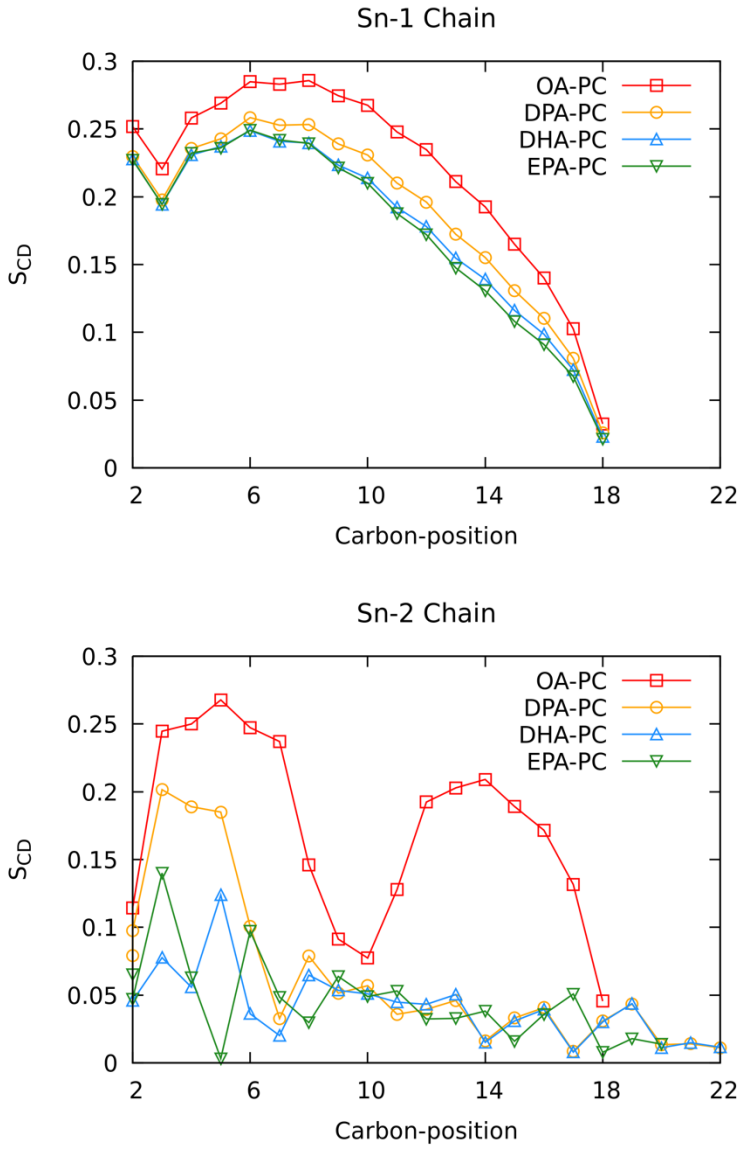

Figure 5.4

Order parameter profile along the *sn*-1 (upper panel) and -2 (lower panel) chains in OA-PC (red), DPA-PC (yellow), DHA-PC (blue) and EPA-PC (green) bilayers following the addition of 20 mol% cholesterol obtained from MD simulations at 37°C. The uncertainty in the simulated data is $\leq \pm 0.003$ in sn-1 chain and $\leq \pm 0.002$ in sn-2 chain, which was estimated from the standard error obtained treating each lipid molecule independently. The uncertainty is smaller in more disordered (lower S_{CD} value) carbon positions.

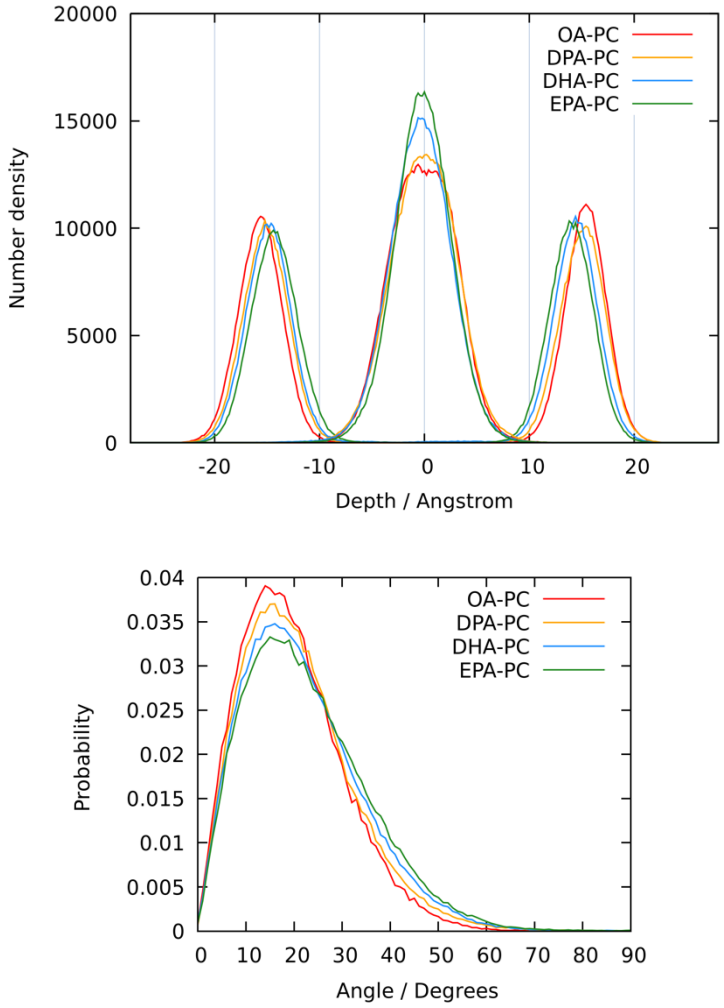

Figure 5.5

Carbon number density profile for the [2,3,4]-carbons (headgroup) and [25,26,27]-carbons (tail) on cholesterol (upper panel) and histogram of the orientation of cholesterol (vector connecting the C13-C10 carbons) relative to the bilayer normal (lower panel) in OA-PC, DPA-PC, DHA-PC and EPA-PC bilayers.

Figure 5.6

Radial distribution function (RDF) for carbon atoms on the sn-1 and-2 chains of OA-PC, DPA-PC, DHA-PC and EPA-PC around the C10 (left panel) and C13 (right panel) atom on cholesterol. The carbon atoms on cholesterol and phospholipid are at the the same depth (within ±1 Å in z direction) as shown in the illustration on two sides.

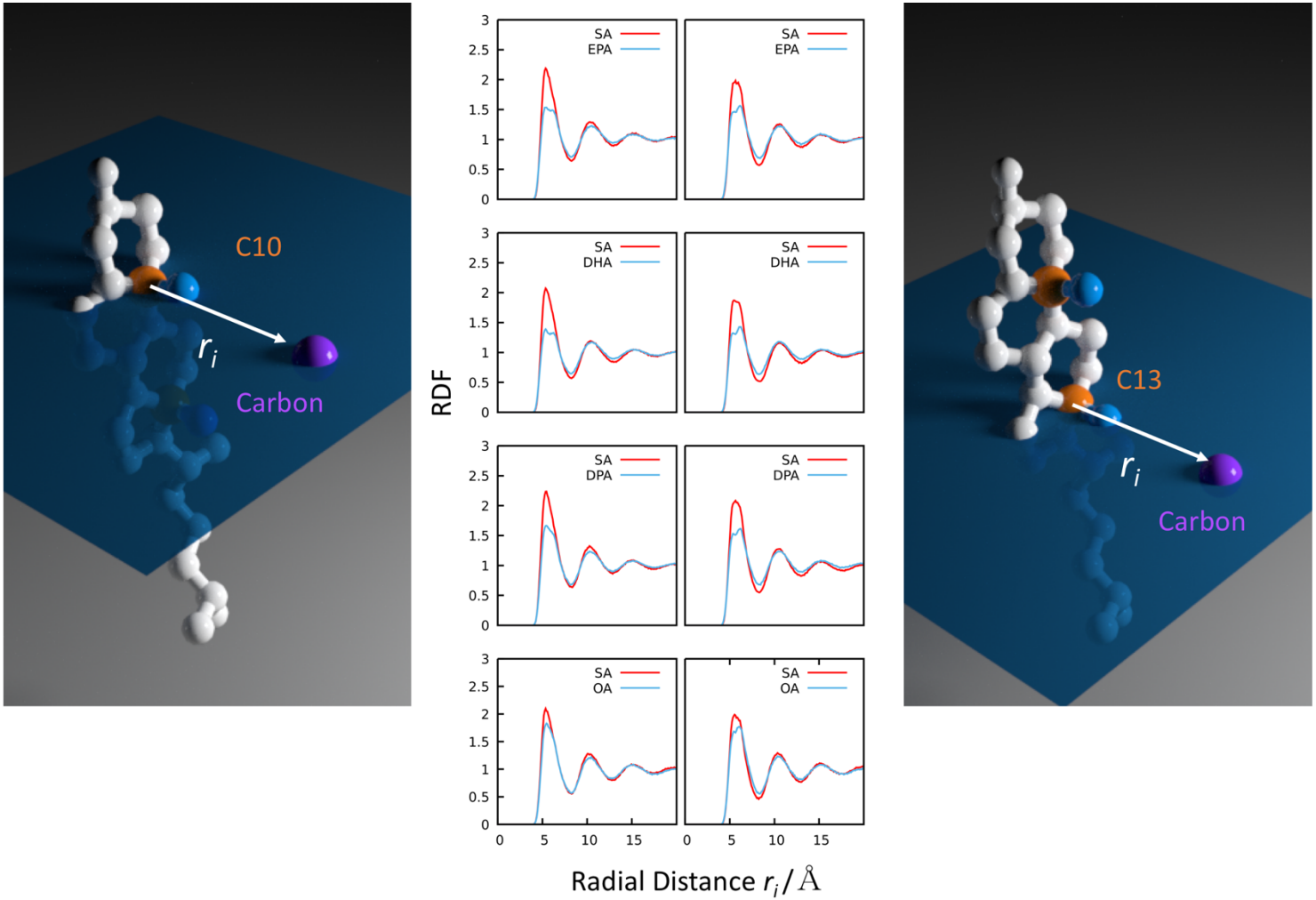
C10
r_i
Carbon
C13
r_i
Carbon
RDF
SA
EPA
SA
DHA
SA
DPA
SA
OA
0
0.5
1
1.5
2
2.5
3
0
5
10
15
Radial Distance r_i / Å

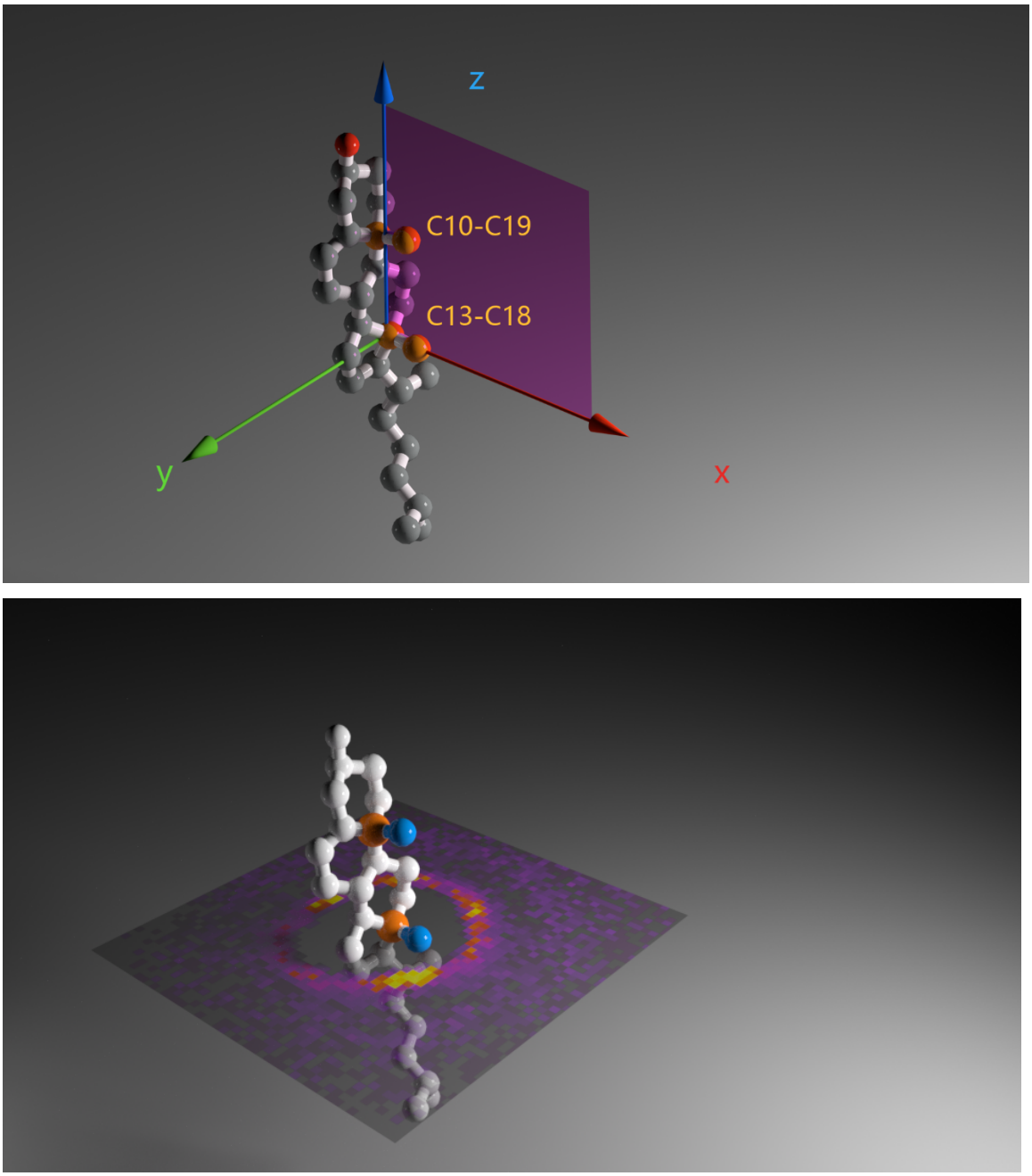

Figure 5.7

Coordinate system (x',y',z') used in the number density profile (NDP) generation relative to the cholesterol molecule (upper panel) and an example of one slice illustrating the set-up of the NDP relative to cholesterol in OA-PC (lower panel). The color scale is the same as in Fig. 5.8.

Figure 5.8

NDP around cholesterol of the carbon atoms on the *sn*-1 (left column) and -2 (right column) chains in OA-PC, DPA-PC, DHA-PC and EPA-PC. Slice is at the depth of the C13 atom on cholesterol. The color represents number of carbons found in the bin within 180 ns by 50/ns sampling rate.

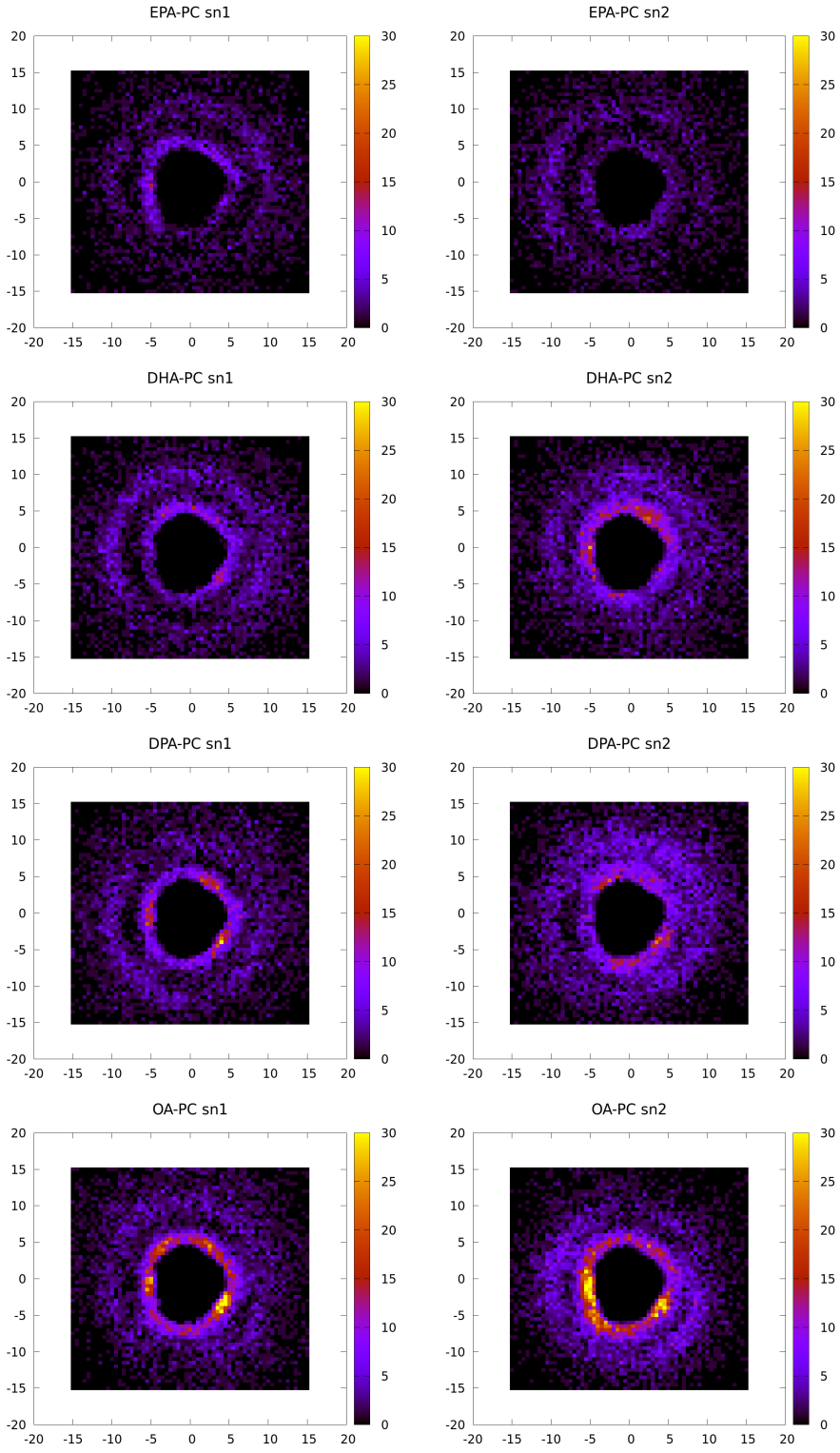
EPA-PC sn1
EPA-PC sn2
DHA-PC sn1
DHA-PC sn2
DPA-PC sn1
DPA-PC sn2
OA-PC sn1
OA-PC sn2

CHAPTER 6. CONCLUSIONS

The main focus of my thesis was characterizing lipid-lipid interaction and lipid dynamics in the PUFA-incorporated lipid membranes. The major techniques applied were standard MD simulation and USMD simulation. In this chapter I will summarize the work done and suggest possible future directions.

6.1 Vitamin E and PUFA

In Chapter 3, we performed standard MD simulations on αtoc in SDPC bilayers, compared with in SOPC bilayers as a control [1]. SDPC represents a PUFA-incorporated phospholipid found in the plasma membrane, and SOPC is monounsaturated and a common bulk lipid in plasma membrane. The simulations were first qualitatively validated by ^{2}H NMR order parameters obtained experimentally. As a molecule that has similar chemical structure to cholesterol, αtoc also orders the corresponding membranes [2,3]. Then comparison was made with neutron scattering data that established there was reasonable agreement on membrane thickness and the disposition of αtoc in the membranes.

We analyzed the interactions between αtoc and different acyl chains in terms of the vdW energy, and further generated a probability distribution function mapping the location of carbon atoms on the lipid chains near αtoc. We found that the DHA chain on SDPC is more likely to come into close proximity with the chromanol ring on αtoc than the OA chain on SOPC. Moreover, flip-flop of αtoc across the bilayer was observed and its rate is about an order of magnitude faster in SDPC than in SOPC. The differences between SDPC and SOPC were attributed to the highly disordered nature of DHA chains. A DHA chain is so flexible that its lower portion can reach the aqueous interface more easily than OA [4], so that the chromanol group, which sits close to the aqueous interface, has a better chance of contact with DHA. The disordered DHA chain also reduces lipid packing, allowing the chromanol ring to penetrate the hydrophobic bilayer interior more easily. The shielding provided by the methyl groups on either side of the OH group on the chromanol group plays a crucial role in letting αtoc to enter the bilayer.

From these results, we conclude that the behavior of αtoc in a PUFA-containing membrane would assist its antioxidant function. The enhanced likelihood of DHA meeting the chromanol group would help the OH group meet and react with lipid peroxyl radicals to stop oxidation. Rapid flip-flop of α-toc across the polyunsaturated phospholipid bilayer would also facilitate termination of lipid chain peroxidation within a membrane as well as at the surface.

To investigate whether αtoc preferentially interacts with PUFA-containing lipid, we performed umbrella sampling MD simulations to calculate its binding energy to lipid bilayers in a subsequent described in Chapter 4. Again we selected SDPC and SOPC to represent the polyunsaturated and monounsaturated lipids, respectively. The vertical (membrane normal) distance between the center of mass of αtoc's chromanol group and the center of the bilayer was chosen to be the reaction coordinate z. The free energy (G(z)) as a function of z was then calculated from umbrella sampling simulations through WHAM. Defining the binding energy as the difference ΔG_{bind} between z_{out} (where αtoc is fully in water) and z_{eq} (where αtoc is at its equilibrium position), the values obtained for ΔG_{bind} are 16.7 kcal/mol in SDPC and 18.3 kcal/mol in SOPC. Greater affinity for SOPC than SDPC is implied, which we ascribe to tighter packing within the monounsaturated phospholipid bilayer. The behavior resembles the higher affinity cholesterol has for ordered, saturated lipid-raft like environments.

From the energy barrier at the center of the membrane in our PMF profiles, defined as ΔG_{flip} between z_{eq} and z_0, we further estimated the rate flip-flop rate for αtoc. The barrier is 0.7 kcal/mol higher in SOPC than SDPC, and the estimated flip-flop rates are 2.5×10^5 s^{-1} for the SOPC and 7.5×10^5 s^{-1} for the SDPC. Like cholesterol, the rates are much faster than reported for phospholipid [5,6]. The faster flip-flop of αtoc in SDPC is consistent with our result from standard MD simulation. The orientation of the chromanol group with respect to depth within the membranes was also mapped. These plots confirm that the chromanol group tends to stay "upright" except at the center of bilayer, where it becomes random in orientation and so can flip to the other leaflet.

Taken together, our umbrella sampling simulations found that αtoc binds less strongly to and flip-flops more quickly in SDPC than SOPC. Preferential affinity for polyunsaturated phospholipid is not seen.

6.2 n-3 PUFA

DPA (22:5), DHA (22:6) and EPA (20:5) are long chain n-3 PUFAs with differing lengths and numbers of double bond consumed in the diet from fish oils. They are associated with a lot of health benefits [7], but whether they have shared or complementary effect is unknown. Our purpose was to investigate how their uptake into phospholipids affect membrane organization and the interaction with cholesterol. In Chapter 5, we applied standard all-atom MD simulation on model membrane-water systems with validation by ^{2}H NMR order parameters. The membrane bilayers are composed of phosphatidylcholine (PC) with stearic acid for the sn-1 chain and different unsaturated fatty acids for the sn-2 chain. The sn-2 chain was either DPA, EPA, DHA or, as a monounsaturated control, OA. Each of these PC lipids were simulated twice: one on a bilayer composed 100 mol% PC, and another with 80 mol% PC and 20 mol% of cholesterol.

The simulations run on single component bilayers showed that, as expected, all three polyunsaturated membranes were more disordered and thinner than the monounsaturated control. Among the polyunsaturated membranes DPA-PC was least disordered and thickest while EPA-PC was most disordered and thinnest. DHA-PC was in between. The interaction with cholesterol was investigated in three steps. First, we observed that cholesterol increases the order and thickness of the polyunsaturated PCs less than monounsaturated OA-PC. Less interaction between cholesterol and lipid chains in the more disordered membranes is implied. Then, we calculated two-dimensional RDFs for carbon atoms on the phospholipid chains (both sn-1 and sn-2) with respect to cholesterol. They showed the disordered n-3 PUFA chains pack around the sterol moiety less compactly than the more ordered saturated SA and, to less extent, mono-unsaturated OA chain. Finally, we generated 3D NDPs of carbons on the phospholipid chains around cholesterol. They confirmed that the n-3 PUFA chains at the sn-2 position do not pack as tightly around the sterol as SA at the sn-1 position or OA at the sn-2 position. Heterogeneity in the NDP

profile, indicating more intimate sterol-FA chain interaction, was most visible for QA-PC, and gradually faded away with more disordered n-3 PUFA-containing PCs.

In general, our simulations and analysis show all three PUFAs disorder the membrane and interact less favorably with cholesterol than OA or SA. EPA has the most disordering effect and packs least well with cholesterol, while DPA has the least disordering effect and packs most well with cholesterol. Such differences have the potential to differentially modulate plasma membrane organization, for example regulating the size of lipid rafts and so modulating the activity of signaling proteins. The results demonstrate, in particular, that possible elongation of EPA to DPA must be taken into account when interpreting the impact of fish oils on membrane organization [8].

6.3 Future directions

Future directions for research include further study of the binding of αtoc to lipid bilayers and its flip-flop within membranes.

The comparison of binding energy measured for SDPC vs. SOPC in our UBSMD simulations shows αtoc has greater affinity to the less unsaturated lipid. However, in these simulations αtoc is in a single component phospholipid environment. Plasma membranes, by contrast, contain many different lipids. Cholesterol, in particular, is a major constituent and its concentration varies drastically between lipid domains. It is possible that αtoc would prefer a PUFA-rich environment depleted in cholesterol over a saturated raft-like domain enriched in cholesterol concentration. Thus, a future direction is to obtain the binding energy of αtoc cholesterol-containing membranes. We would prepare lipid membranes composed of SDPC or SOPC, mixed with different concentrations of cholesterol. A pair of αtoc would then be placed in the membranes to perform UBSMD simulations like in Chapter 4, to so get its binding energy in the presence of cholesterol.

The path that αtoc takes in the flip-flop process would be better described by adding the orientation of the chromanol group as another reaction coordinate in the umbrella sampling. A similar approach was done in studying cholesterol's flip-flop behavior [6]. As another future direction, we propose performing two-dimensional USMD simulations to get the profile of the PMF $G(z,\theta)$ for αtoc as a function of both depth z and orientation θ of the

chromanol group. In this way we would get a more complete analysis of αtoc's flip-flop motion. The same two-dimensional USMD method could also be applied to δ-tocopherol, which undergoes much slower flip-flop according to our earlier all-atom simulations.

6.4 Reference

[1] X. Leng, J. J. Kinnun, D. Marquardt, M. Ghefli, N. Kučerka, J. Katsaras, ... and S. R. Wassall, "α-Tocopherol Is Well Designed to Protect Polyunsaturated Phospholipids: MD Simulations," *Biophysical journal,* vol. 109, no. 8, pp. 1608-1618, 2015.

[2] I. V. Polozov and K. Gawrisch, "NMR detection of lipid domains," *Methods Mol. Biol.,* vol. 398, pp. 107-126, 2007.

[3] M. Mihailescu, O. Soubias, D. Worcester, S. H. White and K. Gawrisch, "Structure and dynamics of cholesterol-containing polyunsaturated lipid membranes studied by neutron diffraction and NMR," *The Journal of membrane biology,* vol. 239, no. 1-2, pp. 63-71, 2011.

[4] S. E. Feller, K. Gawrisch and A. D. MacKerell, "Polyunsaturated fatty acids in lipid bilayers: intrinsic and environmental contributions to their unique physical properties," *Journal of the American Chemical Society,* vol. 124, no. 2, pp. 318-326, 2002.

[5] W. D. Bennett and D. P. Tieleman, "Molecular simulation of rapid translocation of cholesterol, diacylglycerol, and ceramide in model raft and nonraft membranes," *Journal of lipid research,* vol. 53, no. 3, pp. 421-429, 2012.

[6] S. Jo, H. Rui, J. B. Lim, J. B. Klauda and W. Im, "Cholesterol flip-flop: insights from free energy simulation studies," *The Journal of Physical Chemistry B,* vol. 114, no. 42, pp. 13342-13348, 2010.

[7] D. Mozaffarian an

Figure A 1

d J. H. Wu, "Omega-3 fatty acids and cardiovascular disease: effects on risk factors, molecular pathways, and clinical events," *ournal of the American College of Cardiology,* vol. 58, no. 20, pp. 2047-2067, 2011.

[8] G. Kaur, D. Cameron-Smith, M. Garg and A. J. Sinclair, "Docosapentaenoic acid (22: 5n-3): a review of its biological effects," *Progress in lipid research,* vol. 50, no. 1, pp. 28-34, 2011.

APPENDIX A. SUPPLEMENTAL MATERIAL FOR ALPHA-TOCOPHEROL IS WELL-DESIGNED TO PROTECT POLYUNSATURATED PHOSPHOLIPIDS: MD SIMULATIONS

Table A.1

The surface area per lipid calculated from the average bilayer size during the MD simulations on SDPC and SOPC bilayers in the absence and presence of 20 mol% αtoc at 37 °C.

Lipid	SDPC	SDPC+αtoc	SOPC	SOPC+αtoc
Area/lipid ($Å^2$)	71.7 ± 0.2	62.4 ± 0.2	65.7 ± 0.3	58.7 ± 0.2

The uncertainties are the standard error of the areas.

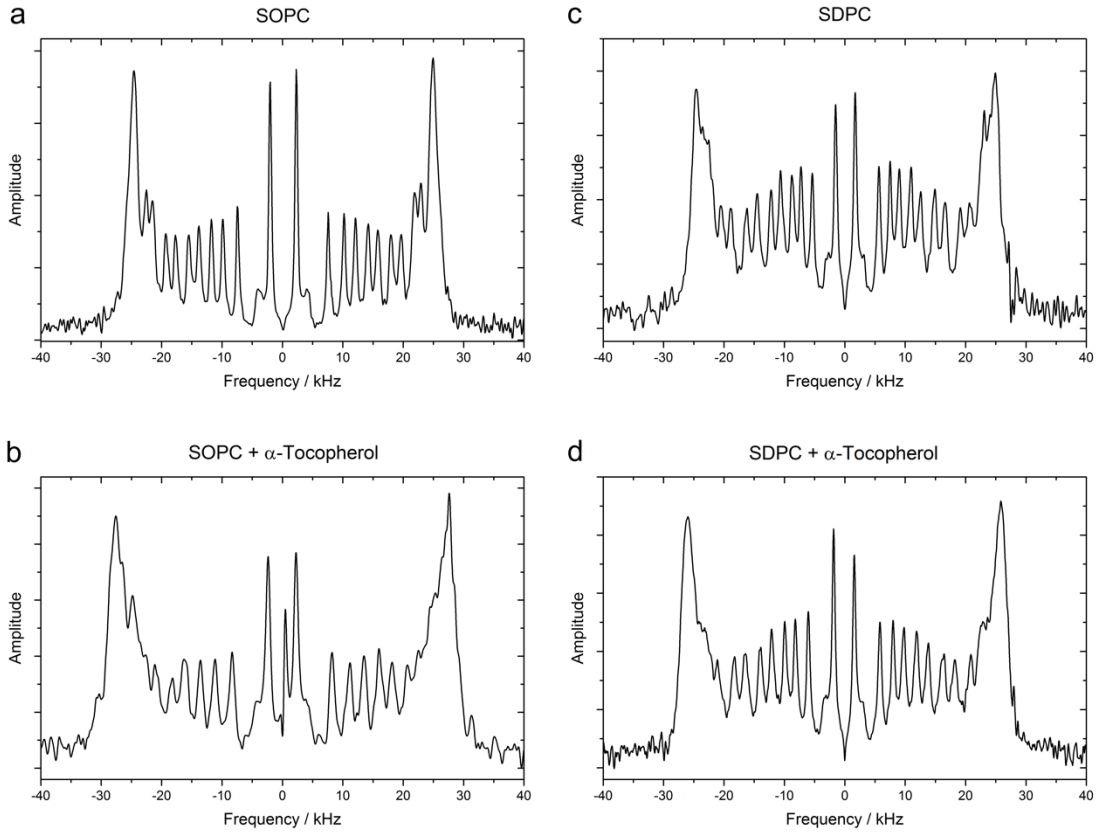

Figure A.2

FFT depaked ^{2}H NMR spectra for 50 wt% aqueous dispersions in 50 mM Tris buffer (pH 7.5) of (a) SOPC-d_{35}, (b) SOPC-d_{35} + 20 mol% αtoc, (c) SDPC-d_{35} and (d) SDPC-d_{35} + 20 mol% αtoc at 37 °C.

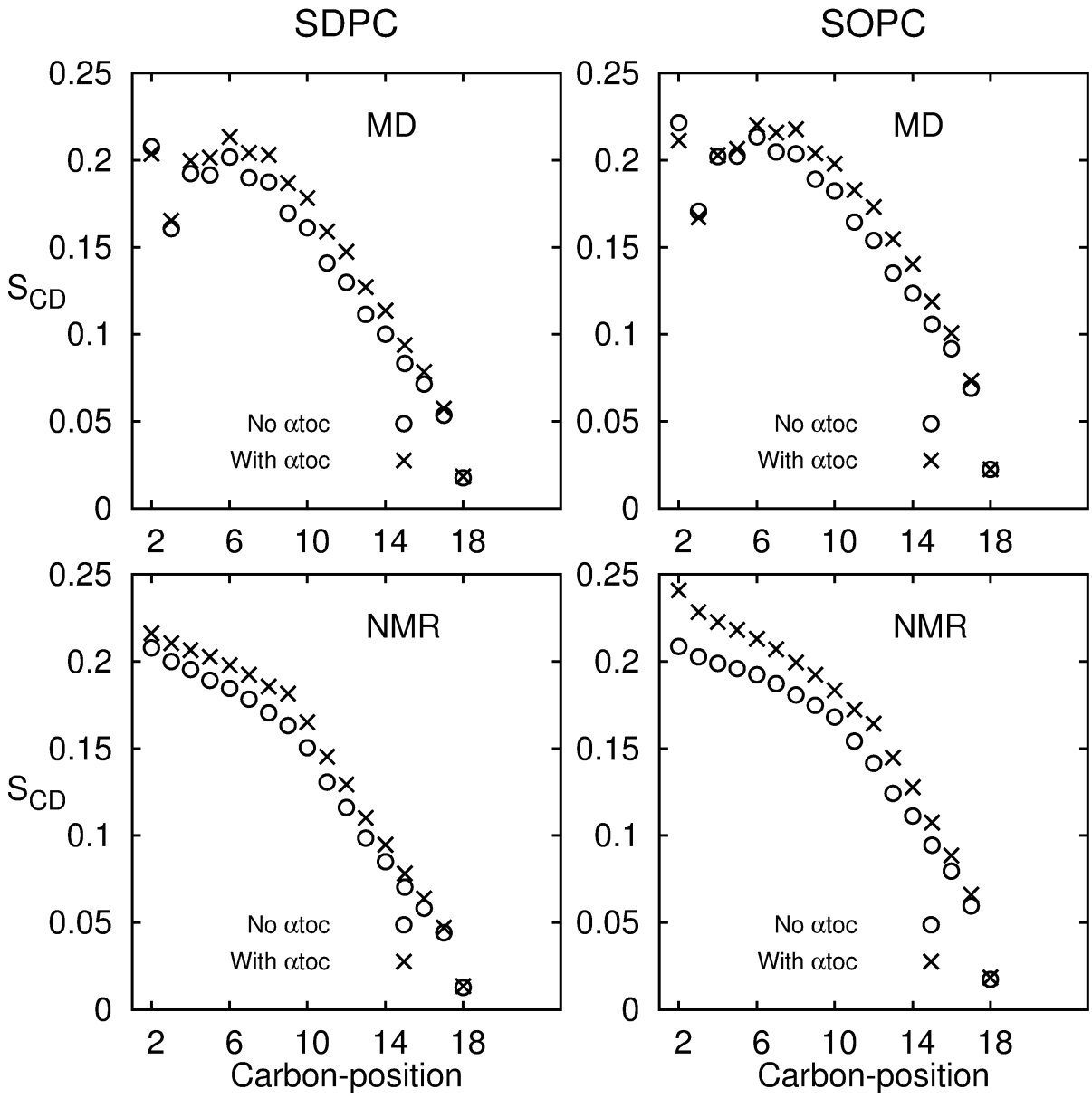

Figure A.3

Order parameter profiles along the *sn*-1 chain in SDPC (left panels) and SOPC (right panels) at 37 ºC obtained in the absence (○) and presence (x) of 20 mol% αtoc from MD simulations (upper panels) and FFT depaked ^{2}H NMR spectra (lower panels).

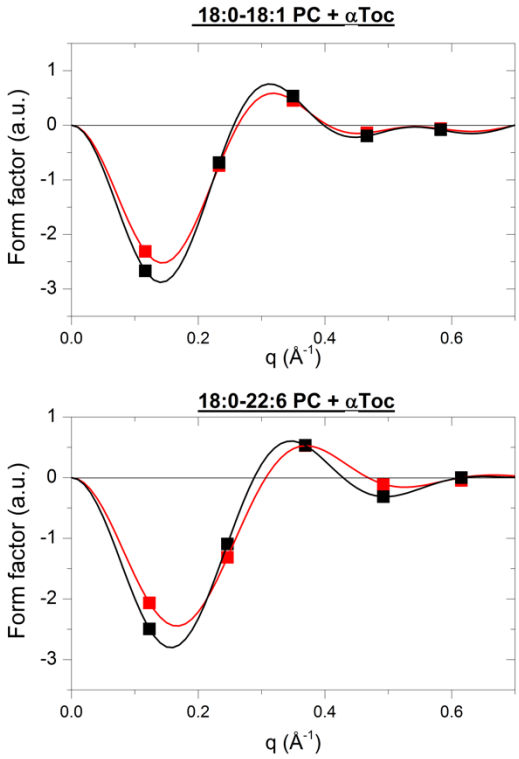

Figure A.4

Measured structure factors for SOPC (18:0-18:1 PC) and SDPC (18:0-22:6 PC) membranes containing protiated αtoc (red) and C5 deuterated αtoc (black), under 94% relative humidity hydration at 37 °C. The solid squares are the measured, phased and scaled structure factors and the line is the fit of Shannon's Theorem generating a continuous form factor.

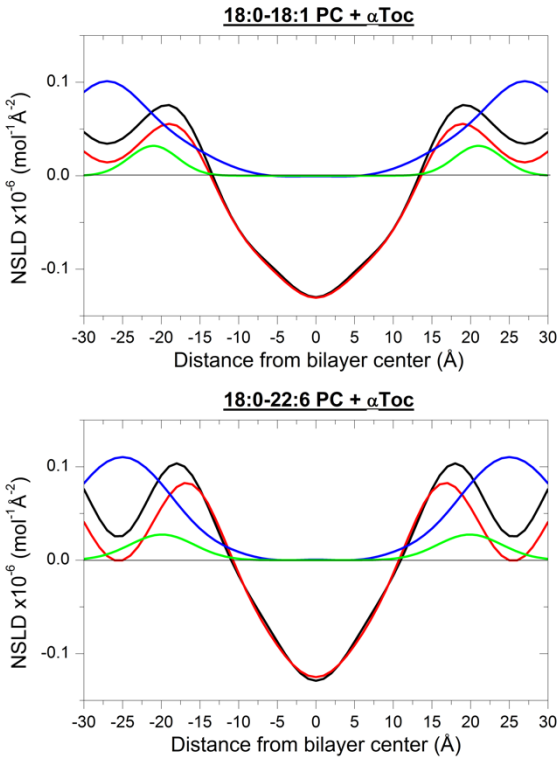

Figure A.5

Scaled neutron scattering length density profiles for SOPC (18:0-18:1 PC) and SDPC (18:0-22:6 PC) with 20 mol% protiated αtoc (red) and 20 mol% αtoc-d_3 (black) hydrated with 8% D_2O at 37°C. The green line is the C5 deuterium label distribution and the blue line represents the water distribution vertically scaled down by a factor 5.

Table A.2

Measured (unit cell) and calculated (other) structural parameters for α-[5-$^2H_3$]tocopherol (αtoc-d_3) in SOPC (18:0-18:1 PC) and SDPC (18:0-22:6 PC) membranes at 37 °C.

Phospholipid	Unit Cell	Bilayer Thickness	Water Centre*	Water Width	Label Centre*	Label Width
18:0-18:1 PC	53.8±0.3	38.8±0.2	26.9±0.1	10.6±0.5	21±1	6.2±0.3
18:0-22:6 PC	50.5±0.9	35±1.6	25.3±0.3	9.9±0.5	19±1.5	8.3±4

*Label position is relative to the bilayer center, and the range that it occupies is determined from the widths, 1/*e*, of Gaussian fits to the data. Units are angstroms (Å).

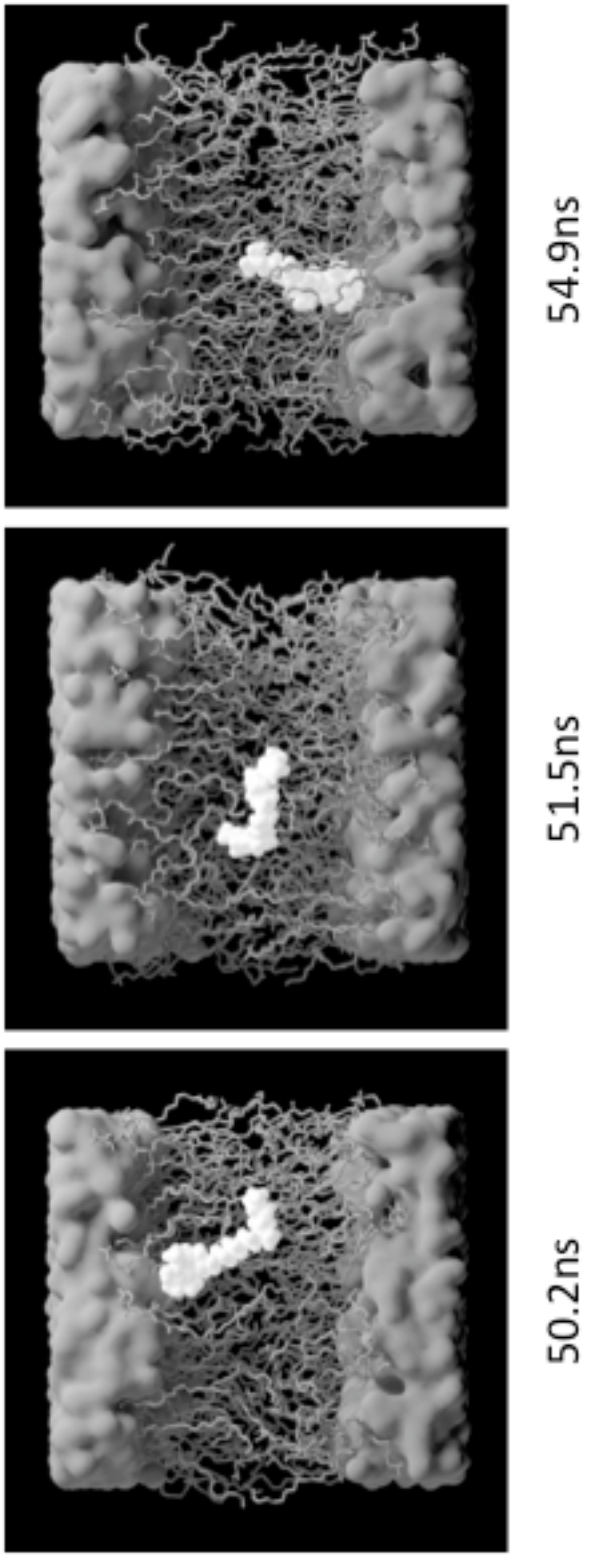

Figure A.6

Enlarged versions of the snapshots presented in Figure 7.

APPENDIX B. SUPPLEMENTAL MATERIAL FOR ALL N-3 PUFA THE SAME? A COMPARISON OF EPA, DHA AND DPA BY MD SIMULATIONS

B.1 Solid state 2H NMR spectroscopy

B.1.1 Materials

1-[$^2H_{35}$]stearoyl-2-oleoylphosphatidylcholine (OA-PC-d_{35}), 1-[$^2H_{35}$]stearoyl-2-eicosapentaenoylphosphatidylcholine (EPA-PC-d_{35}), 1-[$^2H_{35}$]stearoyl-2-docosapentaenoylphosphatidylcholine (DPA-PC-d_{35}), and 1-[$^2H_{35}$]stearoyl-2-docosahexaenoylphosphatidylcholine (DHA-PC-d_{35}) with a perdeuterated *sn*-1 chain were bought from Avanti Polar Lipids (Alabaster, AL). They were either a stock item or custom synthesized. Sigma (St. Louis, MO) and Cambridge Isotope Laboratories (Andover, MA), respectively, were the source of cholesterol and deuterium depleted water.

B.1.2 Sample preparation

Phospholipid (25 mg), on its own or co-dissolved with cholesterol (20 mol%), in chloroform solution was dried with a gentle stream of argon gas (nitrogen gas for OA-PC-d_{35}) and vacuum pumped overnight to remove residual organic solvent. Samples (50 wt% lipid) were hydrated with 50 mM Tris buffer, vortex-mixed and pH was adjusted to 7.5. They were then lyophilized three times with deuterium-depleted water to remove trace amounts of ^{2}HHO. The samples were finally rehydrated with deuterium-depleted water and, following 3 cycles of freezing and thawing, were transferred to 5 mm NMR tubes and stored at -80 °C. Precautions were taken throughout the procedure to minimize oxidation of the samples containing polyunsaturated phospholipid - exposure to direct light was limited and manipulations were performed in a glove box purged with argon gas [1].

B.1.3 NMR spectroscopy

Solid state ^{2}H NMR spectra were acquired on a homebuilt spectrometer operating at 46.0 MHz with a 7.05 T super-conducting magnet (Oxford Instruments, Osney Mead, UK) [2]. As previously described, pulse programming was accomplished with an

programmable pulse generator assembled in house, a phase-alternated quadrupolar echo sequence $(90°_x\text{-}\tau\text{-}90°_y\text{-acquire-delay})_n$ was implemented, signals were obtained in quadrature using a R1200 dual-channel digital oscilloscope (Rapid Systems, Seattle, WA) and temperature was monitored to ±0.1 °C with 1600 Series controller (Love Controls, Michigan City, IN). Parameters were 90° pulse width = 3.6 μs; separation between pulses τ = 50 μs; delay between pulse sequences = 1.5 s; sweep width = ±100 kHz; dataset = 2 K; and number of transients = ~15,000.

B.1.4 Spectral Analysis

The FFT depaking algorithm was applied to enhance resolution of the NMR spectra that are superposition of signals from all positions in the perdeuterated chain at the *sn*-1 position on a phospholipid [3]. The resultant spectra, equivalent to a planar bilayer aligned with its normal in the same direction as the magnetic field (θ = 0°), consist of a series of doublets that are each split according to the magnitude of the order parameter S_{CD} for a C-^{2}H bond. Smoothed profiles of order along the *sn*-1 chain were then generated on the basis of integrated intensity assuming the value of S_{CD} monotonically decreases toward the terminal methyl group [4]

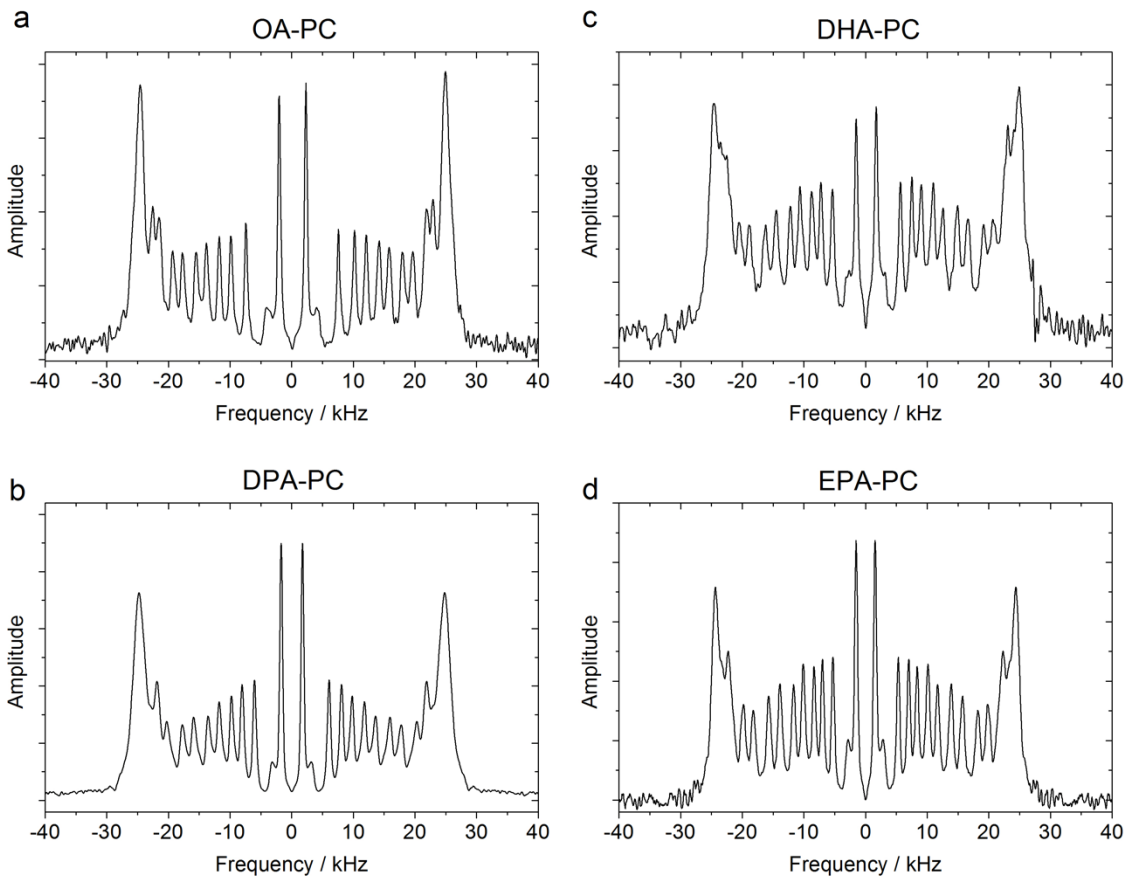

Figure B.1

FFT depaked ^{2}H NMR spectra at 37 °C for 50 wt% aqueous multilamellar dispersions of OA-PC-d_{35}, DPA-PC-d_{35}, DHA-PC-d_{35} and EPA-PC-d_{35} in 50 mM Tris (pH 7.5).

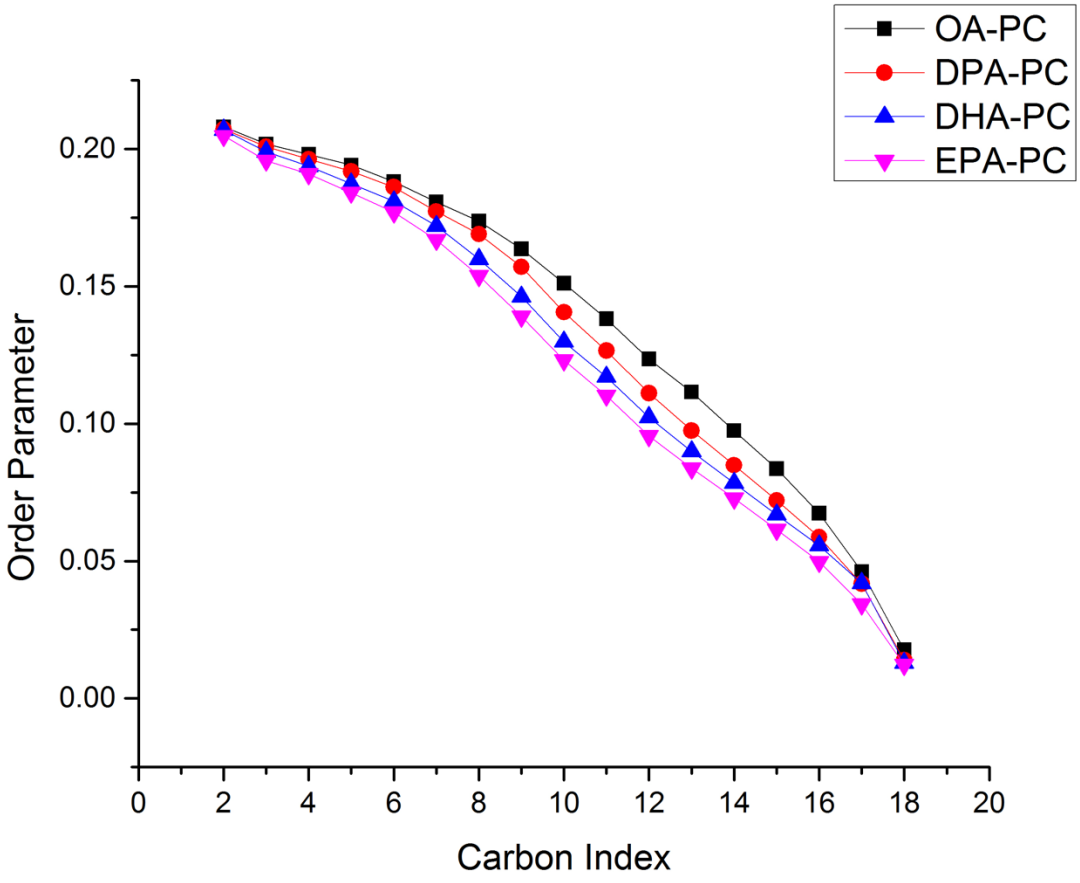

Figure B.2

Smoothed order parameter profiles constructed for the *sn*-1 chain in OA-PC-d_{35}, DPA-PC-d_{35}, DHA-PC-d_{35} and EPA-PC-d_{35} from FFT depaked ^{2}H NMR spectra at 37 °C.

B.2 References

[1] Shaikh, S.R., Brzustowicz, M.R, Gustafson, N., Stillwell, W. and Wassall, S.R. (2002) Monounsaturated PE does not phase-separate from the lipid raft molecules sphingomyelin and cholesterol: Role for polyunsaturation? *Biochemistry* 41, 10593–10602.

[2] Williams, J.A., Batten, S.E., Harris, M., Rockett, B.D., Shaikh, S.R., Stillwell W. and Wassall, S.R. (2012) Docosahexaenoic and eicosapentaenoic acids segregate differently between raft and non-raft domains. *Biophys. J.* 103, 228-237.

[3] McCabe, M.A. and Wassall, S.R. (1997) Rapid deconvolution of NMR powder spectra by weighted fast Fourier transformation. *Solid State Nucl. Magn. Reson.* 10, 53-61.

[4] Lafleur, M., Fine, B., Sternin, E., Cullis, P.R. and Bloom, M. (1989) Smoothed orientational order profile of lipid bilayers by ^{2}H-nuclear magnetic resonance. *Biophys. J.* 56, 1037-1041.

VITA

Education

Ph. D: Physics, anticipated May 2017, Purdue University, Indianapolis, Indiana.

M.S.: Physics, Dec 2011, Purdue University, Indianapolis, Indiana.

B.S.: Applied physics, Jun 2008, Northeastern University, Shenyang, Liaoning, China

M.S. Thesis:

Coarse grained model for RNA

Ph. D Thesis:

Insights on PUFA-containing lipid membranes probed by MD simulations

Awards

Biophysical Society Educational Committee Travel Award, 2013

IUPUI Graduate Student Travel Fellowship Award, 2015

Outstanding Physics Graduate Student Award, 2016

Graduate - Professional Educational Grant, 2016

Research experience

I started working under the supervision of Professor Stephen Wassall at IUPUI on my Ph.D. research in 2011. The main topic was to explore the structure and dynamics of model cell membranes (lipid bilayers) composed of different lipids, especially polyunsaturated fatty acid (PUFA)-containing lipids. In collaboration with Professors Scott Feller at Wabash College and Fangqiang Zhu at IUPUI, I used all-atom MD simulations as my main research tool and performed solid state 2H NMR experiments to provide validation. So far my research has led to three peer-reviewed articles (one as first author and two as a coauthor), five poster presentations at national conferences and two contributed talks at regional meetings. Two more manuscripts (as first author) are currently in preparation.

Before my Ph.D. research, I worked with Professor Marcos Betancourt at IUPUI on my M.S. research from 2009-2011. The main goal was trying to build up a CG model to enhance the speed of simulating RNA molecules. I designed the CG particles for RNA and generated the non-bounded force field for these CG particles using all-atom MD simulation. This CG model has been preliminarily tested by C++ programmed Monte Carlo simulations.

Publications

"α-Tocopherol is well designed to protect polyunsaturated phospholipids: MD simulations." **X. Leng**, J.J. Kinnun, D. Marquardt, M. Ghefli, N. Kučerka, J. Katsaras, J. Atkinson, T.A. Harroun, S.E. Feller and S.R. Wassall. Biophys. J. 109, 1608-1618 (2015).

"How polyunsaturated fatty acids modify molecular organization in membranes: Insight from NMR studies of model systems." S.R. Shaikh, J.J. Kinnun, **X. Leng**, J.A. Williams and S.R. Wassall. Biochim. Biophys. Acta 1848, 211-219 (2015).

"Membrane disordering by EPA in B lymphomas is reduced by elongation to docosapentaenoic acid as revealed with solid state NMR spectroscopy of model membranes." M. Harris, J.J. Kinnun, R. Kosaraju, **X. Leng**, S.R. Wassall and S.R. Shaikh. J. Nutr. 146, 1283-1289 (2016).

Presentations

"Interaction of α-tocopherol with a polyunsaturated lipid studied by MD simulations." Feb. 5, 2013, *Biophysical Society 57th Annual Meeting, poster presentation*

"Interaction of α-tocopherol with a polyunsaturated lipid studied by MD simulations." March 9, *2013, Indiana Academy of Science 128th Annual Meeting, contributed talk*

"Interaction of α-tocopherol with a polyunsaturated lipid studied by MD simulations." April 5, *2013, IUPUI Research Day, poster presentation*

"MD simulations on alpha-tocopherol in PUFA containing lipid." Feb. 16, 2014, *Biophysical Society 58th Annual Meeting, poster presentation*

"α-Tocopherol is well designed to protect polyunsaturated fatty acids." April 11, 2014, *IUPUI Research Day, poster presentation*

"n-3 PUFA-containing phospholipids studied by MD simulations: a comparison of EPA, DPA and DHA." Feb 10, 2015, *Biophysical Society 59th Annual Meeting, poster presentation*

"MD simulations on n-3 PUFA containing phospholipids: a comparison of EPA, DPA and DHA." March 14, 2015 , *Indiana Academy of Science 130th Annual Meeting, contributed talk*

"All n-3 PUFA are not the same: a comparison of DPA, EPA and DHA by MD simulations." March 2, 2016, *Biophysical Society 60th Annual Meeting, poster presentation*

"Binding of vitamin E in model membranes studied by umbrella sampling simulations." March 2, 2016, *Biophysical Society 60th Annual Meeting, poster presentation*